

Impact of Curling and Warping on Concrete Pavement: Phase II

Final Report
May 2023



IOWA STATE UNIVERSITY
Institute for Transportation

Sponsored by
Iowa Highway Research Board
(IHRB Project TR-749)
Iowa Department of Transportation
(InTrans Project 18-659)

About the Program for Sustainable Pavement Engineering and Research

The overall goal of the Program for Sustainable Pavement Engineering and Research (PROSPER) is to advance research, education, and technology transfer in the area of sustainable highway and airport pavement infrastructure systems.

About the Institute for Transportation

The mission of the Institute for Transportation (InTrans) at Iowa State University is to save lives and improve economic vitality through discovery, research innovation, outreach, and the implementation of bold ideas.

Iowa State University Nondiscrimination Statement

Iowa State University does not discriminate on the basis of race, color, age, ethnicity, religion, national origin, pregnancy, sexual orientation, gender identity, genetic information, sex, marital status, disability, or status as a US veteran. Inquiries regarding nondiscrimination policies may be directed to the Office of Equal Opportunity, 3410 Beardshear Hall, 515 Morrill Road, Ames, Iowa 50011, telephone: 515-294-7612, hotline: 515-294-1222, email: eooffice@iastate.edu.

Disclaimer Notice

The contents of this report reflect the views of the authors, who are responsible for the facts and the accuracy of the information presented herein. The opinions, findings and conclusions expressed in this publication are those of the authors and not necessarily those of the sponsors.

The sponsors assume no liability for the contents or use of the information contained in this document. This report does not constitute a standard, specification, or regulation.

The sponsors do not endorse products or manufacturers. Trademarks or manufacturers' names appear in this report only because they are considered essential to the objective of the document.

Iowa DOT Statements

Federal and state laws prohibit employment and/or public accommodation discrimination on the basis of age, color, creed, disability, gender identity, national origin, pregnancy, race, religion, sex, sexual orientation or veteran's status. If you believe you have been discriminated against, please contact the Iowa Civil Rights Commission at 800-457-4416 or the Iowa Department of Transportation affirmative action officer. If you need accommodations because of a disability to access the Iowa Department of Transportation's services, contact the agency's affirmative action officer at 800-262-0003.

The preparation of this report was financed in part through funds provided by the Iowa Department of Transportation through its "Second Revised Agreement for the Management of Research Conducted by Iowa State University for the Iowa Department of Transportation" and its amendments.

The opinions, findings, and conclusions expressed in this publication are those of the authors and not necessarily those of the Iowa Department of Transportation.

Technical Report Documentation Page

1. Report No. IHRB Project TR-749	2. Government Accession No.	3. Recipient's Catalog No.	
4. Title and Subtitle Impact of Curling and Warping on Concrete Pavement: Phase II		5. Report Date May 2023	
		6. Performing Organization Code	
7. Author(s) Kexin Tian (orcid.org/0000-0003-1884-6250), Daniel King (orcid.org/0000-0001-8824-1818), Bo Yang (orcid.org/0000-0002-7774-5233), Sunghwan Kim (orcid.org/0000-0002-1239-2350), Ahmad Alhasan (orcid.org/0000-0002-0091-9899), Halil Ceylan (orcid.org/0000-0003-1133-0366)		8. Performing Organization Report No. InTrans Project 18-659	
9. Performing Organization Name and Address Program for Sustainable Pavement Engineering and Research (PROSPER) Iowa State University 2711 South Loop Drive, Suite 4700 Ames, IA 50010-8664		10. Work Unit No. (TRAIS)	
		11. Contract or Grant No.	
12. Sponsoring Organization Name and Address Iowa Highway Research Board Iowa Department of Transportation 800 Lincoln Way Ames, IA 50010		13. Type of Report and Period Covered Final Report	
		14. Sponsoring Agency Code IHRB Project TR-749	
15. Supplementary Notes Visit https://prosper.intrans.iastate.edu/ for color pdfs of this and other research reports.			
16. Abstract <p>Curling and warping behavior due to temperature and moisture variation has been widely considered an influential factor affecting the smoothness of jointed plain concrete pavement (JPCP). In recent decades, while extensive efforts have been made to quantify the impact of curling and warping-related deflections on the smoothness of JPCP, a standardized method for characterizing the effects of environmental factors on JPCP smoothness is still unavailable. A Phase I study examined curling and warping conditions at six sites using a stationary light detection and ranging (LiDAR) system and developed recommendations to minimize curling and warping based on literature review findings. However, the data collection effort in the Phase I study was limited and was insufficient to validate the recommendations derived from the literature review.</p> <p>The Phase II study described in this report aimed to evaluate and quantify the impact of curling and warping on Iowa concrete pavements and determine the factors that most influence curling and warping behavior. A high-speed profilometer and a LiDAR device were utilized to execute a large-scale field data collection plan for JPCP sites in Iowa, including Long-Term Pavement Performance (LTPP) Program highways, non-LTPP highways, and county roads and city streets. The variables evaluated in this study included temperature and moisture gradients, seasonal and diurnal effects, slab geometry, pavement structural design, mix design, and construction conditions. A validated MATLAB-based algorithm with two different curve-fitting models was coded to evaluate the degrees of curling and warping in multiple ways. This study also used statistical analyses to select the variables that significantly affect curling and warping behavior. The proposed actionable pavement design and construction recommendations will help minimize curling and warping and correct curling and warping-related performance issues.</p>			
17. Key Words concrete slabs—curling and warping—degree of curvature—deflection—International Roughness Index (IRI)		18. Distribution Statement No restrictions.	
19. Security Classification (of this report) Unclassified.	20. Security Classification (of this page) Unclassified.	21. No. of Pages 147	22. Price NA

IMPACT OF CURLING AND WARPING ON CONCRETE PAVEMENT: PHASE II

**Final Report
May 2023**

Principal Investigator

Halil Ceylan, Director
Program for Sustainable Pavement Engineering and Research (PROSPER)
Institute for Transportation, Iowa State University

Co-Principal Investigator

Sunghwan Kim, Research Scientist
Institute for Transportation, Iowa State University

Research Associates

Bo Yang, Kexin Tian, Daniel King

Authors

Kexin Tian, Daniel King, Bo Yang, Sunghwan Kim, Ahmad Alhasan, and Halil Ceylan

Sponsored by

Iowa Highway Research Board and
Iowa Department of Transportation
(IHRB Project TR-749)

Preparation of this report was financed in part
through funds provided by the Iowa Department of Transportation
through its Research Management Agreement with the
Institute for Transportation
(InTrans Project 18-659)

A report from

Program for Sustainable Pavement Engineering and Research (PROSPER)

Iowa State University

2711 South Loop Drive, Suite 4700
Ames, IA 50010-8664

Phone: 515-294-8103 / Fax: 515-294-0467

<https://prosper.intrans.iastate.edu/>

TABLE OF CONTENTS

ACKNOWLEDGMENTS	xi
EXECUTIVE SUMMARY	xiii
1. INTRODUCTION	1
1.1. Background and Motivation	1
1.2. Research Objectives	2
1.3. Overview of Research Approach	2
2. LITERATURE REVIEW	3
2.1. Factors that Influence Curling and Warping	3
2.2. Indicators of Curling and Warping	10
2.3. Summary	13
3. METHODOLOGY	15
3.1. Equipment Used for Data Collection	15
3.2. Algorithm Development and Optimization	16
3.3. Field Data Collection Protocol	25
3.4. Summary	30
4. ANALYSIS APPROACHES AND RESULTS	32
4.1. Analysis Approach	32
4.2. Analysis Results	37
4.3. Summary	92
5. ANALYSIS OF LIDAR SCANNING ON CONCRETE SLABS	95
5.1. Overview of LiDAR	95
5.2. Field LiDAR Data Collection and Processing	96
5.3. Results and Discussion	97
5.4. Summary	102
6. CONCLUSIONS AND RECOMMENDATIONS	103
6.1. General Summary	103
6.2. Algorithm Development and Data Processing	103
6.3. Key Findings	105
6.4. Recommendations	107
REFERENCES	110
APPENDIX A. ADDITIONAL MATERIAL	116
A.1. Operation Manual for SSI High-Speed Profiler	116
A.2. Data Processing Procedure Using MATLAB	118
A.3. Site List and Visited Seasons	130
A.4. Equivalent Temperature Difference Calculation in PMED	133

LIST OF FIGURES

Figure 1. Diurnal slab curvature	4
Figure 2. Schematic of curling in PCC pavements	5
Figure 3. Quarter-car model.....	11
Figure 4. SSI high-speed profiler.....	15
Figure 5. Example profile trace from the SSI profiler	16
Figure 6. Data processing procedure	17
Figure 7. Example site profiles: (a) curled-up site profile (US 18 in Sioux County, Iowa, measured on Aug. 11, 2020) and (b) curled-down site profile (D20 in Hamilton County, Iowa, measured on July 22, 2020).....	18
Figure 8. Algorithm validation: (a) deflection and (b) degree of curvature	19
Figure 9. Joint detection.....	20
Figure 10. ISU portable curling and warping device	22
Figure 11. 2GCI algorithm flowchart	24
Figure 12. Second-order polynomial algorithm flowchart	25
Figure 13. Site locations	26
Figure 14. Typical temperature variation profile throughout a slab	32
Figure 15. Hourly equivalent temperature difference versus (a) curvature IRI, (b) deflection, (c) deflection ratio, (d) degree of curvature	41
Figure 16. Diurnal hourly equivalent temperature difference versus (a) curvature IRI, (b) deflection, (c) deflection ratio, (d) degree of curvature	42
Figure 17. Shrinkage equivalent temperature difference versus (a) curvature IRI, (b) deflection, (c) deflection ratio, (d) degree of curvature	43
Figure 18. Overall equivalent temperature difference versus (a) curvature IRI, (b) deflection, (c) deflection ratio, (d) degree of curvature	43
Figure 19. Configuration of a box-whisker plot	44
Figure 20. Seasonal effects on LTPP sections: (a) curvature IRI, (b) deflection, (c) deflection ratio, (d) degree of curvature (12 sites, 36 data points for each season).....	45
Figure 21. Seasonal effects on non-LTPP sections: (a) curvature IRI, (b) deflection, (c) deflection ratio, (d) degree of curvature (14 sites, 42 data points for each season).....	47
Figure 22. Seasonal effects on county roads and city streets: (a) curvature IRI, (b) deflection, (c) deflection ratio, (d) degree of curvature (7 sites, 21 data points for each season)	48
Figure 23. Summary of seasonal effects on (a) curvature IRI, (b) deflection, (c) deflection ratio, (d) degree of curvature.....	50
Figure 24. Diurnal effects on LTPP sections: (a) curvature IRI, (b) deflection, (c) deflection ratio, (d) degree of curvature (12 sites, 72 data points for each time)	51
Figure 25. Diurnal effects on non-LTPP sections: (a) curvature IRI, (b) deflection, (c) deflection ratio, (d) degree of curvature (14 sites, 66 data points for each time)	52
Figure 26. Diurnal effects on county roads and city streets: (a) curvature IRI, (b) deflection, (c) deflection ratio, (d) degree of curvature (7 sites, 29 data points for each time)	53
Figure 27. Slab width effects on LTPP sections: (a) curvature IRI, (b) deflection, (c) deflection ratio, (d) degree of curvature (12 ft width [6 sites, 108 data points], 14 ft width [6 sites, 108 data points]).....	55

Figure 28. Slab width effects on non-LTPP sections: (a) curvature IRI, (b) deflection, (c) deflection ratio, (d) degree of curvature (12 ft slab width [1 site, 12 data points], 13 ft slab width [1 site, 9 data points], 14 ft slab width [12 sites, 174 data points])	57
Figure 29. Slab width effects on county roads and city streets: (a) curvature IRI, (b) deflection, (c) deflection ratio, (d) degree of curvature (11 ft slab width [4 sites, 39 data points], 12 ft slab width [2 sites, 30 data points], 13 ft slab width [1 site, 15 data points]).....	58
Figure 30. Slab thickness effects on LTPP sections: (a) curvature IRI, (b) deflection, (c) deflection ratio, (d) degree of curvature (8 in. thickness [6 sites, 108 data points], 11 in. thickness [6 sites, 108 data points])	60
Figure 31. Slab thickness effects on non-LTPP sections: (a) curvature IRI, (b) deflection, (c) deflection ratio, (d) degree of curvature (10 in. thickness [10 sites, 138 data points], 11 in. thickness [2 sites, 33 data points])	62
Figure 32. Slab thickness effects on county roads and city streets: (a) curvature IRI, (b) deflection, (c) deflection ratio, (d) degree of curvature (6 in. thickness [1 site, 8 data points], 8 in. thickness [4 sites, 48 data points], 10 in. thickness [2 sites, 30 data points]).....	63
Figure 33. Transverse joint spacing effects on county roads and city streets: (a) curvature IRI, (b) deflection, (c) deflection ratio, (d) degree of curvature (12 ft joint spacing [3 sites, 32 data points], 15 ft joint spacing [3 sites, 39 data points], 20 ft joint spacing [1 site, 15 data points])	64
Figure 34. Dowel bar effects on LTPP sections: (a) curvature IRI, (b) deflection, (c) deflection ratio, (d) degree of curvature (1.25 in. dowel bar [6 sites, 108 data points], (1.5 in. dowel bar [6 sites, 108 data points]).....	66
Figure 35. Dowel bar effects on county roads and city streets: (a) curvature IRI, (b) deflection, (c) deflection ratio, (d) degree of curvature (no dowel bar [4 sites, 56 data points], 1.5 in. dowel bar [2 sites, 30 data points])	67
Figure 36. Joint type effects on non-LTPP sections: (a) curvature IRI, (b) deflection, (c) deflection ratio, (d) degree of curvature (rectangular joints [3 sites, 46 data points], skewed joints [9 sites, 125 data points])	69
Figure 37. Shoulder type effects on non-LTPP sections: (a) curvature IRI, (b) deflection, (c) deflection ratio, (d) degree of curvature (tied PCC shoulder [1 site, 15 data points], untied shoulder [11 sites, 158 data points])	71
Figure 38. Shoulder type effects on county roads and city streets: (a) curvature IRI, (b) deflection, (c) deflection ratio, (d) degree of curvature (tied PCC shoulder [3 sites, 38 data points], untied shoulder [4 sites, 48 data points])	72
Figure 39. Mix design effects on LTPP sections: (a) curvature IRI, (b) deflection, (c) deflection ratio, (d) degree of curvature (high strength [6 sites, 72 data points], low strength [6 sites, 72 data points])	74
Figure 40. Mix design effects on non-LTPP sections: (a) curvature IRI, (b) deflection, (c) deflection ratio, (d) degree of curvature (pre-QMC [6 sites, 89 data points], QMC [6 sites, 82 data points])	76
Figure 41. Mix design effects on county roads and city streets: (a) curvature IRI, (b) deflection, (c) deflection ratio, (d) degree of curvature (C-3WR [2 sites, 24 data points], C-SUD [2 sites, 30 data points], QMC [2 sites, 17 data points]).....	77

Figure 42. Construction season effects on non-LTPP sections: (a) curvature IRI, (b) deflection, (c) deflection ratio, (d) degree of curvature (spring [4 sites, 55 data points], summer [5 sites, 70 data points], fall [3 sites, 46 data points]).....	79
Figure 43. Construction season effects on county roads and city streets: (a) curvature IRI, (b) deflection, (c) deflection ratio, (d) degree of curvature (summer [3 sites, 11 data points], fall [1 site, 6 data points]).....	81
Figure 44. Variables for three groups	83
Figure 45. Multiple linear regression models' prediction results for LTPP sections: (a) curvature IRI, (b) deflection, (c) deflection ratio, (d) degree of curvature	85
Figure 46. Multiple linear regression models' prediction results for non-LTPP sections: (a) curvature IRI, (b) deflection, (c) deflection ratio, (d) degree of curvature	87
Figure 47. Multiple linear regression modelss prediction results for county roads and city streets: (a) curvature IRI, (b) deflection, (c) deflection ratio, (d) degree of curvature.....	89
Figure 48. Hourly equivalent temperature difference versus (a) curvature IRI, (b) deflection, (c) deflection ratio, (d) degree of curvature	90
Figure 49. Shrinkage equivalent temperature difference versus (a) curvature IRI, (b) deflection, (c) deflection ratio, (d) degree of curvature	91
Figure 50. Overall equivalent temperature difference versus (a) curvature IRI, (b) deflection, (c) deflection ratio, (d) degree of curvature	91
Figure 51. Field LiDAR scanning and 3D slab profile.....	95
Figure 52. Schematic diagram of directions for a PCC slab.....	97
Figure 53. Flowchart of the LiDAR data processing procedure.....	97
Figure 54. Profiles at Slab A along the directions of (a) D1, (b) D2, and (3) L	98
Figure 55. Profiles at Slab B along the directions of (a) D1, (b) D2, and (3) L	99
Figure 56. Profiles at Slab C along the directions of (a) D1, (b) D2, and (3) L	99
Figure 57. Profiles at Slab D along directions of (a) D1, (b) D2, and (3) L.....	100
Figure 58. Absolute values of relative deflection for (a) Slab A, (b) Slab B, (c) Slab C, and (d) Slab D	101
Figure A1. Exporting a *.erd proflile in the SSI Profiler software.....	118
Figure A2. Selecting a curling direction in MATLAB	118
Figure A3. Data processing status in MATLAB	119
Figure A4. Code view in MATLAB	119
Figure A5. Detailed site list	130
Figure A6. ThermalPCC.dat image	133

LIST OF TABLES

Table 1. Summary of literature review	14
Table 2. Curled-up non-LTPP highways	27
Table 3. Curled-up LTPP highways.....	28
Table 4. Curled-up county roads and city streets.....	29
Table 5. Curled-down county roads.....	29
Table 6. Definitions of field data collection periods.....	30
Table 7. Summary of engineering variables	36
Table 8. Curled-up LTPP highways for equivalent temperature difference analysis	38
Table 9. Curled-up non-LTPP highways for equivalent temperature difference analysis.....	39
Table 10. Curled-up county roads and city streets for equivalent temperature difference analysis.....	40
Table 11. Summary of seasonal effects	46
Table 12. Summary of diurnal effects.....	52
Table 13. Summary of slab width effects	56
Table 14. Summary of slab thickness effects.....	61
Table 15. Summary of transverse joint spacing effects	65
Table 16. Summary of dowel bar effects	67
Table 17. Summary of joint type effects.....	70
Table 18. Summary of shoulder type effects	72
Table 19. Summary of mix design effects	75
Table 20. Summary of construction season effects	80
Table 21. One-way ANOVA results for LTPP sections	82
Table 22. One-way ANOVA results for non-LTPP sections.....	82
Table 23. One-way ANOVA results for county roads and city streets.....	83
Table 24. Model results summary.....	84
Table 25. Comparison between literature review and findings for highways investigated in the study	94
Table 26. Comparison between literature review and findings for county roads and city streets investigated in the study	94
Table 27. Selected sites for LiDAR scanning.....	96
Table 28. Measured surface temperatures at the investigation sites	98
Table 29. Mix design at the investigation sites.....	100
Table A1. Site list and visited seasons.....	131

ACKNOWLEDGMENTS

The authors gratefully acknowledge the Iowa Department of Transportation (DOT) and the Iowa Highway Research Board (IHRB) for sponsoring this project. The authors also gratefully acknowledge the project technical advisory committee (TAC) members:

- Ben Behnami (Iowa DOT)
- Chris Brakke (Iowa DOT)
- Jason Omundson (Iowa DOT)
- Jonathan Miranda (Iowa DOT)
- Kevin Merryman (Iowa DOT)
- Kent Nicholson (Iowa DOT)
- Michael Kennerly (Iowa DOT)
- Norman Miller (Iowa DOT)
- Todd Hanson (Iowa DOT)
- Vanessa Goetz (Iowa DOT)
- Jim Grove (Federal Highway Administration)
- Lisa McDaniel (Federal Highway Administration)
- Brandon Billings (Cherokee County)
- Lee Bjerke (Winneshiek County)
- Scott Kruse (Boone County)
- Jacob Thorius (Washington County)
- Brian Moore (Iowa County Engineers Association Service Bureau)
- Greg Mulder (Iowa Concrete Paving Association)

Special thanks are due to Steven Tritsch and Peter C. Taylor from the National Concrete Pavement Technology Center at Iowa State University (ISU) for their full technical support. The authors would also like to express their sincere gratitude to the following:

- Yang Zhang, who helped initiate this project and purchase the high-speed profiler.
- Shuo Yang, who helped with the development of the field data collection protocol and light detection and ranging (LiDAR) algorithm
- Muhammad Ahmad Siddique, who helped with the field data collection
- Nianhong Han, who helped upgrade the MATLAB algorithm with more functions
- Surface Systems & Instruments (SSI) Inc., which provided training and technical support in utilizing the high-speed profiler
- Praveen Gopiseti, who provided guidance in extracting temperature gradient data from AASHTOWare Pavement Mechanistic-Empirical Design (PMED) software
- Other research team members, including former members of ISU's Program for Sustainable Pavement Engineering and Research (PROSPER) at the Institute for Transportation, for their assistance during the course of this project

EXECUTIVE SUMMARY

The smoothness of jointed plain concrete pavement (JPCP) has been largely attributed to the curling and warping behavior caused by temperature and moisture variations. Portland cement concrete (PCC) pavements can curl/warp as a result of climatic changes, which can cause either concave or convex deformation. Curling is the nonuniform temperature gradient-induced deformation, and warping is the nonuniform moisture gradient-induced deformation. The top portion of a PCC slab will typically undergo more expansion than the bottom portion of the slab when the top has a higher temperature or moisture content than the bottom. This may cause downward slab curling or warping. In contrast, if the bottom portion of a PCC slab has a higher temperature or moisture content than the top, a negative gradient will result and the bottom portion of the slab will expand more than the top, causing the slab to curl/warp upward.

Concrete pavements display a variety of fatigue failures, including transverse cracking, top-down cracking, and bottom-up cracking, under repeated slab curvature changes and traffic loading. The degree of curling and warping behavior has been measured using a variety of techniques, including walking profilers, light detection and ranging (LiDAR) devices, high-speed profilers, and others. While significant efforts have been made in recent years to quantify the impacts of curling and warping-related deflections on the smoothness of JPCP, a standardized technique for describing the effects of environmental factors on JPCP smoothness is still unavailable.

A Phase I study examined the curling and warping conditions at six sites in Iowa using a stationary LiDAR system and developed recommendations to minimize curling and warping based on literature review findings. However, the data collection effort in the Phase I study was limited and was insufficient to validate the recommendations derived from the literature review.

To evaluate and quantify the impacts of curling and warping on the ride quality of Iowa's concrete pavements, the Phase II study described in this report was performed to collect profile data at 36 sites on Iowa's primary highways and county and city roads. A Surface Systems & Instruments (SSI) high-speed profiler was used to measure the smoothness of the PCC pavement surface. Three to four field visits were scheduled per site from the summer of 2019 to the spring of 2021 to cover all seasons and assess the effects of seasonal fluctuations. To assess the effects of diurnal changes on PCC curling and warping behavior, measurements were taken three times per day (early morning, noon, and late afternoon). Additionally, three Phase I sites on US 30 were rescanned in 2022 using a LiDAR system, and the results were compared with the Phase I data.

By assessing the parameters that most affect the curling and warping behavior of Iowa's concrete pavements, the main objective of this study was to determine the effects of various design considerations on the degree of curling and warping. This research established and examined a number of indicators, including curvature International Roughness Index (IRI), deflection, deflection ratio, and degree of curvature, to study pavement curling and warping. An algorithm using Second-Generation Curvature Index (2GCI)-based and second-order polynomial-based models was developed to interpret the raw profile data from the SSI high-speed profiler during pavement profile collection.

To test these methods and examine how temperature gradients and moisture gradients affect curling and warping, pavement sites near reliable Modern-Era Retrospective Analysis for Research and Applications (MERRA) climate stations were chosen to compute the equivalent temperature difference using the American Association of State Highway and Transportation Officials' (AASHTO's) AASHTOWare Pavement Mechanistic-Empirical Design (PMED) software.

The findings of this study show that for curled-up sites, the curling and warping behavior become less pronounced with reductions in the total equivalent temperature difference. Trendlines for three curling/warping indicators (curvature IRI, deflection, and deflection ratio) reached values of zero near a total equivalent temperature difference of 0°F in this study, so using -10°F as the default effective permanent curling/warping temperature difference in PMED is a reasonable assumption.

Statistical analysis was performed to study the relationships between curling and warping behavior and environmental and pavement design and construction factors, including seasonal and diurnal effects, slab geometry, shoulder type, mix type, construction season, and so on. A one-way analysis of variance (ANOVA) was used to determine which variables significantly impacted curling and warping behavior. The different variables were then used to create multiple linear regression models to predict curling and warping behavior and analyze how construction factors and environmental variables impact curling and warping behavior.

Based on the findings obtained from the sites selected for this study, quality management concrete (QMC) mix designs are recommended because they result in reduced curling and warping behavior compared to other mix design types. Constructing pavements with rectangular slabs and tied PCC shoulders can also effectively decrease curling and warping behavior relative to other slab geometries and shoulder types.

1. INTRODUCTION

Pavement performance is critical to the traveling public and the local economy. Factors affecting pavement performance include traffic volume and load, layer structures and material engineering properties, and environment. The primary function of the pavement surface is to provide a smooth riding surface with good friction, and commuters and members of the public who live in an area expect that local roads will maintain excellent smoothness during the roads' lifetimes.

1.1. Background and Motivation

Iowa is one of the leading states in terms of miles of portland cement concrete (PCC) pavements on roadways (FHWA 2020). Thanks to their rigidity and flexural strength, concrete pavements disperse traffic loads to underlying pavement layers over a large area. PCC pavements offer many options in terms of color, texture, structure, and reinforcement capabilities and are capable of achieving good long-term performance in terms of factors such as smoothness, cracking, durability, and service life.

Many concrete pavements are constructed as jointed plain concrete pavements (JPCP), where sawcut joints are placed to control early-age shrinkage cracking. Curling and warping of the slabs formed by these joints is a common occurrence, and it is widely assumed that this behavior impacts pavement ride quality (Chang et al. 2008). According to an investigation by Merritt et al. (2015), International Roughness Index (IRI) and Profilograph Index (PrI) are the most common smoothness indices used in many state highway agency (SHA) requirements. While many specifications allow for IRI to be measured in both wheel paths, acceptance is usually based on the average IRI of the two wheel paths.

Since the mid-1920s, the effects of the curling and warping behavior of PCC pavements have been well known and thoroughly examined (Westergaard 1926). However, curling and warping behavior still has unknown effects on the long-term performance of pavements. While some researchers have found a strong link between the two, others have claimed that the link is not as crucial as it appears. Engineers continue to look for more cost-effective ways to design and construct pavements that do not compromise performance, which requires a deeper understanding of the relationship between curling and warping behavior and long-term performance.

The study described in this report was undertaken to collect concrete pavement performance measurements, determine critical threshold magnitudes across Iowa, and better understand the link between the diurnal and seasonal temperature/moisture fluctuations in these measurements and long-term pavement performance.

An innovative computational approach was created for this study to assess the degree of curling and warping from profiles produced by an inertial profiler. The developed algorithm could be used to obtain different curling and warping indicators, including curvature IRI, deflection, deflection ratio, and degree of curvature, from raw profile data and immediately identify the

effects of curling and warping. This method can provide a more objective comparison than relying on comparisons of IRI alone.

1.2. Research Objectives

This study aimed to determine curling and warping tendencies in Iowa pavements using several indicators and to assess their impact on pavement performance. As a follow-up to the Phase I study documented in Ceylan et al. (2016a), this Phase II study used a high-speed profiler to quantify the effects of curling and warping. The study's specific goals were as follows:

- Evaluate the use of a high-speed inertial profiler for curling and warping measurements
- Determine the engineering factors with the most influence on the curling and warping behavior of PCC slabs in Iowa
- Evaluate the effects of diurnal and seasonal variations on the curling and warping behavior of PCC slabs in Iowa
- Develop an advanced algorithm to quantify the degree of curling and warping of PCC slabs used in Iowa's highways, county roads, and city streets
- Make actionable recommendations for minimizing and correcting curling and warping-related issues in Iowa's PCC slabs

1.3. Overview of Research Approach

To collect raw pavement profile data, a Surface Systems & Instruments (SSI) high-speed profiler (SSI Inertial Profiling System CS9300) was installed on a truck. Laser sensor units were equipped at the front of the truck to measure the pavement surface's left and right tracks. This instrument has a profile data resolution of 1 in. longitudinally and 0.01 in. for elevation. It measures humidity and surface temperature along with profile data and integrates an IRI calculation algorithm to provide results in terms of IRI.

To evaluate the seasonal variations in PCC curling and warping behavior, 36 sites, including highways, county roads, and city streets, were visited in four seasons over three years (2019 through 2021). Each field visit included at least three field surveys performed at different times of day (early morning, noon, and late afternoon) to assess diurnal differences in PCC curling and warping behavior.

2. LITERATURE REVIEW

Pavement performance is a critical parameter in highway engineering strategic plans that substantially impact society and the economy. Factors affecting pavement performance include traffic, climate, material characteristics, pavement structural parameters, and service age. Curling and warping caused by temperature and moisture changes have long been thought to be significant factors in the smoothness of PCC pavement. Curling and warping can increase maintenance costs, shorten the service life of a pavement, and increase transverse, longitudinal, and corner cracking both from the top down and bottom up. In recent decades, the impact of curling and warping-related deflections on the smoothness of PCC pavements has been extensively studied.

Since many studies have shown that rough roads lead to discomfort for users, increased travel time due to slower speeds, and higher vehicle operating costs, pavement roughness is one of the main indicators of pavement performance. Several devices have been used to measure road smoothness, ranging from simple rulers showing local surface deviations to inertial profilers equipped with laser sensors that record actual elevation measurements along the pavement.

Smith and Ram (2016) mentioned that the use of lightweight inertial profilers on concrete pavements has become increasingly common over the past two decades to guarantee sufficient strength for opening to regular traffic operations. Data collection using lightweight inertial profilers typically requires lane closures, and a short lead-in distance is also needed to achieve appropriate test speeds at the testing zones. Still, a high-speed profiler has high accuracy and repeatability under highway speeds and does not require lane closures.

Můčka (2017) published a paper summarizing the currently most-used equipment for rating pavement smoothness using IRI:

- **Inertial profilers.** The inertial profiler is currently one of the most complex roadway profiler systems. It provides a relatively accurate and repeatable simulation of a pavement profile, then analyzes the profile to generate various roughness statistics. This type of equipment includes high-speed inertial profilers and lightweight inertial profilers.
- **Inclinometer-based devices.** This type of instrument measures the surface profile as the instrument moves along the test surface. Such instruments are commonly used for shorter lengths of ground data collection, such as for airport runways. This type of equipment includes walking profilers and dipsticks.

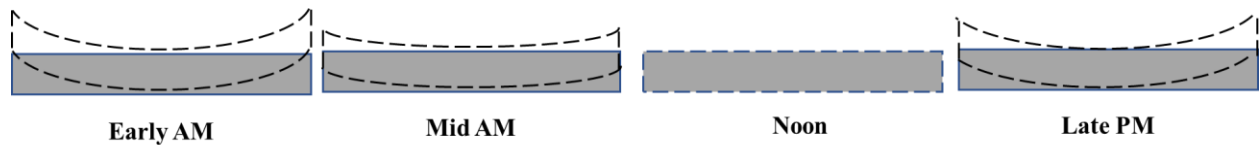
2.1. Factors that Influence Curling and Warping

2.1.1. Seasonal and Diurnal Effects

The curling effect of temperature reversals on slab deflection is often diurnal, whereas the warping effect of moisture on slab deflection is usually seasonal, and diurnal variation (curling) is typically larger than seasonal variation (warping) (Chang et al. 2008). Nantung (2011) pointed

out that diurnal ambient temperature fluctuations only affect the top half of a PCC slab's temperature profile, while seasonal ambient temperature variations can affect the entire depth of a PCC slab's temperature profile. The temperature differential due to diurnal effects between the mid-depth and bottom of a slab is nonexistent. Severe temperature fluctuations in a concrete slab, particularly noticeable during winter, late spring, or early summer, determine the maximum and minimum strains in a concrete pavement.

Temperature and moisture gradients arise in a concrete slab because of daily and seasonal fluctuations in both temperature and moisture conditions (Asbahan 2009). Tayabji et al. (2010) tested concrete slabs at experimental sites during different times of the day and noticed that, at any given time, the slabs might be curled differently in terms of curvature level or even orientation, as illustrated in Figure 1. In conclusion, the seasonal variation of slab curvatures was generally equal to or smaller than the diurnal variation. Seasonal slab curvature trends may also differ with diurnal analysis periods; this must be addressed site by site because it has been shown that diurnal and seasonal impacts can vary dramatically among locations.



Tayabji et al. 2010

Figure 1. Diurnal slab curvature

Merritt et al. (2015) evaluated a report on the effects of concrete pavement curling and warping on ride quality. In a project on US 34 near Greeley, Colorado, slab IRI caused by curling and warping can result in IRI values of up to 40 in./mile. To examine the impact of extreme seasonal conditions, the researchers collected eastbound and westbound profile data during two winter and summer seasons. Four measurements were collected each day during the four visits. The authors found that the roughness of the August profile data was higher than that for February and that August exhibited more significant diurnal variation in roughness than February.

Johnson et al. (2010) looked at slab curling resulting from daily and seasonal temperature changes and found that the change in IRI due to daily temperature changes in South Carolina was projected to be less than 10 in./mile based on the data acquired in this study effort. The change in IRI due to seasonal fluctuations in pavement curvature was predicted to be less than 5 in./mile. These differences are minor, especially when compared to the variability in single-point laser profiler observations caused by the diamond-ground concrete pavement's surface texture. The authors concluded that the difference in roughness measurements caused by pavement curvature was insignificant for network data collection.

Temperature and moisture gradients can fluctuate across seasons and even between measurement times within a day. Yu and Khazanovich (2001) tested a section six months a year and monitored temperature gradients every two hours. The authors mentioned that multi-axle loads during nighttime temperatures become more critical if the built-in curling magnitude is large enough,

and slabs can split from the top down rather than from the bottom up. Built-in curling during concrete setting and diurnal curling during the concrete pavement’s service life are integrated as performance parameters in the American Association of State Highway and Transportation Officials (AASHTO) Mechanistic-Empirical Pavement Design Guide (MEPDG)/AASHTOWare Pavement Mechanistic-Empirical Pavement Design (PMED) software model for curling.

Masad et al. (1996) claimed that the influence of nonlinear temperature distribution is greatest at night and early in the morning (2:00 a.m., 6:00 a.m., and 11:00 p.m.). Compared to concrete’s high compressive strength, the maximum compressive stress resulting from temperature distribution nonlinearity is insignificant. Ceylan et al. (2005) indicated that the pavement temperature differential is typically positive throughout the daytime and nighttime and negative late at night and early in the morning.

2.1.2. Temperature and Moisture Gradients

The two most critical environmental factors affecting geometric changes in PCC are temperature and humidity. In the 1940s, Thomlinson (1940) calculated the curling stresses in PCC under the premise of a nonlinear temperature distribution in the slab. Curling refers to the deformation caused by a nonuniform temperature gradient, while warping refers to the deformation caused by a nonuniform moisture gradient. When the temperature or moisture content at the top of a PCC slab is higher than at the bottom, a positive gradient is created and the top section expands more than the bottom, resulting in downward slab curling or warping. In contrast, if the temperature or moisture content at the bottom of a PCC slab is higher than at the top, a negative gradient occurs and the bottom half of the slab expands more than the top, resulting in upward curling or warping of the slab.

The definitions of curled-up and curled-down slab behaviors are illustrated in Figure 2. The slab deformation caused by temperature gradient is called curling deformation, while the slab deformation caused by moisture gradient is called warping deformation. However, since moisture deformation can be transformed into temperature deformation, the term “curling” is used in the definition of curling direction. Depending on the directional properties of the temperature and moisture changes, there can be either an upward curling (curl up) or downward curling (curl down).

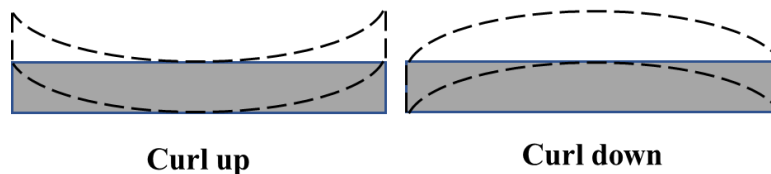


Figure 2. Schematic of curling in PCC pavements

It has been observed that the curled-down condition (daytime) is more harmful than the curled-up condition (nighttime). Curling during the day may be more critical when fatigue consumption is considered because of the presence of maximum tension (the bottom of the plate under a load)

and the higher amount of traffic loading applied (Ioannides and Salsilli-Murua 1989). Because of initial deformation, the slab is always curled up to some degree (Lee et al. 2017).

Nassiri (2011) and Choi and Won (2009) indicated that curling is downward when the slab is warmer at the top than at the bottom. When a positive temperature gradient exists in the slab (the temperature at the top of the slab is higher than that at the bottom), the top area expands more than the bottom, so the slab curls down.

Wang et al. (2009) proposed a method for predicting the temperature profile in a multilayered pavement. They proposed a new approach to solve the axisymmetric temperature field of a multi-layer pavement system in which a multi-layer pavement system is modeled as a two-dimensional (2D) heat transfer problem. The derived analytical solution calculates the temperature at any position and time t in the N -layer pavement system. Temperatures in a continuously reinforced concrete pavement (CRCP) test section were continuously predicted for 71.5 hours at half-hour intervals under both winter and summer conditions.

Based on the measured road surface temperature data from falling weight deflectometer (FWD) testing, Wang (2016) proposed an infinite-series solution for predicting the change in road surface temperature with time. The primary purpose of the study was to systematically offer a new analytical solution for predicting the temperature distribution of the pavement surface over time during FWD testing and to validate the model based on Long-Term Pavement Performance (LTPP) Program FWD temperature data. The developed MATLAB algorithm used in situ pavement surface and subsurface temperatures extracted from the LTPP FWD temperature database to verify the model.

A simple empirical model for predicting the temperature gradient in JPCP was proposed by Zhao et al. (2020). In their study, pavement temperatures were measured by temperature sensors installed at one corner and the center of a slab. At each location, nine sensors were installed at different pavement depths. Weather data were gathered from a nearby weather station. No significant difference was found between the measured temperatures at the center and corner of the concrete slab, indicating that measurement location had little effect on temperature monitoring results.

Qin et al. (2019) considered the influence of thermal conductivity, heat capacity, density, surface emissivity, and albedo on road surface temperature fluctuations and built a theoretical model for the maximum, minimum, and amplitude of the surface temperature. The authors chose the weather data from a summer day with stable solar radiation and wind speed and found that thermal conductivity, heat capacity, and density similarly affect the pavement surface temperature. Increasing the thermal conductivity, heat capacity, density, or a combination of the three linearly reduced the maximum road surface temperature while raising the minimum.

Moisture gradients, similar to temperature gradients, form in a slab when the concrete moisture levels at the top of the slab differ from those at the bottom, and the distribution of moisture within concrete slabs and the resulting warping strains have been extensively studied. In situ tests have revealed that the moisture gradient varies dramatically up to a depth of about 2 in.,

with the deeper areas of the pavement slab remaining at about 80% saturation or higher (Philip and De Vries 1957). When the moisture at the top of a slab is higher than at the bottom, a positive moisture gradient occurs, leading to downward curvature. In contrast, a negative gradient occurs when the moisture content at the bottom of the slab is higher than at the top, causing upward slab curvature (Asbahan 2009, Harr 1958, Ceylan et al. 2016a). Moisture distribution is often nonlinear through the depth of the concrete, with the top 2 in. of the slab varying the most (Yu and Khazanovich 2001).

Lee et al. (2011) demonstrated that moisture-related curling of concrete slabs is not a simple occurrence, since concrete's material characteristics and behaviors are time-dependent and the geometric boundary between the slab and the base changes as curling progresses.

Asbahan and Vandebossche (2011) found that temperature gradients cause concrete slabs to curl upward and downward daily and seasonally, but moisture gradients lead slabs to curl upward. Mateos et al. (2020) mentioned that because of the low water-to-cementitious materials (w/cm) ratio of concrete mixtures, the majority of the shrinkage that concrete experiences is due to self-desiccation (autogenous shrinkage). Self-desiccation occurs because capillary pore water is consumed during cement hydration to allow chemical reactions to progress, which reduces capillary pore humidity (Wei and Hansen 2011). Lowering the paste content and raising the aggregate content can reduce the shrinkage resulting from this process. The paste hardens and becomes stronger during hydration, becoming concrete, and too much cement paste can cause the concrete to crack quickly, increasing curling and warping behavior (Hajibabae and Ley 2016).

When the slab's top surface is exposed to external drying, differential drying is thought to be the source of moisture warping. Still, if poor drainage and saturated soil conditions prevail, experience has shown that significant uplift due to moisture warping develops in slabs on grade. As a result, two further moisture transport processes may be implicated in establishing a considerable moisture gradient throughout the depth of a slab, causing additional slab warping and differential drying from the slab's top surface. The first process is self-desiccation, linked to cement hydration, and the second is water absorption at the slab's base (Qin 2011).

Asbahan (2009) summarized that pavement drying shrinkage, pavement drainage characteristics, and meteorological factors such as relative humidity, rainfall, and snow can all affect moisture gradients. However, temperature gradients have received more attention in the literature than moisture gradients, partly because even today temperature gradients are more straightforward to quantify due to the lack of commercial humidity sensors for long-term studies on concrete pavements (Yang 2014).

2.1.3. Pavement Structure

Slab curvature is influenced by several parameters related to the concrete pavement structure, including temperature and moisture conditions at the time of placement, concrete material properties, slab geometry, and slab deformation restrictions. Dowel bars, slab self-weight, and friction at the interface between the slab's base and the subbase could all influence the

deformation of the slab (Olidis and Hein 2004). As mentioned in Suprenant (2002), while curling is caused by moisture gradients, many factors affect the degree of curling, such as drying shrinkage, modulus of subgrade reaction, reinforcement ratio, slab thickness, joint spacing, and so on.

Some studies have shown that using thin slabs and long joint spacing tends to increase pavement curling (Siddique and Hossain 2005, Rao and Roesler 2005, Masad et al. 1996). In Iowa, most roadway pavement designs feature a 20 ft joint spacing rather than a 15 ft joint spacing. However, some county roads were built during the previous century using shorter (12 ft) or much longer (40 ft) joint spacings. Ytterberg (1987) observed that upward curling increases when slab length is increased from 15 to 20 ft.

The 1993 *AASHTO Guide for Design of Pavement Structures* (AASHTO 1993) suggested that using skewed joints with or without dowel bars can improve the performance of plain and reinforced concrete pavements. The use of a skewed joint could reduce the deflection and stress at the joint, thereby increasing the slab's load-bearing capacity and prolonging the road surface's service life, and could also reduce the impact response when a vehicle passes over the joint. However, Rasmussen et al. (2007) demonstrated that a typical 5% increase in stress due to the presence of a skewed joint could be expected due to curling and warping restraint. Skewed joints appear to be an essential factor in the observed distresses that can lead to increased stresses and deflections at the active plate corners, leading to delamination and corner cracking. Also, the slab size is effectively increased when skewed joints are used, raising the possibility of mid-panel cracking. Rasmussen et al. (2007) recommended that skewed joints be abandoned.

Bischoff (1996) compared the performance of skewed joints with and without dowel bars in non-reinforced concrete pavement. The author found that the dowelled joints performed better than the non-dowelled joints, with the dowelled joints estimated to last 2.5 times longer than the non-dowelled joints before any maintenance or rehabilitation was required.

By splitting the LTPP sections into three groups based on time versus IRI performance, Khazanovich et al. (1998) examined roughness patterns in JPCP, CRCP, and jointed reinforced concrete pavements (JRCP). The three groups included categories for poor, normal, and good performance. The authors discovered that pavements with a larger percentage of steel reinforcement were smoother and that pavements built on coarse-grained subgrades fared better than those built on fine-grained subgrades in general. The pavements built on fine-grained subgrades accounted for 63% of all poorly performing sections while the pavements built on coarse-grained subgrades accounted for 37% of the sections in that category. The researchers investigated the effects of joint spacing, slab thickness, and base type and found a correlation between higher IRI values and increased JRCP slab thickness but no correlation between joint spacing and IRI performance. According to the findings, the base type (granular versus stabilized) had little effect on the performance of pavement segments categorized as poor and normal. However, granular rather than stabilized bases were used in 82% of the sections exhibiting high performance in terms of IRI.

Yu et al. (1998) summarized that because both the length and width of a slab affect the curling stresses at the slab corners, the corner load stress in widened slab sections may be much higher if loads are applied directly at the slab corners. In summary, widened slabs should be controlled to be equal to or less than 14 ft wide to avoid built-in upward curling (Yang et al. 2020a, Yang et al. 2020b).

Perera et al. (1998) discovered significant differences in the rate of increase in IRI values between dowelled and non-dowelled JPCPs. When compared to dowelled pavements, non-dowelled pavements exhibited higher rates of roughness growth. Byrum (2001) also observed that dowel bars at joints might help to minimize the upward curvature that is locked in. Thermal gradients present during the transformation of PCC from a fluid to a solid are thought to be connected to construction-related locked-in curvatures.

2.1.4. Concrete Mix Design

Pavements can have a high level of smoothness just after they are built, but that smoothness can quickly deteriorate due to changes in slab form caused by curling and warping. Another difficulty with achieving high initial smoothness occurs when paving contractors use construction practices or make adjustments to the PCC mix design that result in high initial smoothness but are damaging to a pavement's long-term performance (Perera et al. 2005). In 2004, ACI Committee 302 (2016) found that "curling is related to the concrete mixture paste content and is not a result of the vapor retarder." In Phase I of the present research, Ceylan et al. (2016a) concluded that PCC slabs may exhibit less warping if the concrete mix contains more coarse particles and less paste. A moderate w/cm ratio is also preferred because a larger w/cm ratio can result in more drying shrinkage while a lower w/cm ratio can result in more significant autogenous shrinkage.

The thermal qualities of concrete or aggregates, such as coefficient of thermal expansion (CTE), thermal conductivity, and heat capacity, have garnered attention as critical material properties for limiting the curling of PCC pavements. These qualities have been identified as essential elements in mechanics-based thickness design systems such as the MEPDG/PMED program for estimating PCC pavement performance (Chung 2012). The elastic modulus of concrete, or the ratio of stress to strain, has also been identified as an important factor in curling and warping. Because elastic modulus is related to concrete's creep and stress relaxation behavior, concrete with a greater elastic modulus value may exhibit more curling. According to Rao and Roesler (2005), curling and warping are also affected by the CTE of concrete. When exposed to similar temperature gradients, PCC pavements with higher CTE values experience larger volume shifts, resulting in greater curling deformation. Thermal conductivity, which indicates a material's capacity to conduct heat, also affects curling and warping. As most recently summarized by Asadi et al. (2018), humidity, temperature, type of aggregate, use of phase change materials, type of cementitious material, and density can all affect the thermal conductivity of concrete. It has been observed that concrete pavements with a higher modulus of elasticity, a higher coefficient of thermal expansion, and a lower thermal conductivity exhibit higher curling stress (Kim et al. 2021).

2.1.5. Construction Period

A positive temperature differential between a concrete slab's top and bottom surfaces during the day leads slab corners to curl downwards, while a negative temperature differential during the night causes slab corners to curl upwards. Additionally, the irreversible drying shrinkage fraction that gradually increases as the concrete matures and eventually reaches a plateau causes permanent warping (Nassiri 2011). This is commonly referred to as upward built-in curling. The permanent curling and warping and other pavement deformation behaviors are influenced to some extent by the pavement's construction age. The pavement will experience different curvature changes over time, and this change is more steady at a later age than at a younger age.

Rao et al. (2001) observed that installing pavement late in the day or late at night during cloudy weather tends to prevent significant built-in curling. As the concrete ages, it can be observed that the slab experiences upward curvature (Nassiri 2011).

2.2. Indicators of Curling and Warping

2.2.1. Pseudo Strain Gradient

Chang et al. (2008) devised a practical method, i.e., the Second-Generation Curvature Index (2GCI), to help address some of the disadvantages of existing curvature indices in terms of accuracy, stability, and portability. According to Chang et al. (2008), pseudo strain gradient (PSG) is the gross strain gradient required to deform a slab from a flat baseline into the shape seen in the measured slab profile. The PSG value for a slab is calculated using the Westergaard (1926) equation to fit a curve between the measured profile and an expected curled slab form. Estimates of mechanical pavement parameters are required by the Westergaard (1926) equation (summarized by the radius of relative stiffness, l). The 2GCI surpasses other curvature indices because it can be linked to the physical qualities of JPCP that are sensitive to curling and warping in the field (geometry, elastic modulus, Poisson's ratio, and subgrade support). PSG can thus always be used to summarize the level of curling and warping (Lee et al. 2020).

Karamihas and Senn (2012) assessed the use of the PSG as an indicator of curling and warping behavior. To see whether there were any links between PSG and curling and warping behavior, the PSG and variations in PSG over time were compared to changes in roughness. Using the relationship between IRI and PSG, the authors were able to demonstrate the possibility of isolating the effects of concrete pavement curling and warping from other sources of roughness (faulting, cracking, etc.). According to the study, long-term increases in IRI may be produced by changes (i.e., progression) in curling and warping over time.

Karamihas and Senn (2012) calculated the PSG values for a series of slabs using objective algorithms to estimate the gross strain gradient required to deform each slab into the shape seen in the measured profile. The average absolute PSG value for each tested slab was used to summarize the levels of curling and warping within each test section. The level of curling and warping in each slab was measured using PSG. The average PSG value of each slab was used to

quantify the overall curling and warping observed over the entire segment for the sake of monitoring trends over time.

2.2.2. Curvature IRI

The rideability or the relative discomfort induced by a vehicle traveling over a section of concrete pavement can be affected by curling and warping (Johnson et al. 2010).

Measuring longitudinal profile is a common pavement management activity for documenting pavement surface roughness. Longitudinal road profile data are typically summarized by an index such as IRI that compresses thousands of elevation readings into a single value. While IRI is the most often used index, the information quality is only as good as the profile measurement, no matter what index is generated from the longitudinal profile (Karamihas 1999). In 1982, the World Bank performed an IRI study in Brazil to produce a standard that could be used to quantify smoothness. IRI is based on a mathematical simulation of the response of a tire on a vehicle traveling at a speed of 50 mph. This is referred to as a quarter-vehicle or quarter-car model. Normalized parameter values for sprung mass, unsprung mass, suspension spring stiffness, and linear suspension damping are used to depict this quarter-vehicle model (Figure 3).

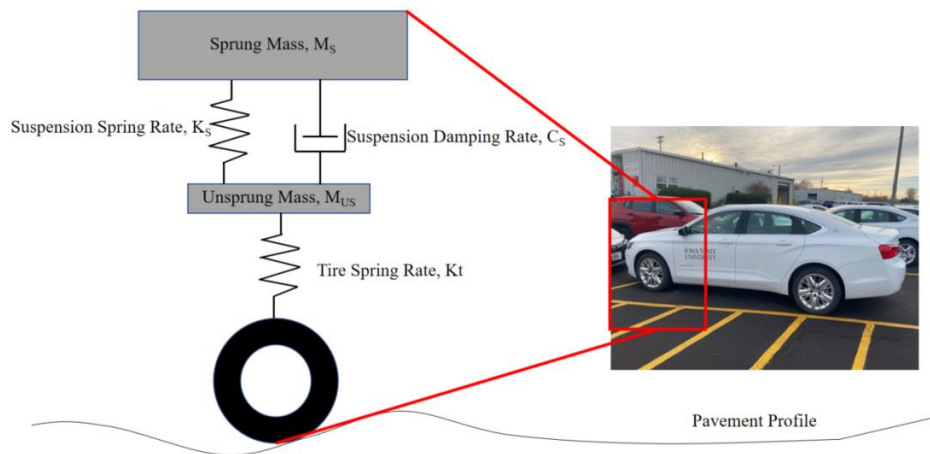


Figure 3. Quarter-car model

Mackiewicz et al. (2018) studied the influence of pavement structure, foundation type, temperature, and service time on the roughness and texture of selected concrete pavements. The results showed that the texture index depends considerably on the pavement service time. Temperature slightly influences transverse roughness values but does not affect the registered IRI values.

Pradena and Houben (2018) compared the stability of ride quality produced by traditional and short-slab JPCPs. The authors measured IRI using a walking profiler. For non-dowelled traditional JPCPs, Δ IRI values up to 38 in./mile were obtained. The results indicated that the IRI values produced by the short-slab JPCPs were essentially the same regardless of the time of day. Thus, the IRI values measured at different times of day all indicate the representative IRI value

of the short-slab JPCP surface. This stability provided by the short-slab JPCPs may have been caused by the shorter slab lengths and limited effective aggregate interlock at the joints, the latter of which changes the slab curvature due to smaller crack widths under the joints.

Perera et al. (1998) found that higher IRI values for JRCPs were linked to higher amounts of precipitation, higher subgrade moisture contents, thicker slabs, longer joint spacings, lower w/cm ratios, and higher PCC modulus values. Byrum (2001) found that IRI appeared to primarily reflect the faulting features of LTPP pavement sections, followed by slab curvature and settlement-like effects. Differential settlement and slab form appeared to affect IRI by as much as 140 in./mile in LTPP pavements. A study by Lee et al. (2020) proposed a new method for distinguishing curvature-related IRI (i.e., due to curling and warping) from non-curvature-related IRI (i.e., due to other distresses such as spalling, faulting, etc.).

2.2.3. Deflection and Deflection Ratio

Bending or distortion of slabs over time due to shrinkage and temperature effects is known as long-term deflection. The state of cracking and concrete creep can have an impact on this parameter. Every type of pavement deflection testing equipment works in the same way: a known load is applied to the pavement, and the highest surface deflection, or a series of surface deflections at fixed distances from the load, is measured in a deflection basin.

The FWD is the most widely used deflection testing equipment at the moment. FWD testing is a distinct stop-and-go activity, and its discrete testing sites are supposed to reflect a certain length of the pavement under consideration. Stop-and-go operations take longer than continuous operations, increase operational costs, and disrupt traffic, all of which contribute to an unhealthy working environment (Arora et al. 2007).

Built-in curling cannot be evaluated based only on the pavement surface profile; it must be analyzed in conjunction with pavement reaction data such as deflections (Yu and Khazanovich 2001). According to Yang (2019), PCC can expand and/or contract at different rates at different PCC slab depths, causing curvature in the slab due to unique repeated-deflection behavior resulting from temperature and moisture fluctuations through the depth of the pavement. The most considerable deflection on a PCC slab's surface is commonly seen along the diagonal line between two opposite corners. To measure such diagonal profiles in the field, traditional inclinometers and walking profilers require lane closures, while inertial profilers typically record longitudinal profiles along the pavement's wheel paths. Also, due to differences in constraints along the slab, the deflection of a PCC slab in the field is frequently asymmetric. McCracken (2008) observed that the influence of temperature gradient on pavement deflection is greater than that of moisture gradient.

2.2.4. Degree of Curvature

Dealing with curvature is essential in structural analysis and applied mechanics, mainly when evaluating soil-structure interaction issues such as slab curling and warping. Each structurally

continuous slab in a jointed concrete pavement system has an elevation function, $z = f(x)$, along any line across the slab (Byrum 2009).

To improve safety in inclement weather and low-light situations, permanent raised pavement markings (PRPMs) are frequently employed to increase the markings' visibility and advise drivers on upcoming maneuvers. Byrum (2005) discovered that the degree of curvature of a pavement had a strong relationship with the safety benefits of PRPMs. As the degree of curvature of a pavement rises (i.e., as the radius of curvature increases) on two-lane highways, the safety value of PRPMs decreases. Contrary to widespread assumption, PRPMs are more effective at night on roads with a gentler curvature (a degree of curvature of 3.5 or a radius of 0.3 miles). PRPMs are ineffective on roads with low annual average daily traffic (AADT) values (less than 5,000) and sharper curvature (a degree of curvature of more than 3.5 degrees or a radius of less than 0.3 miles).

Yang et al. (2022) used a key criterion for determining the degree of curling and warping from the degree of curvature. Morning and afternoon measurements were performed in this investigation, and the degree of curling and warping was expressed as a degree of curvature (Byrum 2009) to account for the rate of slope change along the slab length. In this approach, each structurally continuous slab has an elevation function, $z = f(x)$, along any line across the slab that can be calculated as shown in equation (1).

$$k = \frac{\frac{d^2z}{dx^2}}{\left[1 + \left(\frac{dz}{dx}\right)^2\right]^{3/2}} \quad (1)$$

When the slope is small, or when the slope changes, the simplified small strain estimate for curvature shown in equation (2) can be used:

$$k \approx \frac{d^2z}{dx^2} = z'' \quad (2)$$

2.3. Summary

Curling and warping are two distinct bending phenomena linked with temperature and moisture differentials in PCC slabs. Slab restrictions cause tensile strains that can be amplified several times over when paired with traffic loading. Many studies have evaluated the curling and warping of concrete pavements. The curling and warping of concrete slabs can be assessed using various measurement devices, analysis methodologies, and indicators. According to the literature review findings presented in this chapter, many factors influence PCC curling and warping. Temperature and moisture gradients, slab geometry design, concrete mix composition, construction time and season, and seasonal and diurnal effects are only a few examples.

Many factors should be considered in order to provide durable PCC pavements in Iowa by decreasing curling and warping. Table 1 outlines methodologies drawn from a comprehensive

literature review for minimizing PCC curling and warping. While it is commonly documented that reduced initial roughness decreases roughness development over time and extends pavement life, comprehensive testing has not revealed the parameters with the most significant impact on curling and warping behavior.

Table 1. Summary of literature review

Factor	Literature Review	Reasons	Reference
Slab Thickness	A thicker slab can result in lower curling and warping.	Structural integrity and strength entirely depend on concrete pavement thickness. The thicker the concrete slab is, the stronger it is and less likely it is to bend, resulting in less curling and warping.	Wei et al. (2017)
Transverse Joint Spacing	A shorter slab length can result in lower curling and warping.	Joint spacing for unreinforced concrete pavements depends on slab thickness, the concrete aggregates used, subgrade/subbase support, and environmental conditions. Transverse joints are provided to control cracking. Reducing joint spacing can increase resistance to bending stresses.	Roesler et al. (2012)
Slab Width	A wider slab can result in higher curling and warping.	Reducing slab width can increase resistance to bending stresses.	Yu et al. (1998)
Total Cementitious Content	Curling is related to the concrete mixture's paste content.	Shrinkage can be decreased by reducing the paste content and increasing the aggregate content of a mix.	Hajibabae and Ley (2016)
w/cm	Increasing or decreasing w/cm ratio from an optimal range can lead to higher curling and warping.	A higher w/cm ratio can lead to higher drying shrinkage, while a lower w/cm ratio can lead to higher autogenous shrinkage, which results in greater warping.	Mateos et al. (2020)
Joint Type	Skewed joints are not recommended for widened JPCPs.	Skewed joints caused performance problems, in that slabs are prone to cracking at locations where a skewed joint makes an acute angle with the pavement edge or longitudinal joint. Skewed joints can lead to higher curling stresses at the slab corners.	Rasmussen et al. (2007)
Shoulder Type	Slabs with tied concrete shoulders experience less curling and warping than slabs with granular or hot-mix asphalt (HMA) shoulders.	Tied concrete shoulders reduce pavement stresses from curling and edge deflections.	Yang et al. (2018)
Construction Season	Paving in the late fall and in the evening can minimize curling.	Paving during hot weather can lead to a large temperature gradient in a flat slab when the slab hardens. During fall paving, less built-in curling occurs when the concrete is fresh and temperatures are not as hot during the day and the pavement is less prone to evaporation.	Kasu et al. (2021)
Dowel Bar Diameter	Dowel bars can restrain vertical curling deflection at joints but can also increase curling and warping stresses by restraining vertical deflection.	Dowel bars are short steel bars that provide a mechanical connection between slabs without restricting horizontal joint movement. They reduce the probability of temperature changes and moisture changes that cause curling of the slab edges. Larger diameter dowel bars increase load transfer efficiency and decrease curling.	Ceylan et al. (2016a)

3. METHODOLOGY

3.1. Equipment Used for Data Collection

Profilers such as inclinometers, walking profilers, and inertial profilers can measure the pavement profile along defined paths in two dimensions (Ceylan et al. 2016b). To collect profile data for this study, an SSI high-speed profiler (SSI Inertial Profiling System CS9300) was installed on a truck. A standard method for assessing large-scale highway pavements is to use this type of high-speed inertial profiler (Byrum 2001). As shown in Figure 4, three laser sensor units were installed at the front of the truck to measure the left, central, and right tracks of a roadway surface. This instrument has a profile data resolution of 1 in. longitudinally and 0.01 in. for elevation. It measures humidity and surface temperature along with profile data and integrates an IRI calculation algorithm to provide results in terms of IRI. The operation manual for the high-speed profiler used in this study is provided in Appendix A.1.



Figure 4. SSI high-speed profiler

The operational speed range of the high-speed profiler is 5 to 70 mph, and the optimal data collection speed is between 20 and 55 mph. Since the sampling interval is 1 in., IRI results are usually given in units of inches per mile. The height measurement resolution is 0.01 in., and the operating temperature range is 32°F to 110°F. The IRI is a universal ride quality index for concrete and asphalt roads worldwide. The profile is analyzed using a quarter-car simulation weighted toward body and vehicle bounce frequencies and the most uncomfortable riding conditions. Because high-speed profiler devices rely on accelerometers, the data will be inaccurate if the vehicle is driven at less than 10 mph (Sayers and Karamihas 1998). The accelerometer should be calibrated for each field trip before arriving at the site. When collecting data, the driving speed should rigorously match the speed limit for the type of road, with highways measured at 60 mph, county roads at 50 mph, and city streets at 25 mph.

3.2. Algorithm Development and Optimization

The SSI profiler output at each site included three tracks corresponding to the left, middle, and right scanners attached to the front of the truck, as shown in Figure 4. During scanning, scans were processed using the SSI profiler software, and the real-time profile was shown in the Toughbook connected to the profiler. Figure 5 shows a sample profile collected at one of the testing sites. As shown in this figure, the three tracks exhibit very similar trends, with the different heights caused by the different reference heights of the three tracks.

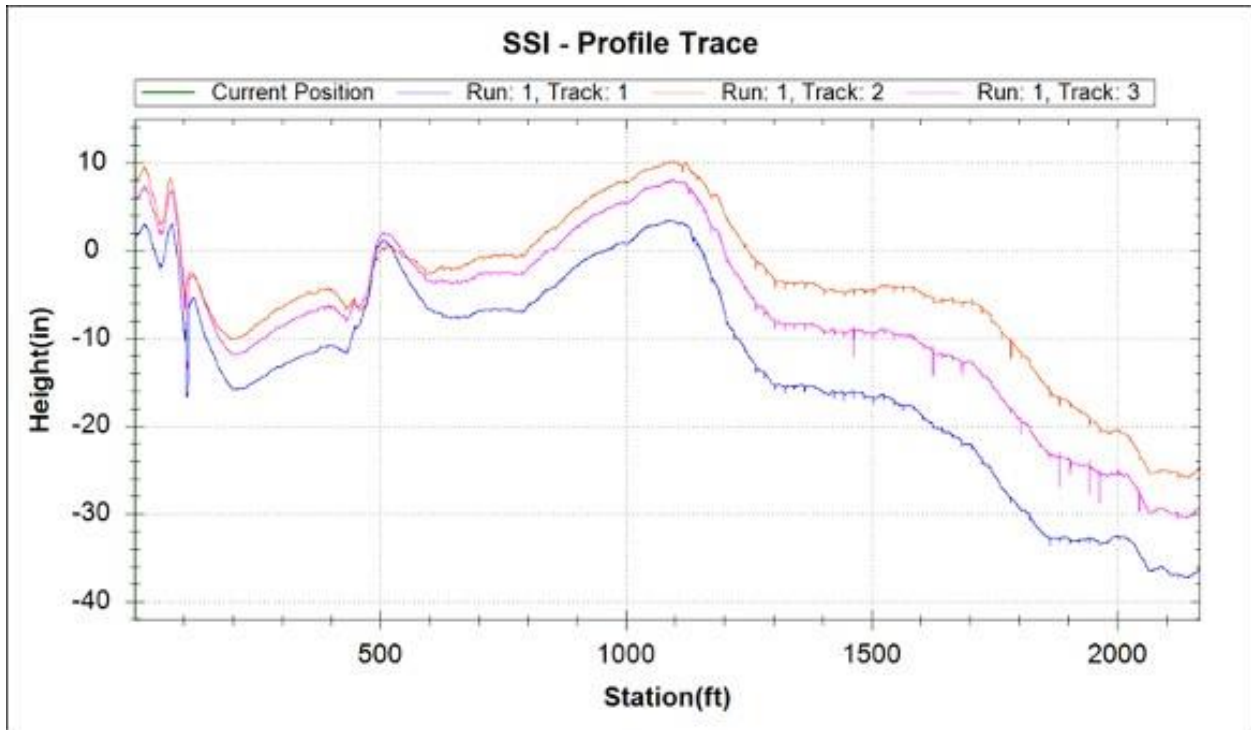


Figure 5. Example profile trace from the SSI profiler

To analyze the data from the raw profile, the data gathered by the SSI profiler were converted to a ProVAL profile, after which the processed data were exported for further analysis using MATLAB-based algorithms to quantify the degree of curling and warping. The detailed analysis procedure is shown in Figure 6.

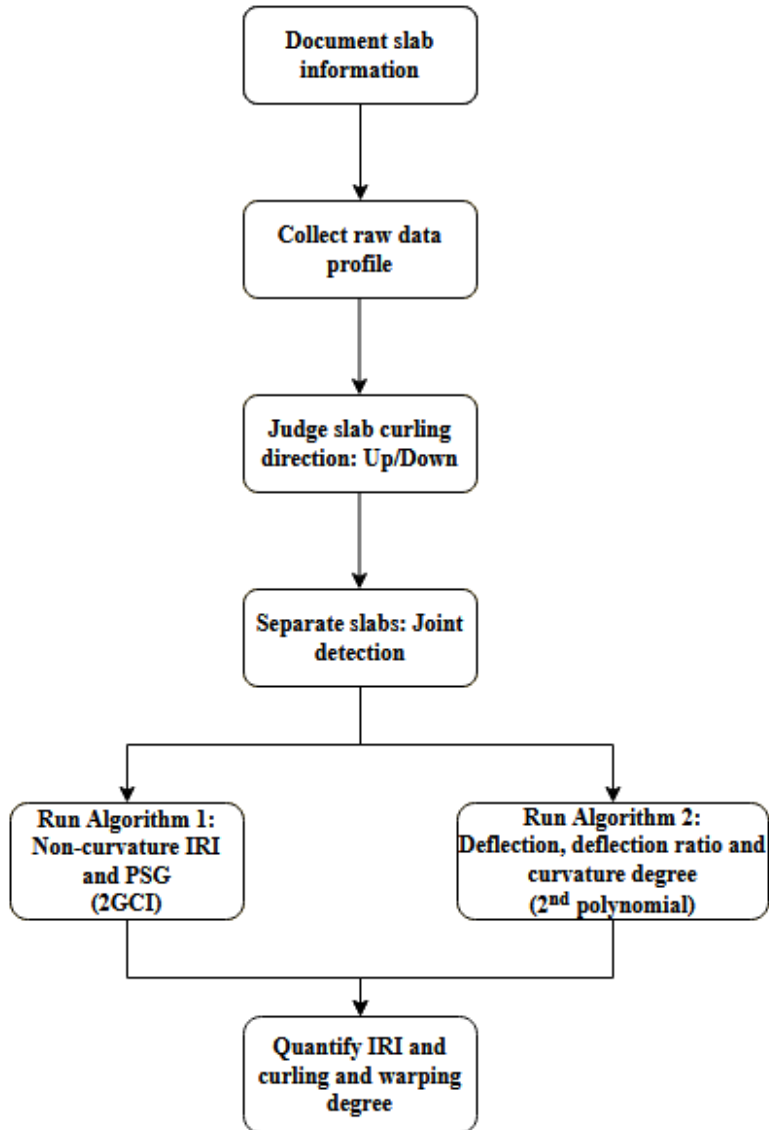
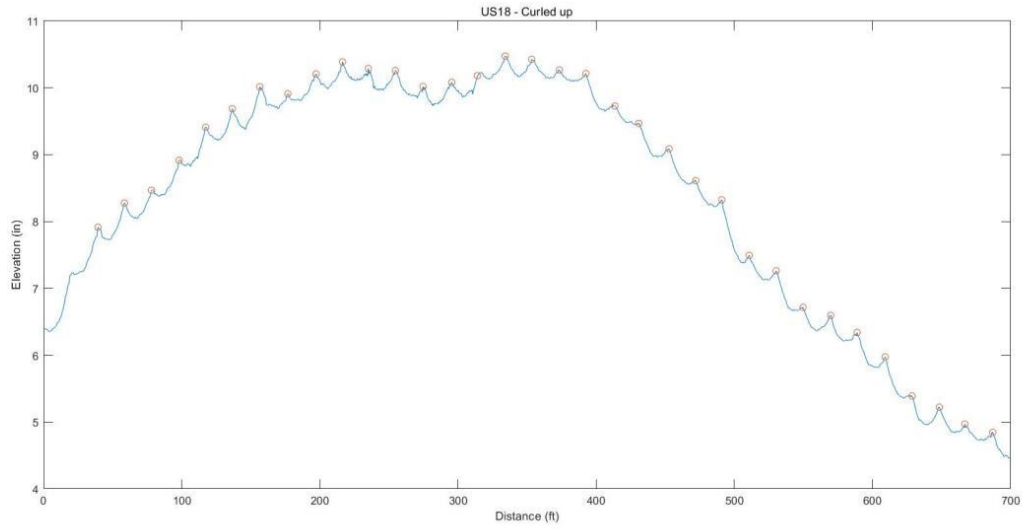
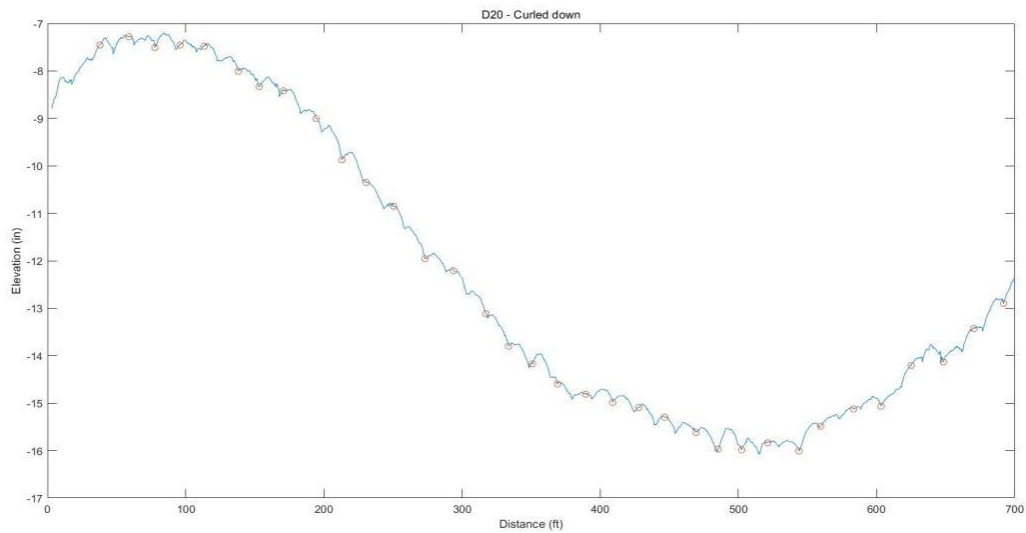


Figure 6. Data processing procedure

There are two basic curling directions for PCC slabs: curled up and curled down. Example profiles for each curling direction are shown in Figure 7(a) and 7(b), respectively. Field validation data were collected in the parking lot of Reiman Gardens in Ames, Iowa. Three slabs with 9 ft lengths were selected, and a high-speed profiler, walking profiler, and the Iowa State University (ISU) portable curling and warping measuring device were used.



(a)



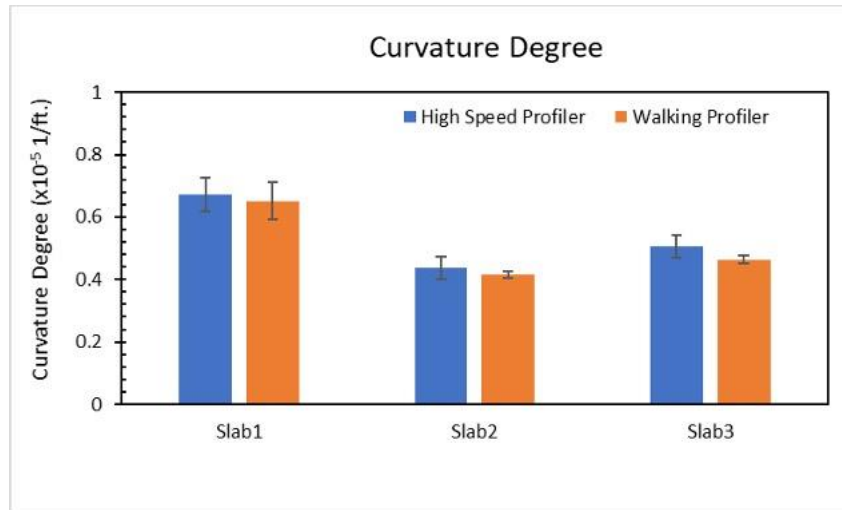
(b)

Figure 7. Example site profiles: (a) curled-up site profile (US 18 in Sioux County, Iowa, measured on Aug. 11, 2020) and (b) curled-down site profile (D20 in Hamilton County, Iowa, measured on July 22, 2020)

After four repeated runs for the three devices, similar degrees of curling and warping (degrees of deflection and curvature) were obtained, as shown in Figure 8.



(a)



(b)

Figure 8. Algorithm validation: (a) deflection and (b) degree of curvature

3.2.1. Joint Detection

In profile data analysis, deciding where to locate the joints in the profile is a complex process. Karamihas and Senn (2012) summarized a straightforward method for locating pavement joints. In brief, this is accomplished by locating negative spikes with a value less than a threshold, i.e., by identifying the joints in a pavement profile as those places where negative spikes repeatedly appear in the same exact locations. To begin the scanning procedure for a single site, the transverse joint spacing for the specific site was first obtained, then scanning was begun at a joint. Due to local building constraints, the joint spacing for some county roads and city streets was sometimes larger or smaller than the stipulated joint spacing. In such cases, the algorithm searched for peaks in the second derivative within a 2 to 3 in. window to locate joints, after which the joint locations were marked and plotted (Figure 9). This step helped increase analysis accuracy by reducing a potential error source in the curve-fitting process for each slab.

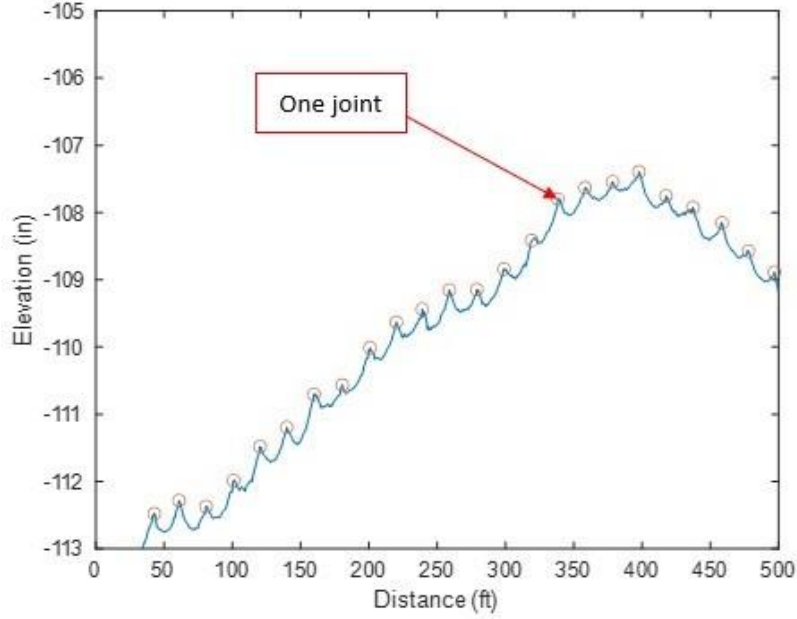


Figure 9. Joint detection

3.2.2. 2GCI Fit Model

3.2.2.1. Curvature and Non-curvature Profiles

For PCC pavements, curling caused by temperature and warping caused by moisture are two well-known phenomena that have a major impact on ride quality. Recognizing this effect on pavement roughness, Karamihas et al. (2008) developed a curve-fitting approach for observed slab profiles based on an idealized Westergaard (1926) shape. As illustrated in equations (3) through (6), which include both moisture gradient ($\Delta\varepsilon_{sh}$) and temperature gradient (ΔT), the idealized profile connects slab elevation (z) to a position along the slab.

$$z = -z_0 \frac{2 \cos \lambda \cosh \lambda}{\sin 2\lambda - \sinh 2\lambda} \left[(-\tan \lambda + \tanh \lambda) \cos \frac{x}{l\sqrt{2}} \cosh \frac{x}{l\sqrt{2}} + (\tan \lambda + \tanh \lambda) \sin \frac{x}{l\sqrt{2}} \sinh \frac{x}{l\sqrt{2}} \right] \quad (3)$$

$$z_0 = \frac{-(1+\mu)(\alpha\Delta T + \Delta\varepsilon_{sh})}{h} l^2 \quad (4)$$

$$\lambda = \frac{b}{l\sqrt{8}} \quad (5)$$

$$l = \sqrt[4]{\frac{Eh^3}{12(1-\mu^2)k}} \quad (6)$$

where

x = horizontal coordinate along the slab profile, referenced to the slab center (L)

z_0 = uplift at the slab ends (L)

l = radius of relative stiffness (L)

b = slab width (used here as slab length)

E = slab elastic modulus (F/L²)

μ = Poisson's ratio (–)

k = the modulus of subgrade support (F/L²/L)

The PSG is given the prefix “pseudo” since it is calculated experimentally. The 2GCI approach defines the PSG to include temperature gradients, moisture gradients, and additional factors that affect PCC slab curling and warping (Karamihas and Senn 2012). The PSG is written mathematically in equation (7):

$$PSG = \frac{(\alpha\Delta T + \Delta\epsilon_{sh})}{l\sqrt{2}} \quad (7)$$

where $\Delta\epsilon_{sh}$ is the extra strain gradient due to moisture gradient and other factors within the PCC slab.

The displacement at the slab's edge z_0 can be rewritten as follows with the PSG defined above (Lee et al. 2020):

$$Z_0 = PSG \cdot (1 + \mu)l^2 \quad (8)$$

Thus, PSG becomes one of the coefficients in the 2GCI fitting model, and l is the other coefficient, as shown in equation (8). In the proposed 2GCI model, x is the horizontal coordinate along the slab profile, referenced to the slab center; l is the radius of relative stiffness, also a coefficient in the 2GCI fitting model (with a range of 16 to 56 in. in the algorithm); λ is the non-dimensional parameter; and b is the profile distance.

To identify the curve closest to the data and adjust the model parameters (PSG , l), the nonlinear least squares method was used to build a regression model in which the sum of the squares of the vertical distances between different points and the regression curve is smallest.

3.2.2.2. Deflection and Deflection Ratio

This study proposed a new indicator, deflection ratio, to evaluate the degree of curling and warping behavior. This indicator minimizes the effect of transverse joint spacing on the degree of curling and warping. The research team developed an algorithm to calculate the slab deflection and degree of curvature using profile data. The analysis results demonstrated that the second-order polynomial method and 2GCI method could evaluate the acquired high-speed profiler data as an indicator of curling and warping behavior. These two methods could represent a new way of measuring curling and warping with appropriate precision and accuracy.

The algorithm needed field measurement validation. Two devices other than a high-speed profiler were used to compare the deflection results: a portable curling and warping device and a walking profiler. The ISU PCC Research Laboratory built a portable curling and warping measurement system to support ISU research needs in documenting maximum pavement deflection in the field (Ceylan et al. 2016b). A taut rope is used to set up a static pavement deflection measurement device on the surface of a concrete slab. The string is linked to two steel columns standing erect at opposing joints on a plate for randomly spaced mid-chord deflection measurements (Figure 10). Plate deflection can be measured by measuring the distance between the cord and the plate's surface at various positions with a step ruler or digital ruler. The precision of the portable device is 0.05 in.

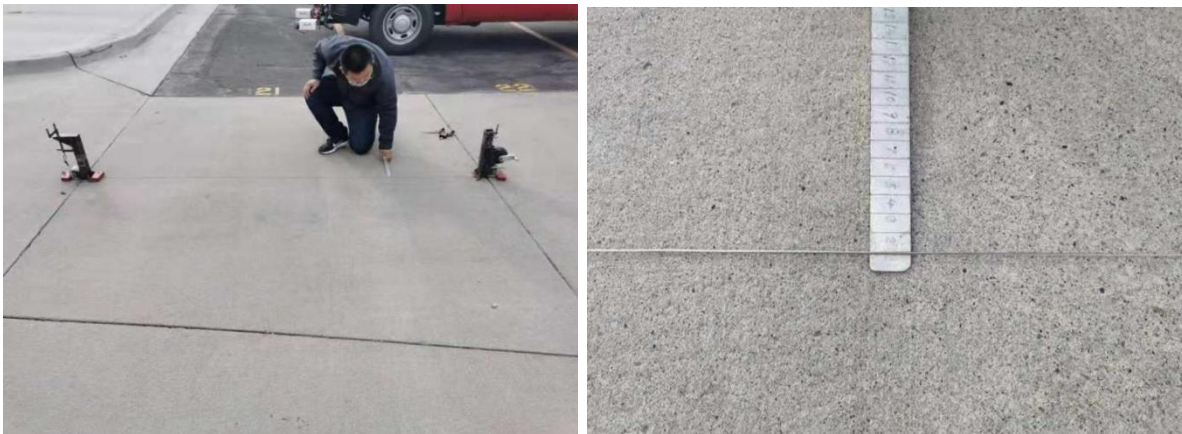


Figure 10. ISU portable curling and warping device

A PCC slab's maximum deflection is commonly found along the diagonal line between two opposite corners of the pavement slab. To measure this diagonal profile, traditional inclinometers and walking profilers in the field require lane closures, while inertial profilers normally measure longitudinal profiles along the wheel paths. Because the values acquired along these longitudinal sections are frequently underestimated, slab deflection readings from inertial profilers offer a gently distorted image of the maximum slab deflection (Byrum 2005).

Slabs in the Reiman Gardens parking lot in Ames, Iowa, were used to compare slab profile measurements taken by a high-speed profiler to those taken by a standard ARRB G3 Class 1 walking profiler and the ISU portable curling and warping device. The walking profiler, a high-

precision surface profiler that can provide profile measurements at a walking pace, was industrially calibrated to provide good accuracy and reproducibility. The test area in this section of the pavement consisted of three continuous PCC slabs, each measuring 9 ft in length. Three high-speed profiler speeds (30, 40, and 50 mph) were used, with three repeat runs at each speed. As shown in Figure 8, the three devices produced identical degrees of deflection and curvature, indicating that the developed algorithm is accurate enough to be applied to the high-speed profiler database.

3.2.3. Second-Order Polynomial Fitting Model

The positions and magnitudes of critical slab stresses are influenced by slab curvature, which indicates how concrete pavement slabs react to environmental pressures and impacts long-term pavement performance. Because curvature is a constant value, second-order polynomials are the easiest to utilize when fitting slab shapes. The pavement slab's shape is also physically represented by a quadratic equation. Although a second-order polynomial function cannot depict variations in the actual slab surface profile over the length of the slab due to cracks and surface defects, it can be used to identify the slab's neutral axis (Lederle et al. 2011). Using a higher-order polynomial or adding more variables to the model can enhance R^2 , but this does not necessarily imply that the model is more predictive (Ahammed and Tighe 2008). Lederle et al. (2011) concluded that when analyzing profilometer data, a higher-order polynomial has no physical meaning and is simply the line that connects the most contour points.

The profile data collected in this study were fitted using a second-order polynomial curve calculated using linear algebra after each slab's raw profile was retrieved; the fitting equation is shown in equation (9). The second derivative is taken to find the constant curvature (k) of the best-fit polynomial for each curve. At $k = 2a$, the second-order polynomial's curvature is constant. The second-order fitting in equation (9) is utilized in this fitting model to fit the entire slab surface and calculate the slab's maximum deflection and representative degree of curvature.

$$z = a_{20}x^2 + a_{02}y^2 + a_{11}xy + a_{10}x + a_{01}y + a_{00} \quad (9)$$

Although the second-order polynomial function cannot depict variations in the actual slab surface profile over the length of the slab due to cracks and surface defects, it can be used to identify the slab's neutral axis (Lederle et al. 2011). In previous studies, some researchers have compared quadratic or even higher-order polynomial fitting curves for slabs, but no guidance has been established on using the results of a second-order polynomial fitting model as an indicator to evaluate the degree of curling and warping.

3.2.4. Data Processing Procedure

In this study, the advanced 2GCI technique was used. Figure 11 roughly illustrates the 2GCI method, and the following further outlines the method:

1. Identify the curling direction and determine the joint locations for a particular PCC pavement profile.
2. For each PCC slab, extract the pavement profile.
3. Remove the pavement grade for each slab.
4. Perform the 2GCI method to fit a curve for each slab.
5. Re-apply the pavement grade for each slab.
6. Repeat steps 2 through 5 until all of the PCC slabs have been fitted using the 2GCI method.
7. Generate a 2GCI curvature-related profile that incorporates all of the slabs' curled shapes and a 2GCI non-curvature-related profile that eliminates the effects of curling and warping behavior.

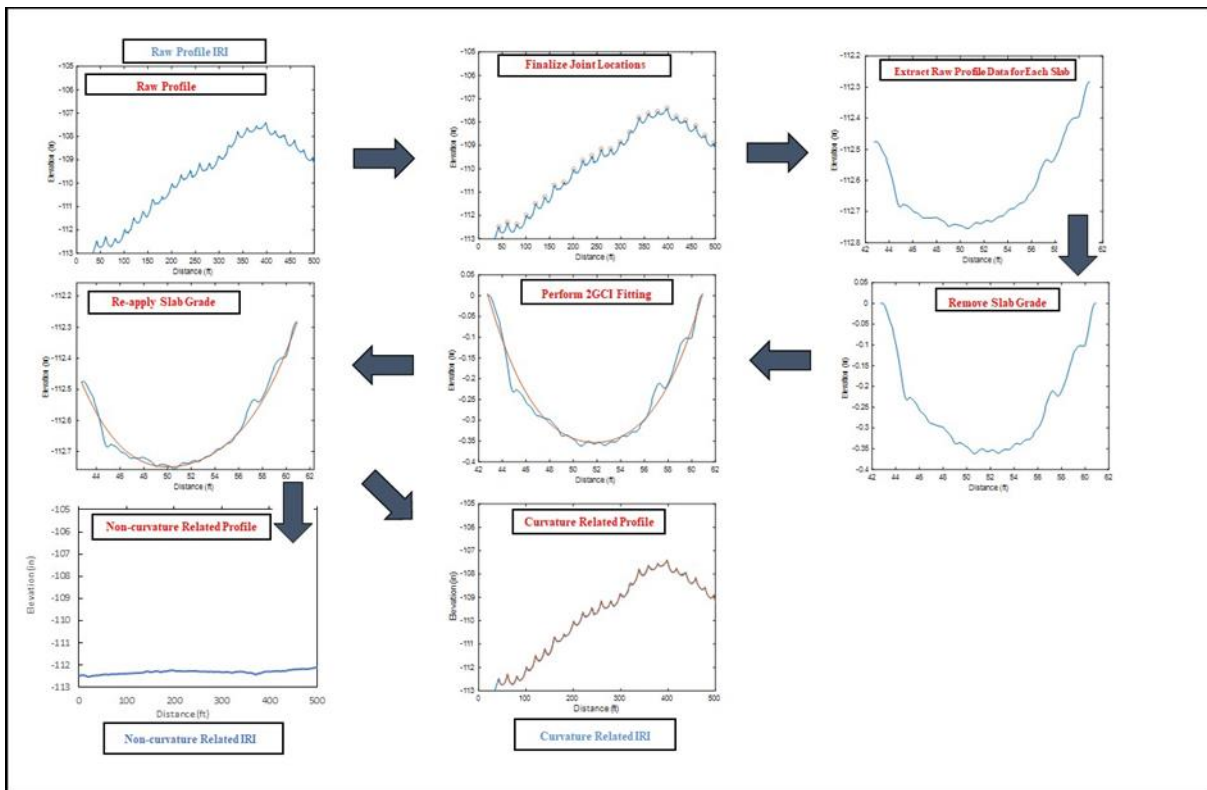


Figure 11. 2GCI algorithm flowchart

In this study, the second-order polynomial fitting model algorithm was also used. Figure 12 roughly illustrates the novel second-order polynomial method, and the following further outlines the method:

1. Identify the curling direction and determine the joint locations for a particular PCC pavement profile.
2. For each PCC slab, extract the pavement profile.
3. Perform the second-order polynomial method to fit a curve for each slab.
4. Remove the pavement grade for each slab. Repeat steps 2 through 5 until all of the PCC slabs have been fitted using the second-order polynomial fitting curve.

5. Generate a second-order polynomial curvature-related profile, which incorporates the slabs' curled shapes.

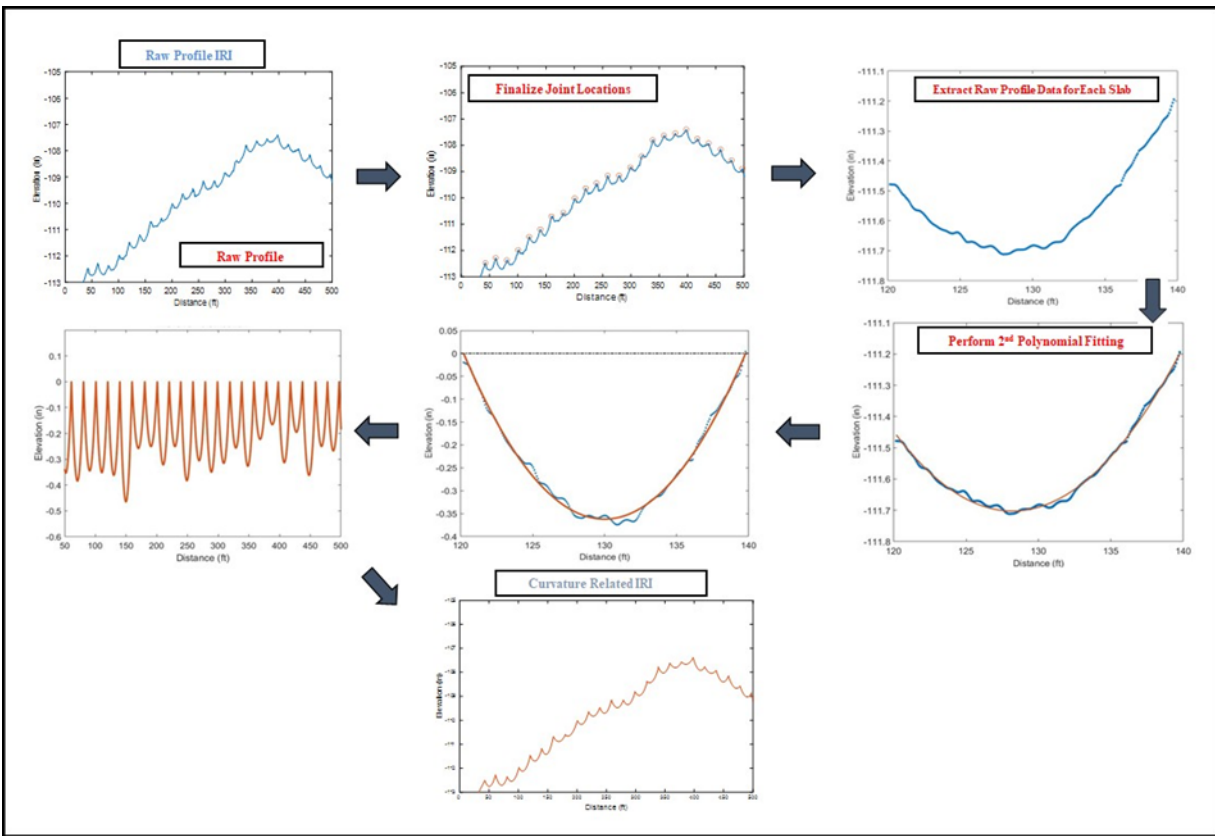


Figure 12. Second-order polynomial algorithm flowchart

For both methods, the input includes the *.erd profile data file from ProVAL, the estimated curling direction (up/down), and the transverse joint spacing (feet). The output includes curvature IRI, curvature-related profile, non-curvature IRI, non-curvature-related profile, radius of relative stiffness, PSG, deflection, deflection ratio, and degree of curvature.

Appendix A.2 provides a full description of the data processing procedure.

3.3. Field Data Collection Protocol

3.3.1. Site List and Measurement Schedule

Field data collection started in the summer of 2019 and continued into the summer of 2021. As shown in Figure 13, there were 36 sites in total across Iowa. A detailed site list is provided in Appendix A.3.

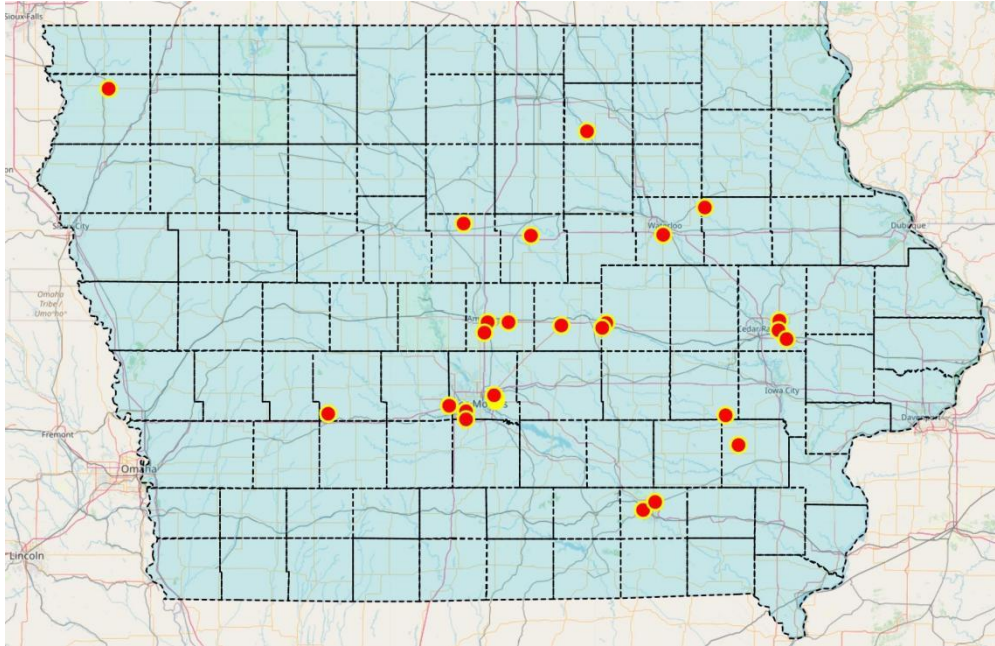


Figure 13. Site locations

The 36 sites selected for data collection included 6 sites from Ceylan et al. (2016a), an LTPP site with 12 sections, county roads, and city streets. It should be noted that LTPP section 19-0259 was categorized as a non-LTPP section, as shown in Table 2, because this section was built following Iowa DOT specifications for different purposes than other LTPP sections. All of these sites differ with respect to construction time, geometry, geographic location, and other factors. When evaluating the site location data, an attempt was made to extract locations with a high degree of similarity to allow for comparisons, more in-depth analysis, and the drawing of conclusions. The sites were grouped according to two considerations: curling direction, as shown in Figure 7(a) and 7(b) (curled up/down), and road type (LTPP highways, non-LTPP highways, county roads, and city streets).

The site lists are shown in Table 2 through Table 5.

Table 2. Curled-up non-LTPP highways

County	Route	GPS BP	GPS EP	Direction	Joint Spacing (ft)	Slab Width (ft)	Thickness (in)	Shoulder Type	Construction Year	Joint Type	Dowel Bar Diameter (in.)	Mix Design Type
Linn County	US 151 (1)*	42.015006, -91.550325	41.977795, -91.551462	SB	20	14	10	Gravel	1997	Skewed	1.5	Pre-QMC
Linn County	US 151 (2)*	41.969667, -91.551846	41.938959, -91.544902	SB	20	14	10	Gravel	2000	Skewed	1.5	QMC
Linn County	US 30*	41.921808, -91.500884	41.925681, -91.513144	WB	20	14	10	HMA	1999	Skewed	1.5	Pre-QMC
Marshall County	US 330	41.993521, -93.040868	42.004982, -93.023629	NB	20	14	10	HMA	2002	Skewed	1.5	QMC
Sioux County	US 18	43.185815, -96.148269	43.185728, -96.174479	WB	20	14	10	HMA	2000	Skewed	1.5	QMC
Story County	US 30*	42.008738, -93.550531	42.008749, -93.545509	EB	20	14	10	HMA	2013	Rectangular	1.5	QMC
Story County	US 30*	42.007997, -93.406686	42.008016, -93.411022	WB	20	14	10	Gravel	1995	Skewed	1.5	Pre-QMC
Story County	I-35	41.954742, -93.569622	41.982961, -93.570533	NB	20	14	11	PCC	2017/2018	Rectangular	1.5	QMC
Tama County	US 30*	42.005827, -92.736966	42.005086, -92.731025	EB	20	14	10	HMA	2005	Rectangular	1.5	QMC
Hardin County	US 20	42.448073, -93.251695	42.435761, -93.203982	EB	20	14	10	Gravel	2003	Rectangular	1.5	QMC
Polk County	IA-5	41.513942, -93.694281	41.514770, -93.711057	SB	20	14	10	HMA	2002	Skewed	1.5	QMC
Wapello County	US 63	41.089022, -92.398171	41.057160, -92.374412	WB	15	12	10	Gravel	2007	Rectangular	1.5	QMC
Black Hawk County	US 20	42.452778, -92.345000	42.454894, -92.309267	EB	20	13	11	PCC	2019	Rectangular	1.5	QMC
Polk County	US 65, 19-0259	41.629044, -93.500031	41.630937, -93.501583	NB	20	14	11	HMA	1994	Skewed	1.5	Pre-QMC

* Site included in the Phase I study

Pre-QMC: mix used in projects constructed before 2000; QMC: mix used in projects constructed after 2000

Table 3. Curled-up LTPP highways

County	Route	GPS BP	GPS EP	Direction	Joint Spacing (ft)	Slab Width (ft)	Thickness (in.)	Shoulder	Construction Year	Joint Type	Dowel Bar Diameter (in.)	Mix Design Type
Polk County	US 65, 19-0217	41.608011, -93.495366	41.609899, -93.494963	NB	15	14	8	HMA	1994	Rectangular	1.25	Low Strength
Polk County	US 65, 19-0218	41.609899, -93.494963	41.612946, -93.494257	NB	15	12	8	HMA	1994	Rectangular	1.25	High Strength
Polk County	US 65, 19-0219	41.612946, -93.494257	41.615219, -93.493786	NB	15	12	11	HMA	1994	Rectangular	1.5	Low Strength
Polk County	US 65, 19-0220	41.615219, -93.493786	41.619170, -93.492904	NB	15	14	11	HMA	1994	Rectangular	1.5	High Strength
Polk County	US 65, 19-0215	41.619170, -93.492904	41.621468, -93.493012	NB	15	12	11	HMA	1994	Rectangular	1.5	Low Strength
Polk County	US 65, 19-0216	41.621468, -93.493012	41.624623, -93.495144	NB	15	14	11	HMA	1994	Rectangular	1.5	High Strength
Polk County	US 65, 19-0213	41.624623, -93.495144	41.626883, -93.497545	NB	15	14	8	HMA	1994	Rectangular	1.25	Low Strength
Polk County	US 65, 19-0214	41.626883, -93.497545	41.629044, -93.500031	NB	15	12	8	HMA	1994	Rectangular	1.25	High Strength
Polk County	US 65, 19-0221	41.630937, -93.501583	41.632663, -93.502705	NB	15	14	8	HMA	1994	Rectangular	1.25	Low Strength
Polk County	US 65, 19-0222	41.632663, -93.502705	41.635370, -93.504418	NB	15	12	8	HMA	1994	Rectangular	1.25	High Strength
Polk County	US 65, 19-0223	41.635370, -93.504418	41.637358, -93.505661	NB	15	12	11	HMA	1994	Rectangular	1.5	Low Strength
Polk County	US 65, 19-0224	41.637358, -93.505661	41.638608, -93.506498	NB	15	14	11	HMA	1994	Rectangular	1.5	High Strength

Table 4. Curled-up county roads and city streets

County	Route	GPS BP	GPS EP	Direction	Joint Spacing (ft)	Slab Width (ft)	Thickness (in.)	Shoulder	Construction Year	Joint Type	Dowel Bar Diameter (in.)	Mix Design Type
Floyd County	T26	42.972175, -92.869775	42.987609, -92.888543	NB	15	11	8	Gravel	2017	Rectangular	N/A	C-3WR
Wapello County	H21	41.046907, -92.480172	41.084129, -92.526112	EB	20	11	8	Gravel	2017	Rectangular	N/A	C-3WR
Polk County	Park Avg.	41.555459, -93.699586	41.555446, -93.691851	EB	15	13	10	PCC curb	2017	Rectangular	1.5	C-SUD
Polk County	Ashworth Rd.	41.582495, -93.812445	41.581991, -93.818358	WB	15	12	10	PCC curb	2017	Rectangular	1.5	C-SUD
Buchanan County	V62 (1)	42.541153, -92.062575	42.569117, -92.062248	NB	12	11	6	PCC	2018	Rectangular	N/A	C-3WR
Guthrie County	N54	41.542452, -94.643460	41.519050, -94.643450	SB	12	11	8	Gravel	2016	Rectangular	N/A	QMC
Tama County	E49	41.978133, -92.761044	41.978699, -92.727949	EB	12	12	8	Gravel	2017	Rectangular	N/A	C-3WR

QMC: mix used in projects constructed after 2000; C-3WR: mix most often used for county pavements in recent years; C-SUD: urban durability mix

Table 5. Curled-down county roads

County	Route	GPS BP	GPS EP	Direction	Joint Spacing (ft)	Slab Width (ft)	Thickness (in.)	Shoulder	Construction Year	Joint Type	Dowel Bar Diameter (in.)	Mix Design Type
Hamilton County	D20	42.507348, -93.713137	42.514416, -93.639516	WB	15	11	6	Gravel	1984	Skewed	N/A	N/A
Iowa County	F67	41.532808, -91.919650	41.540449, -91.887120	WB	20	11	7	Gravel	1993	Skewed	N/A	N/A
Washington County	G26 (2)	41.381407, -91.642522	41.380797, -91.714506	WB	40	11	6	Gravel	1973	Rectangular	N/A	N/A

Based on the developed experimental plan, field profile data were collected from these sites in all four seasons. On the day of data collection in each season, measurements were taken at three times, including the early morning, noon, and late afternoon. The seasons and times are shown in Table 6.

Table 6. Definitions of field data collection periods

Period	Definition
Spring	March 16–May 15
Summer	May 16–Aug. 15
Fall	Aug. 16–Nov. 15
Winter	Dec. 16–March 15
Early Morning	7:30 a.m.–9:00 a.m. CST
Noon	12:00 p.m.–1:30 p.m. CST
Late Afternoon	4:30 p.m.–6:00 p.m. CST

3.3.2. Operation Procedure

Activities at each site included the following:

1. According to location information such as station number, milepost number, and GPS coordinates from Ceylan et al. (2016a), find the site’s beginning point (BP) and ending point (EP).
2. Record slab information: slab width, transverse joint spacing, shoulder type, and transverse joint type.
3. Referring to the operation manual, calibrate the motion sensors on the SSI high-speed profiler.
4. For safety, turn on the truck’s headlights when profiling to alert other drivers and coworkers.
5. Check for the presence of cracks and take photographs of any cracks found.
6. Drive the truck at a constant speed and use the profiler device to scan the pavement surface. Choose the “EE start” function when close to the site’s BP to start the measurement, and choose the “EE stop” function when close to the site’s EP to end the measurement.
7. Check the report produced by the profiler to determine whether the surface temperature and moisture content results are reasonable.

A detailed operation manual is provided in Appendix A.1.

3.4. Summary

For the field investigation, 36 sites with a variety of slab structures and design characteristics were selected on primary highways and county and city roads in Iowa. The research team used a high-speed profiler to collect raw pavement profile data and performed the appropriate calibration procedure on the profiler before each measurement. During the project, at least four

field visits were scheduled per site to cover all seasons and to investigate the effects of seasonal variation on PCC curling and warping behavior. During each field visit, three measurements (early morning, noon, and late afternoon) were conducted at each site to assess diurnal differences in PCC curling and warping behavior.

Two innovative algorithms, one based on the 2GCI model and one based on a second-order polynomial fitting model, were developed to transform the raw profile data and measure the amount of curling and warping in the profiled pavements. Curvature profile, non-curvature profile, and other indicators of the degree of curling and warping were among the algorithms' outputs.

4. ANALYSIS APPROACHES AND RESULTS

4.1. Analysis Approach

Previous research has shown that changes in slab curvature caused by temperature and moisture changes substantially impact pavement smoothness evaluations (Karamihas 1999). Several rigid pavement design and analysis methods have been developed to account for the effects of temperature differences. Choubane and Tia (1992) introduced the total nonlinear temperature profile shown in Figure 14. The temperature profile contains three components: (1) a component causing axial displacement, (2) a component causing bending, and (3) a nonlinear temperature component. For a more mechanistic pavement design, Wells (2006) highlighted the importance of temperature- and moisture-related slab deflection.

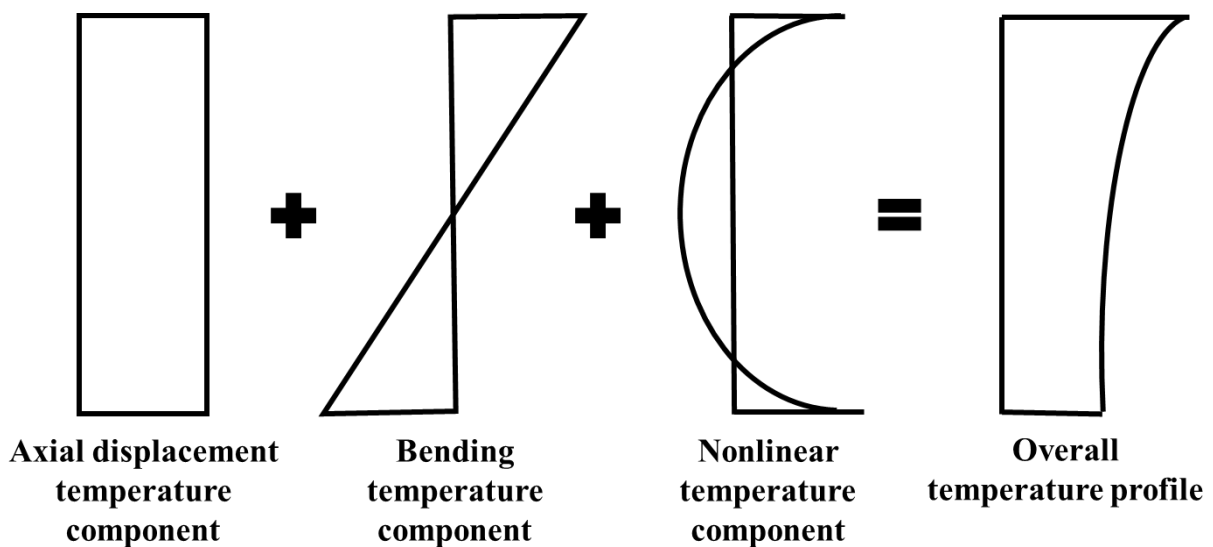


Figure 14. Typical temperature variation profile throughout a slab

Although the nonlinear distribution of temperature throughout a concrete slab has long been acknowledged, some methods are nevertheless predicated on the premise that the temperature change in a concrete slab from top to bottom is linear. Arlington Road experiments in the early 1930s were the first to detect nonlinearity in the temperature distribution of concrete road panels (Engineering and Contracting Volume 57). Even if the bending gradient is a more typical temperature distribution, Teller and Sutherland (1935) argued that a uniform temperature gradient results in the most severe stress situations. Lang (1942) claimed that the temperature distribution varies slightly from linear to nonlinear. Because of the importance of warp stress and the several variables that affect design, slight changes in alignment are unimportant; therefore, the temperature gradient can be taken as roughly linear for simplicity.

Moisture gradients through the depth of a PCC slab cause warping and reversible contraction. Daily and seasonal weather variations, as well as pavement materials, influence moisture

gradients (Rao and Roesler 2005). Seasonal changes may be more impactful than daily differences because of the limited hydraulic conductivity of concrete (Yu et al. 2004). The top and bottom surfaces of concrete pavement are exposed to the elements. The bottom of the slab, because it is in touch with the soil or base layer, usually has a high moisture content, but the top surface loses moisture as it dries because it is exposed to air. As a result, various moisture gradients form throughout the depth of the slab. The top surface of the slab shrinks relative to the bottom surface due to a negative moisture gradient with a lower moisture content at the top than at the bottom, resulting in slab warping. Due to the various responses of internally cured concrete to self-drying, water absorption, and external drying processes, the moisture gradient distribution would be expected to differ from that of a control mix. Grasley et al. (2006) developed a moisture gradient model based on diffusion theory and drying stress gradient models. The moisture gradient is first created using internal relative humidity (RH) readings directly related to stress development (rather than otherwise approximating or calculating the moisture distribution). Second, in addition to considering only freely shrinking concrete, the issue of totally constrained concrete must be addressed.

Slab curling and warping, as well as joint motion deformation, are caused by temperature and moisture gradients in slabs (Wei and Hansen 2011). The influence of temperature gradients on slab deformation has been extensively studied, and moisture gradients can easily be converted to temperature gradients for assessing slab deformation (Wei et al. 2015).

4.1.1. Equivalent Temperature Difference

The temperature gradient within a concrete slab is usually calculated by predicting the temperature of the pavement. Two types of methodologies are typically utilized to predict the temperature gradient of pavements: theoretical or statistical approaches (Tan et al. 2013). Statistical approaches usually involve a regression process based on climate, meteorological data from large databases, and temperature measurements taken on road surfaces. Statistical methods are comparatively straightforward compared to theoretical approaches, and as a result they are more commonly employed. Statistical methods, however, are region-specific and necessitate using a vast database. The common theoretical approach involves solving heat transfer equations using numerical methods. Dempsey (1969) was among the first to use one-dimensional heat transfer models and explicit finite-difference approaches to formulate numerical simulation methods. The Climate-Material-Structure (CMS) Pavement Analysis program developed at the University of Illinois is one of the most commonly used theoretical models for temperature prediction. It uses one-dimensional, forward finite-difference heat transfer analysis to estimate temperatures throughout the pavement layers based on atmospheric conditions. It also estimates how much frost gets through the layers (Hasan and Tarefder 2018). The CMS model requires input in the form of pavement material parameters and climate data such as air temperature, precipitation, radiation, and so on.

While the theoretical approach is widely known for its time-consuming solution process and the high number of required inputs, it has been incorporated into the Enhanced Integrated Climate Model (EICM). The EICM was utilized in the AASHTO 2002 *Mechanistic-Empirical Pavement Design Guide* (AASHTO 2002) to determine instantaneous hourly positive and negative

temperature gradients generated by solar radiation and other elements while considering the impacts of temperature and humidity in the design of JPCP. To quantify the effects of temperature-, moisture-, and construction-related curling and warping, Yu et al. (2004) explained the methods and procedures utilized for JPCP design in the 2002 design guide.

A complete evaluation of the impact of climate on pavement materials, reactions, and hazards is one of the fundamental advancements in pavement design included in PMED. The EICM is used in that software for simulating temperature and humidity within each pavement layer and in the foundation. To estimate pavement surface temperature and humidity conditions, the climate model uses hourly ambient climate data from meteorological stations across the United States, including temperature, precipitation, wind speed, cloud cover, and relative humidity.

The temperature difference is calculated as the temperature at the top of the slab minus the temperature at the bottom of the slab. A positive equivalent temperature difference indicates that the equivalent temperature at the top of the slab is more significant than at the bottom, while a negative number indicates the inverse. Suppose the equivalent temperature difference increases from zero to a positive value early on, indicating that the equivalent temperature at the top of the slab is higher than at the bottom. In that case, the slab is forced to curl down. Because concrete shrinkage occurs mainly near the top of the slab, if the equivalent temperature difference decreases to a negative value, indicating that the equivalent temperature at the bottom of the slab is higher than at the top, the slab is forced to curl upward. As concrete ages, the corresponding temperature difference drops to greater negative values, indicating that the slab is more likely to curl.

4.1.2. Equivalent Temperature Difference Calculation

Based on the theory proposed by Yu et al. (2004), all slab deformation impacts, including the pavement slab's original shape and any settlement that may occur over time, are stated as equivalent temperature differences. The permanent curling/warping effective temperature difference ($\Delta T_{\text{Permanent}}$) is the equivalent temperature difference that corresponds to the effective permanent curling and warping locked into the pavement at a temperature and moisture difference of zero. The permanent curling/warping effective temperature difference in PMED is defined as -10°F based on national calibration results (Olidis and Hein 2004). Solar radiation and other effects generate a transient hourly negative and positive temperature difference (ΔT_{Hourly}). The EICM calculates the equivalent linear hourly temperature difference using the temperatures of 11 uniformly spaced points through the slab. For each month of the year, the transient shrinkage (reversible shrinkage) at the top of the pavement slab induced by variations in atmospheric relative humidity is transformed into an equivalent temperature difference ($\Delta T_{\text{Shrinkage}}$).

The atmospheric relative humidity primarily determines the quantity of reversible shrinkage in hardened concrete at any particular time. According to Eisenmann and Leykauf (1990), slab warping produced by shrinkage is transformed into an equivalent temperature difference. The calculation procedure is shown in equations (10) through (13):

$$\Delta T = \Delta T_{\text{Permanent}} + \Delta T_{\text{Hourly}} + \Delta T_{\text{Shrinkage}} \quad (10)$$

$$ETG_{SHi} = \frac{3 \cdot (\phi \cdot \varepsilon_{su}) \cdot (S_{hi} - S_{have}) \cdot h_s \cdot \left(\frac{h}{2} - \frac{h_s}{3}\right)}{\alpha \cdot h^2 \cdot 100} \quad (11)$$

where

ETG_{SHi} = temperature difference equivalent to the deviation in moisture warping in month i from the annual average, °F

ϕ = reversible shrinkage factor in terms of the fraction of total shrinkage (0.5 assumed)

S_{have} = annual average relative humidity factor

h_s = depth of the shrinkage zone (typically 2 in.)

h = PCC slab thickness, in.

α = PCC coefficient of thermal expansion, /°F

S_{hi} = relative humidity factor for month i :

$$S_{hi} = 1.4 - 0.01 \cdot RHa, \text{ RHa} < 80\%$$

$$S_{hi} = 3.0 - 0.03 \cdot RHa, \text{ RHa} \geq 80\% \quad (12)$$

RHa = ambient average relative humidity, percent

ε_{su} = ultimate shrinkage

The ultimate shrinkage may be estimated based on PCC mix properties using equation (13):

$$\varepsilon_{su} = C_1 \cdot C_2 \cdot \{26w^{2.1}(f'_c)^{-0.28} + 270\} \quad (13)$$

where

C_1 = cement type factor (1.0 for Type I, 0.85 for Type II, and 1.1 for Type III cement)

C_2 = curing type factor (1.0 for moist curing, 1.2 if cured using a curing compound)

w = water content, lb/ft³

f'_c = 28-day PCC compressive strength, psi (typically 4,000 psi)

The present study used PMED, which integrates equation (10) to calculate temperature differences. Temperature difference data were used to evaluate influences on curling and warping behavior. The detailed analysis procedure used to calculate the temperature difference is described in Appendix A.4.

4.1.3. Description of Statistical Analysis Approaches

4.1.3.1. One-Way ANOVA

To examine the significance of the effect of different variables on curling and warping behavior, a one-way analysis of variance (ANOVA) was done. This analysis must ensure that the samples are independent, residuals are normally distributed, and variances are homogeneous. The four indicators of curling and warping behavior (curvature IRI, deflection, deflection ratio, and degree of curvature) were considered as dependent variables, while slab geometry, shoulder type, joint type, seasonal effect, diurnal effect, and mix design were considered as fixed factors. The p-value at a confidence of 95% shows the significance of the coefficients. The higher the level of significance, the smaller the p-value (a p-value smaller than 0.05 indicates a significant factor).

4.1.3.2. Multiple Linear Regression Model

Due to the data's wide dispersion and relatively large scale, a multiple linear regression analysis provided more information for assessing the association between pavement design parameters and the degree of curling and warping. Based on the variables identified in this study, multiple linear regression models were developed to quantify critical engineering variables that determine the degree of curling and warping (curvature IRI, deflection, deflection ratio, and degree of curvature). These variables are shown in Table 7.

Table 7. Summary of engineering variables

Variable	LTPP	Non-LTPP	County Roads and City Streets
Seasonal Time	1 (Spring), 2 (Summer), 3 (Fall), 4 (Winter)		
Diurnal Time	1 (Morning), 2 (Noon), 3 (Afternoon)		
Slab Thickness (in.)	8, 11	10, 11	6, 8, 10
Transverse Joint Spacing (ft)	-	-	12, 15, 20
Slab Width (ft)	12, 14	12, 13, 14	11, 12, 13
Joint Type	1 (Rectangular), 2 (Skewed)		
Shoulder Type	1 (Untied Shoulder), 2 (Tied Shoulder)		
Dowel Bar Diameter (in.)	1.25, 1.5	-	0, 1.5
Mix Type	900 (High-Strength Mix), 500 (Low-Strength Mix)	1 (Pre-QMC), 2 (QMC)	2 (QMC), 3 (C-SUD) 4 (C-3WR)

Pre-QMC: mix used in projects constructed before 2000; QMC: mix used in projects constructed after 2000; C-3WR: mix most often used for county pavements in recent years; C-SUD: urban durability mix

The following relationship was assumed to apply to the progression of the curling and warping indicators:

Degree of curling and warping = F (slab geometry, mix design, shoulder type, and joint type)

Regarding the variables in the argument, function F has partial derivatives. The function is reduced to the following linear regression equation:

Degree of curling and warping = $aX_1 + bX_2 + cX_3 \dots$

where

Degree of curling and warping = dependent variable

X_1, X_2, X_3 = independent variables

a, b, c = linear regression coefficients

4.2. Analysis Results

4.2.1. Curled-Up Sites

The curled-up sites included in the equivalent temperature difference analysis are shown in Table 8 to Table 10. Sites with nearby reliable climate stations included those near Ames, Des Moines, and Cedar Rapids, Iowa. During each site visit, three high-speed profiler measurements were taken at three times throughout the day: early morning, noon, and late afternoon (Table 6).

The North American Regional Reanalysis (NARR) climatic data set produced by the National Centers for Environmental Prediction (NCEP) assimilates high-resolution precipitation data throughout North America. While this data set has shown improvements over NCEP's Global Reanalysis II data set in several variables (Mesinger et al. 2006), the Modern-Era Retrospective Analysis for Research and Applications (MERRA) data set was chosen as the source of climatic data for the present study because it provides comparably high-resolution diagnostic output over a similar period. It was released only last year (2022), so there is limited information concerning its quality. PMED automatically requests NARR climatic inputs when rigid designs are selected, but the pavement data for this study were analyzed using the MERRA data set through the creation of "custom" climate files.

Table 8. Curled-up LTPP highways for equivalent temperature difference analysis

Route	Group	County	Visit Season	Testing Date	Curling Direction
LTPP 217	Highway	Polk County	summer	8/17/2019	Up
			spring	3/16/2020	Up
			summer	7/24/2020	Up
			fall	11/12/2020	Up
LTPP 218	Highway	Polk County	summer	8/17/2019	Up
			spring	3/16/2020	Up
			summer	7/24/2020	Up
			fall	11/12/2020	Up
LTPP 219	Highway	Polk County	summer	8/17/2019	Up
			spring	3/16/2020	Up
			summer	7/24/2020	Up
			fall	11/12/2020	Up
LTPP 220	Highway	Polk County	summer	8/17/2019	Up
			spring	3/16/2020	Up
			summer	7/24/2020	Up
			fall	11/12/2020	Up
LTPP 215	Highway	Polk County	summer	8/17/2019	Up
			spring	3/16/2020	Up
			summer	7/24/2020	Up
			fall	11/12/2020	Up
LTPP 216	Highway	Polk County	summer	8/17/2019	Up
			spring	3/16/2020	Up
			summer	7/24/2020	Up
			fall	11/12/2020	Up
LTPP 213	Highway	Polk County	summer	8/17/2019	Up
			spring	3/16/2020	Up
			summer	7/24/2020	Up
			fall	11/12/2020	Up
LTPP 214	Highway	Polk County	summer	8/17/2019	Up
			spring	3/16/2020	Up
			summer	7/24/2020	Up
			fall	11/12/2020	Up
LTPP 221	Highway	Polk County	summer	8/17/2019	Up
			spring	3/16/2020	Up
			summer	7/24/2020	Up
			fall	11/12/2020	Up
LTPP 222	Highway	Polk County	summer	8/17/2019	Up
			spring	3/16/2020	Up
			summer	7/24/2020	Up
			fall	11/12/2020	Up
LTPP 223	Highway	Polk County	summer	8/17/2019	Up
			spring	3/16/2020	Up
			summer	7/24/2020	Up
			fall	11/12/2020	Up
LTPP 224	Highway	Polk County	summer	8/17/2019	Up
			spring	3/16/2020	Up
			summer	7/24/2020	Up
			fall	11/12/2020	Up

Table 9. Curled-up non-LTPP highways for equivalent temperature difference analysis

Route	Group	County	Visit Season	Testing Date	Curling Direction
LTPP 259	Highway	Polk County	summer	8/17/2019	Up
			spring	3/16/2020	Up
			summer	7/24/2020	Up
			fall	11/12/2020	Up
US 30	Highway	Story County	summer	6/20/2019	Up
			winter	1/6/2020	Up
			spring	2/28/2020	Up
			summer	6/29/2020	Up
			fall	10/7/2020	Up
US 30	Highway	Story County	summer	6/20/2019	Up
			winter	1/6/2020	Up
			spring	2/28/2020	Up
			summer	6/29/2020	Up
			fall	10/7/2020	Up
US 30	Highway	Linn County	summer	7/19/2019	Up
			summer	7/1/2020	Up
			fall	10/8/2020	Up
US 20	Highway	Black Hawk County	summer	8/19/2019	Up
			summer	7/1/2020	Up
			fall	11/23/2020	Up
I-35	Highway	Story County	summer	8/23/2019	Up
			spring	5/21/2020	Up
			summer	8/3/2020	Up
			fall	10/7/2020	Up
IA 5	Highway	Polk County	summer	7/24/2020	Up
			fall	11/12/2020	Up
US 151 (1)	Highway	Linn County	summer	7/19/2019	Up
			summer	7/1/2020	Up
			fall	10/8/2020	Up
US 151 (2)	Highway	Linn County	summer	7/19/2019	Up
			summer	7/1/2020	Up
			fall	10/8/2020	Up

Table 10. Curled-up county roads and city streets for equivalent temperature difference analysis

Route	Group	County	Visit Season	Testing Date	Curling Direction
N54	County Road	Guthrie County	summer	9/25/2019	Up
			summer	8/18/2020	Up
			fall	11/18/2020	Up
E49	County Road	Tama County	summer	8/19/2019	Up
			summer	6/17/2020	Up
			fall	10/21/2020	Up
V62	County Road	Buchanan County	summer	8/19/2019	Up
			summer	7/2/2020	Up
			fall	11/23/2020	Up
T26	County Road	Floyd County	summer	8/15/2019	Up
			summer	7/13/2020	Up
			fall	11/23/2020	Up
Park Avg.	City Street	Polk County	summer	9/5/2019	Up
			summer	7/24/2020	Up
			fall	11/12/2020	Up
Ashworth Rd.	City Street	Polk County	summer	9/5/2019	Up
			summer	7/24/2020	Up
			fall	11/12/2020	Up

4.2.1.1. Equivalent Temperature Difference Effects

A positive or negative temperature difference exists between the top and the bottom surfaces of a concrete slab. Figure 15 shows the hourly equivalent temperature difference versus curling and warping behavior for the pavements evaluated in this study. As shown in Figure 16, for the hourly component of the overall estimated temperature difference, the noon ΔT_{Hourly} parameter always has positive values, which explains the positive temperature difference between the concrete slab's top and bottom surfaces in the daytime. The hourly equivalent temperature difference for the early morning and late afternoon periods shows positive and negative values. A previous study showed that the diurnal temperature effect has a maximum impact during the nighttime and the morning of the following day (Masad et al. 1996).

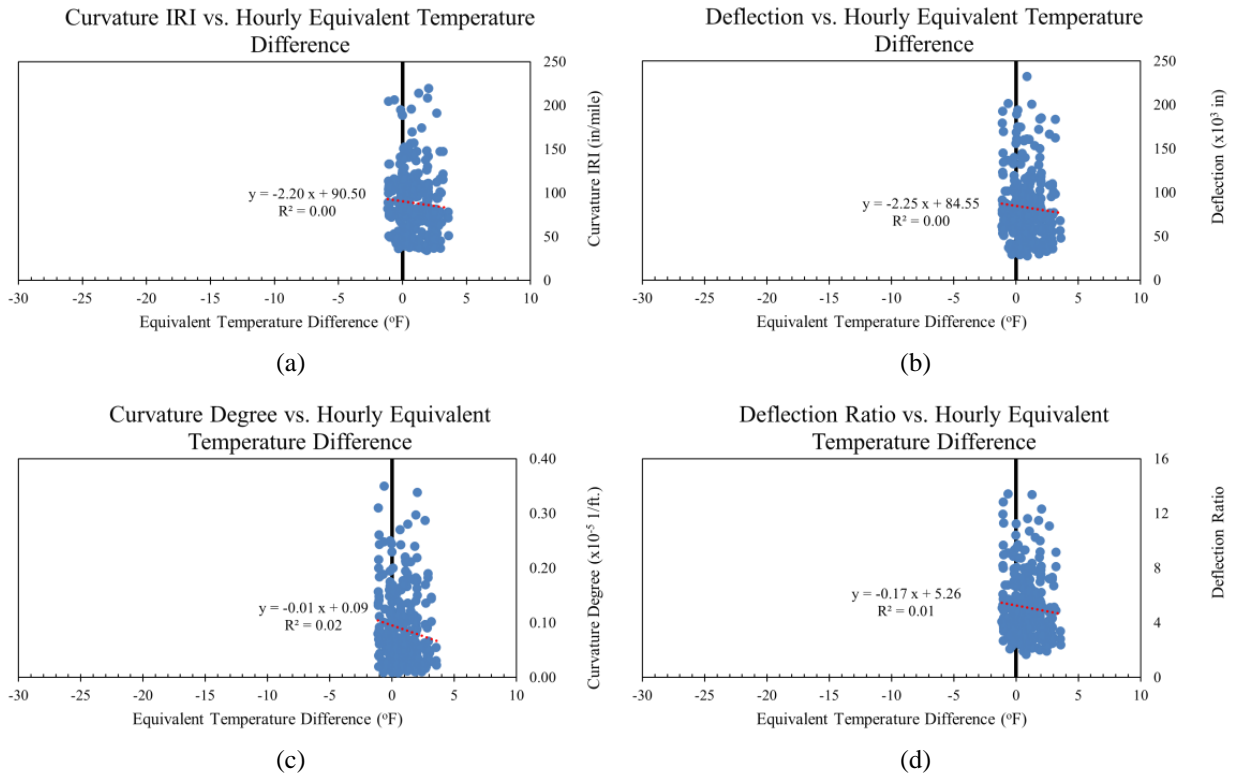


Figure 15. Hourly equivalent temperature difference versus (a) curvature IRI, (b) deflection, (c) deflection ratio, (d) degree of curvature

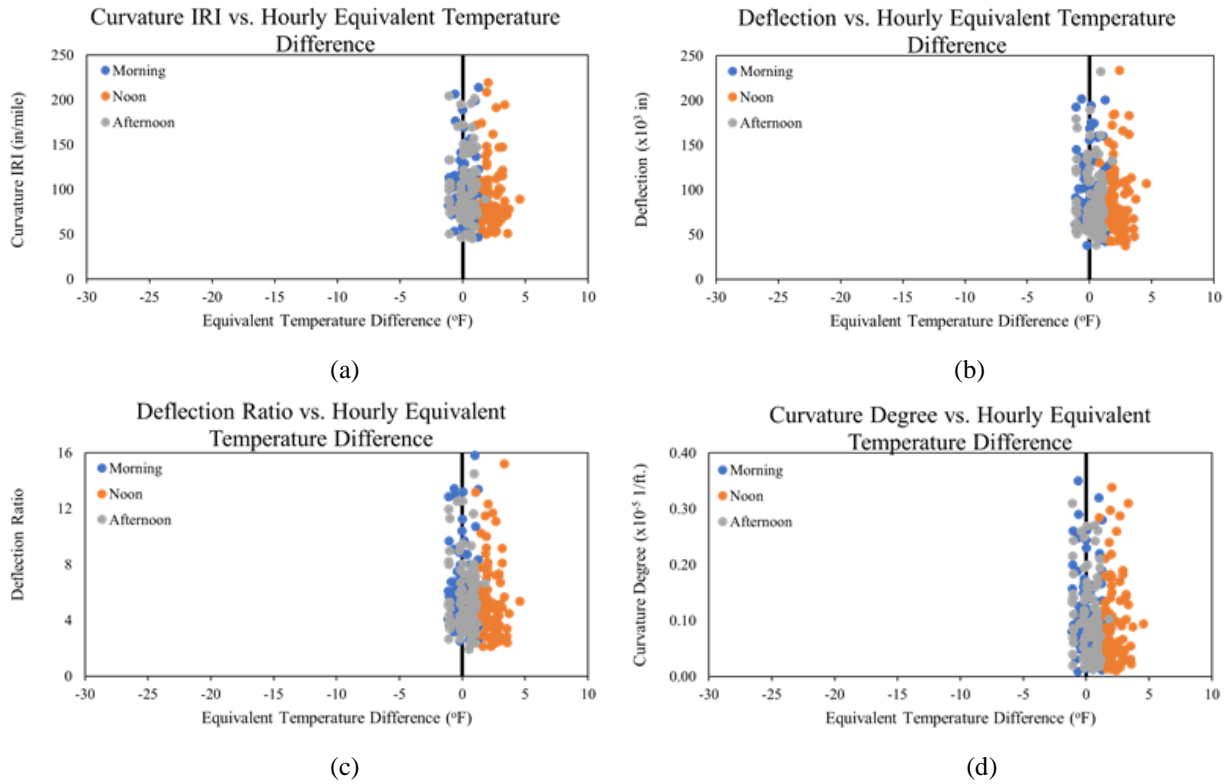


Figure 16. Diurnal hourly equivalent temperature difference versus (a) curvature IRI, (b) deflection, (c) deflection ratio, (d) degree of curvature

Figure 17 and Figure 18 depict curling and warping behavior versus shrinkage equivalent temperature difference and overall equivalent temperature difference, respectively. The general trend is shown by three of the four indicators of curling and warping (curvature IRI, deflection, and deflection ratio) decreasing as the equivalent temperature difference approaches 0°F.

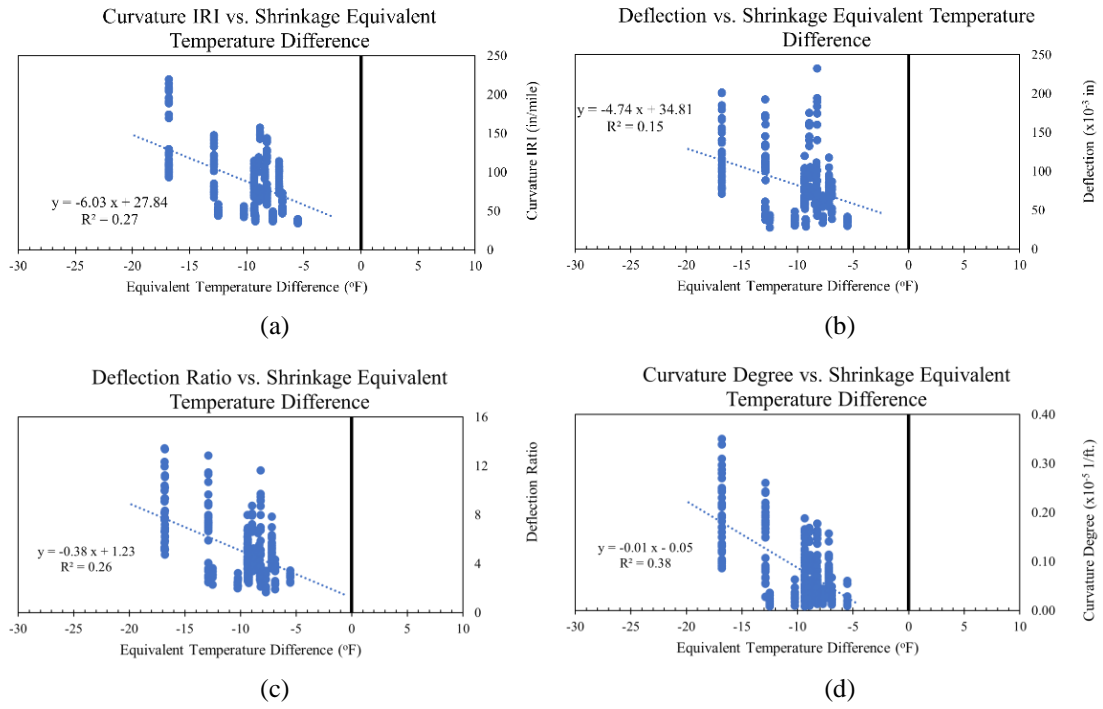


Figure 17. Shrinkage equivalent temperature difference versus (a) curvature IRI, (b) deflection, (c) deflection ratio, (d) degree of curvature

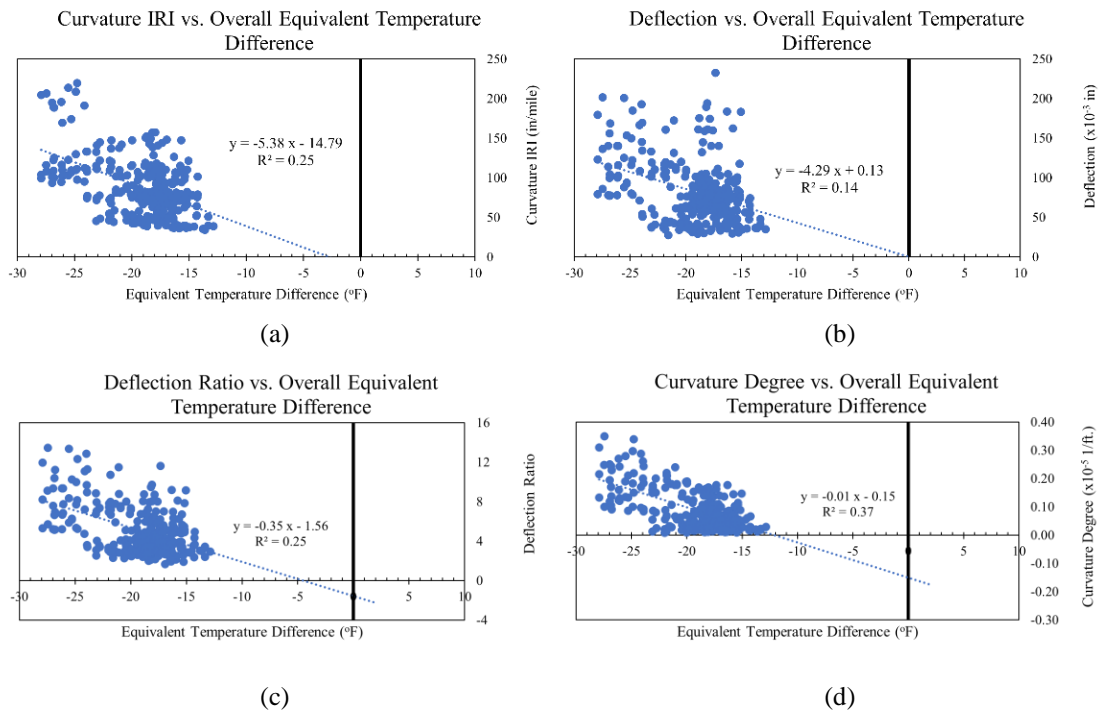


Figure 18. Overall equivalent temperature difference versus (a) curvature IRI, (b) deflection, (c) deflection ratio, (d) degree of curvature

There are permanent and transient components to the temperature difference. The permanent components can be summed to form a single quantity, expressed as an effective linear temperature difference throughout a PCC slab. For the transient components, the moisture impacts are based on monthly changes in atmospheric relative humidity, while the temperature effects are based on hourly climatic data.

A positive equivalent temperature difference indicates that the equivalent temperature at the top of the slab is more significant than at the bottom, while a negative number indicates the inverse. The slab curls downwards as the equivalent temperature difference increases from zero to a positive number, which indicates a higher equivalent temperature at the top of the slab than at the bottom. The equivalent temperature difference decreases to a negative value when the drying shrinkage of the concrete occurs mainly near the top of the slab, which indicates a higher equivalent temperature at the bottom of the slab than at the top, causing the slab to curl upwards.

In the MEPDG, the permanent effective curling/warping temperature gradient is represented by a nationwide default value of -10°F . Even though the environmental conditions and the climate database employed vary by county across Iowa, the testing results show that -10°F can accurately reflect local conditions in the state. It is worth mentioning that changes in relative humidity can impact transient moisture shrinkage in the PCC slab's top surface (Shafiee et al. 2019). Curling and warping behavior was found to decrease when the absolute equivalent temperature difference decreases at locations near accurate climatic stations. When the equivalent temperature is 0°F , the concrete slab is flat with no curling and warping behavior. The trendlines shown in Figure 18 indicate that when the curvature IRI, deflection, and deflection ratio reached zero values, their corresponding overall temperature differences were near 0°F . Since the permanent effective curling/warping temperature was hypothesized as -10°F , the trendlines indicate that this hypothesis is reasonable for concrete pavements in Iowa. In terms of the hourly component, the effective temperature difference at midday is always positive, whereas the values in the morning and afternoon are always the opposite. The scattered distribution of data (Figure 16) shows that the hourly temperature difference is not as important for curling and warping behavior as other variables. In comparison to the hourly and overall equivalent temperature differences, the shrinkage equivalent temperature difference has a greater impact.

4.2.1.2. Seasonal Effects

The following statistical analyses are summarized using box-whisker plots (Figure 19) to provide an overview of how each variable affects the degree of curling/warping for three groups of roads: LTPP highways, non-LTPP highways, and county roads and city streets.

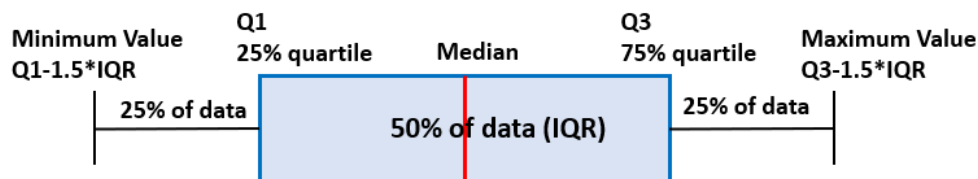


Figure 19. Configuration of a box-whisker plot

All 12 LTPP sections (0217, 0218, 0219, 0220, 0213, 0214, 0215, 0216, 0221, 0222, 0223, and 0224) were measured in four seasons. Spring data were measured on March 16, 2020; summer data were measured on July 24, 2020; fall data were measured on November 12, 2020; and winter data were measured on February 16, 2021. The exact time of each visit is shown in Appendix A.3.

Figure 20 shows the seasonal effects on the curling and warping behavior of the LTPP sections via four indicators: curvature IRI, deflection, deflection ratio, and degree of curvature.

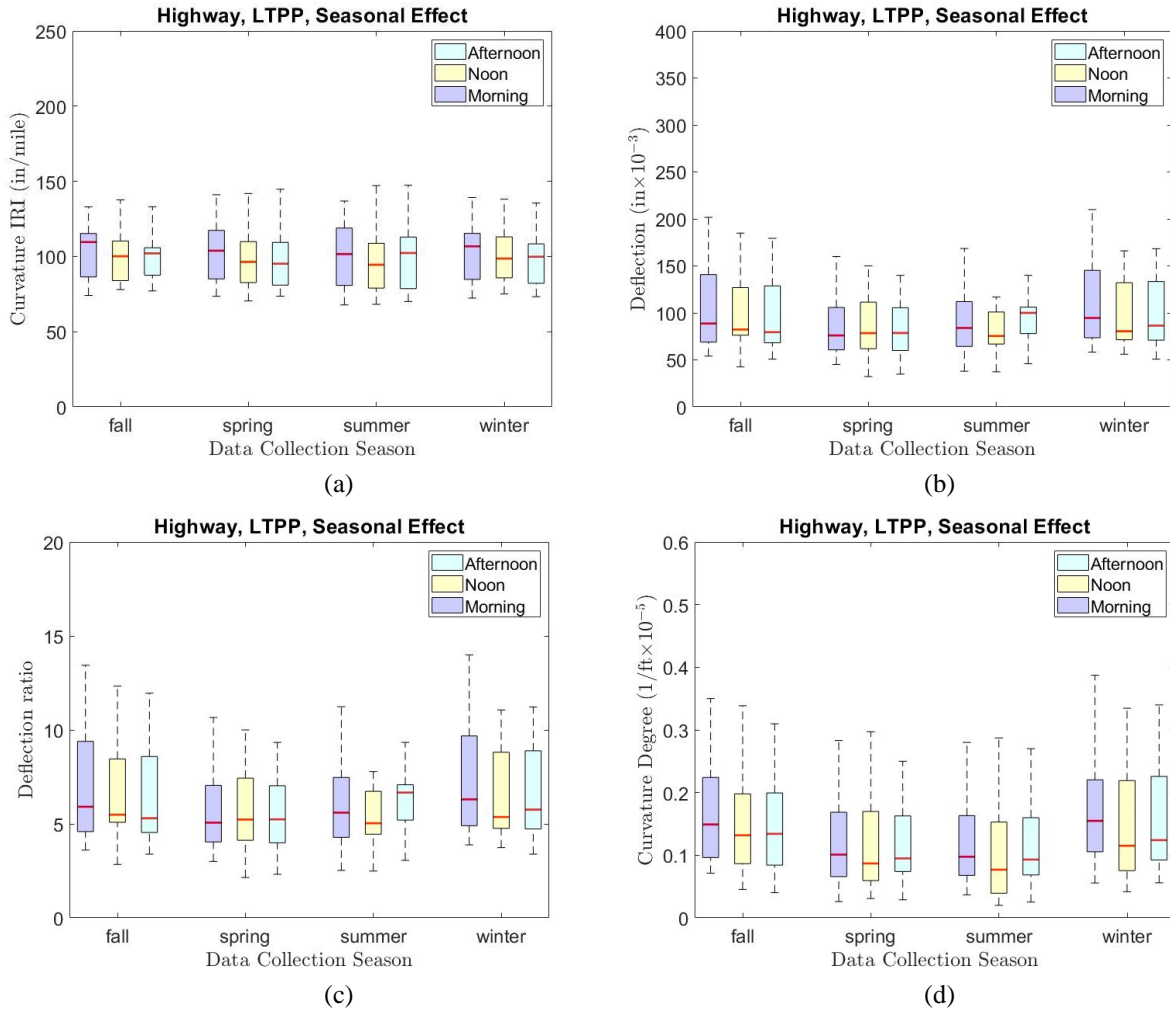


Figure 20. Seasonal effects on LTPP sections: (a) curvature IRI, (b) deflection, (c) deflection ratio, (d) degree of curvature (12 sites, 36 data points for each season)

The key findings for this group are as follows:

- For the LTPP sections, curvature IRI is in the range of 70.5 to 212.6 in./mile in the spring, 67.8 to 213.9 in./mile in the summer, 74.1 to 219.4 in./mile in the fall, and 72.3 to 200.9

in./mile in the winter. Fall has the highest average curvature IRI of 109.2 in./mile, while spring has the lowest average curvature IRI of 106.6 in./mile.

- For the LTPP sections, deflection is in the range of 32.2 to 159.9 x10⁻³ in. in the spring, 37.3 to 200.6 x10⁻³ in. in the summer, 42.6 to 201.6 x10⁻³ in. in the fall, and 50.8 to 209.9 x10⁻³ in. in the winter. Fall has the highest average deflection of 102.8 x10⁻³ in., while spring has the lowest average deflection of 85.6 x10⁻³ in.
- For the LTPP sections, deflection ratio is in the range of 2.15 to 10.66 in the spring, 2.49 to 13.37 in the summer, 2.84 to 13.44 in the fall, and 3.39 to 13.99 in the winter. Fall has the highest average deflection ratio of 6.85, and spring has the lowest average deflection ratio of 5.71.
- For the LTPP sections, degree of curvature is in the range of 0.03 to 0.30 x10⁻⁵ 1/ft in the spring, 0.02 to 0.29 x10⁻⁵ 1/ft in the summer, 0.04 to 0.39 x10⁻⁵ 1/ft in the fall, and 0.05 to 0.22 x10⁻⁵ 1/ft in the winter. Fall has the highest average degree of curvature of 0.154 x10⁻⁵ 1/ft, and spring has the lowest average degree of curvature of 0.119 x10⁻⁵ 1/ft.
- According to the average degrees of curling/warping due to seasonal effects for the LTPP sections (Table 11), curling and warping behavior tends to be slightly lower in the spring than in other seasons, and for all indicators fall has the highest degree of curling/warping.

Table 11. Summary of seasonal effects

Road Type	Season	Avg. Curvature IRI (in./mile)	Avg. Deflection (x10 ⁻³ in.)	Avg. Deflection Ratio	Avg. Degree of Curvature (x10 ⁻⁵ 1/ft)
LTPP	Spring	106.6	85.6	5.71	0.12
	Summer	104.5	91.9	6.13	0.11
	Fall	109.2	102.8	6.85	0.15
	Winter	106.6	101.9	6.82	0.15
Non-LTPP	Spring	91.8	104.7	5.32	0.09
	Summer	87.2	103.0	5.22	0.08
	Fall	92.5	112.4	5.74	0.10
	Winter	91.3	100.4	5.10	0.08
County roads and city streets	Spring	68.0	67.1	4.20	0.05
	Summer	58.4	58.7	4.08	0.06
	Fall	60.9	70.9	4.91	0.07
	Winter	71.0	68.3	4.29	0.05

The non-LTPP group includes 13 non-LTPP highway sites and one LTPP section (0259). Figure 21 shows the seasonal effects on the curling and warping behavior of the non-LTPP sections. All sites were visited in four seasons; more detailed information on the site visits is provided in Appendix A.3.

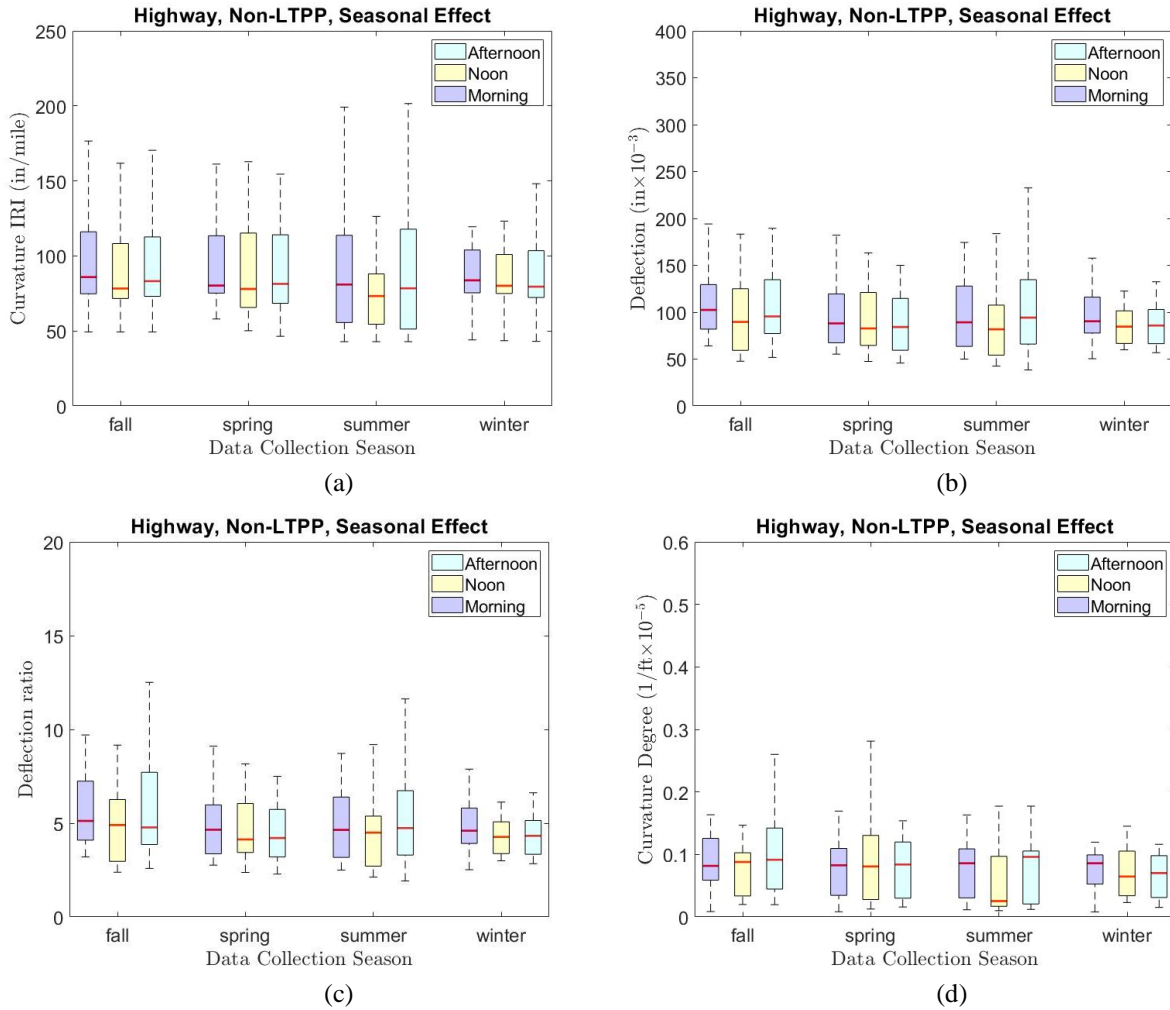


Figure 21. Seasonal effects on non-LTPP sections: (a) curvature IRI, (b) deflection, (c) deflection ratio, (d) degree of curvature (14 sites, 42 data points for each season)

The key findings for this group are as follows:

- For the non-LTPP sections, curvature IRI is in the range of 46.4 to 215.7 in./mile in the spring, 42.9 to 201.6 in./mile in the summer, 49.4 to 176.6 in./mile in the fall, and 43.1 to 171.9 in./mile in the winter. Fall has the highest average curvature IRI of 92.5 in./mile, and summer has the lowest average curvature IRI of 87.2 in./mile.
- For the non-LTPP sections, deflection is in the range of 45.8 to 329.2 $\times 10^{-3}$ in. in the spring, 38.4 to 316.1 $\times 10^{-3}$ in. in the summer, 47.8 to 259.9 $\times 10^{-3}$ in. in the fall, and 50.4 to 263.9 $\times 10^{-3}$ in. in the winter. Fall has the highest average deflection of 112.4 $\times 10^{-3}$ in., and winter has the lowest average deflection of 100.4 $\times 10^{-3}$ in.
- For the non-LTPP sections, deflection ratio is in the range of 2.29 to 16.46 in the spring, 1.92 to 15.81 in the summer, 2.39 to 13.00 in the fall, and 2.52 to 13.19 in the winter. Fall has the highest average deflection ratio of 5.74, and winter has the lowest average deflection ratio of 5.10.

- For the non-LTPP sections, degree of curvature is in the range of 0.01 to 0.33×10^{-5} 1/ft in the spring, 0.01 to 0.32×10^{-5} 1/ft in the summer, 0.01 to 0.29×10^{-5} 1/ft in the fall, and 0.01 to 0.28×10^{-5} 1/ft in the winter. Fall has the highest average degree of curvature of 0.097×10^{-5} 1/ft, and summer has the lowest average degree of curvature of 0.078×10^{-5} 1/ft.
- According to the average degrees of curling/warping due to seasonal effects for the non-LTPP highways (Table 11), fall has the highest curling/warping behavior for all indicators, summer has the lowest curvature IRI and degree of curvature, and winter shows the lowest deflection and deflection ratio values.

The third group comprises five county roads (T26, H21, V62, N54, and E49) and two city streets (Park Ave. and Ashworth Rd.) in Polk County, Iowa. Figure 22 shows the seasonal effects on the curling and warping behavior of these county roads and city streets; more detailed information on the site visits is provided in Appendix A.3.

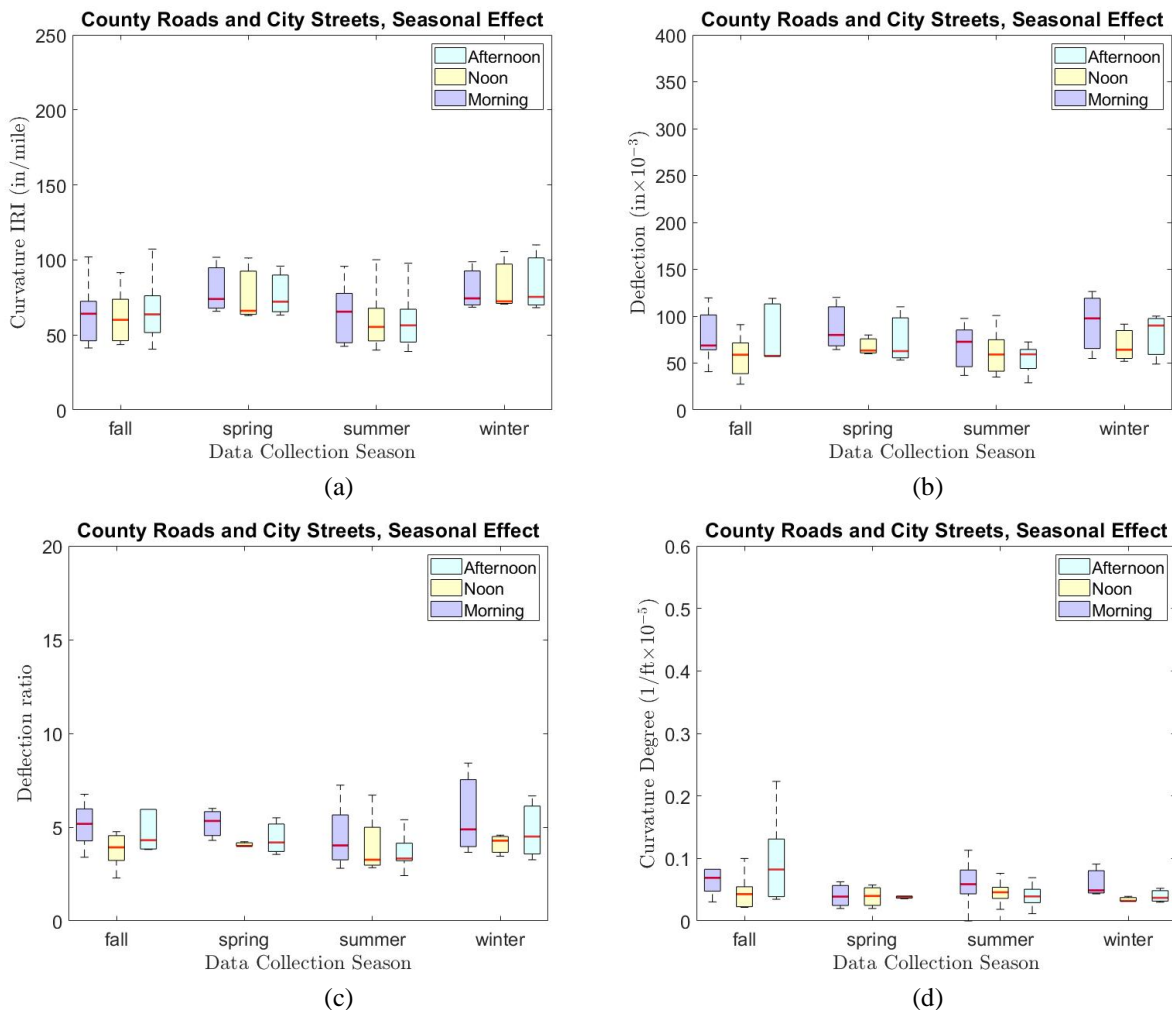


Figure 22. Seasonal effects on county roads and city streets: (a) curvature IRI, (b) deflection, (c) deflection ratio, (d) degree of curvature (7 sites, 21 data points for each season)

The key findings for this group are as follows:

- For county roads and city streets, curvature IRI is in the range of 36.2 to 101.7 in./mile in the spring, 35.3 to 103.2 in./mile in the summer, 34.1 to 107.2 in./mile in the fall, and 33.9 to 110.0 in./mile in the winter. Winter has the highest average curvature IRI of 71.0 in./mile, and summer has the lowest average curvature IRI of 58.4 in./mile.
- For county roads and city streets, deflection is in the range of 29.7 to 120.0 $\times 10^{-3}$ in. in the spring, 29.0 to 128.1 $\times 10^{-3}$ in. in the summer, 43.51 to 99.3 $\times 10^{-3}$ in. in the fall, and 29.7 to 126.3 $\times 10^{-3}$ in. in the winter. Fall has the highest average deflection of 70.9 $\times 10^{-3}$ in., and summer has the lowest average deflection of 58.7 $\times 10^{-3}$ in.
- For county roads and city streets, deflection ratio is in the range of 2.47 to 6.00 in the spring, 2.42 to 10.68 in the summer, 2.29 to 10.84 in the fall, and 2.48 to 8.42 in the winter. Fall has the highest average deflection ratio of 4.91, and summer has the lowest average deflection ratio of 4.08.
- For county roads and city streets, degree of curvature is in the range of 0.02 to 0.10 $\times 10^{-5}$ 1/ft in the spring, 0.01 to 0.29 $\times 10^{-5}$ 1/ft in the summer, 0.01 to 0.22 $\times 10^{-5}$ 1/ft in the fall, and 0.03 to 0.09 $\times 10^{-5}$ 1/ft in the winter. Fall has the highest average degree of curvature of 0.072 $\times 10^{-5}$ 1/ft, and spring has the lowest average degree of curvature of 0.048 $\times 10^{-5}$ 1/ft.
- According to the average degree of curling/warping for seasonal effects on county roads and city streets (Table 11), curling and warping behavior tends to be relatively higher in the fall and summer in the spring.

Figure 23 shows the summarized seasonal effects on different site groups. The fall season exhibited the highest curling and warping behavior based on the average values of all indicators.

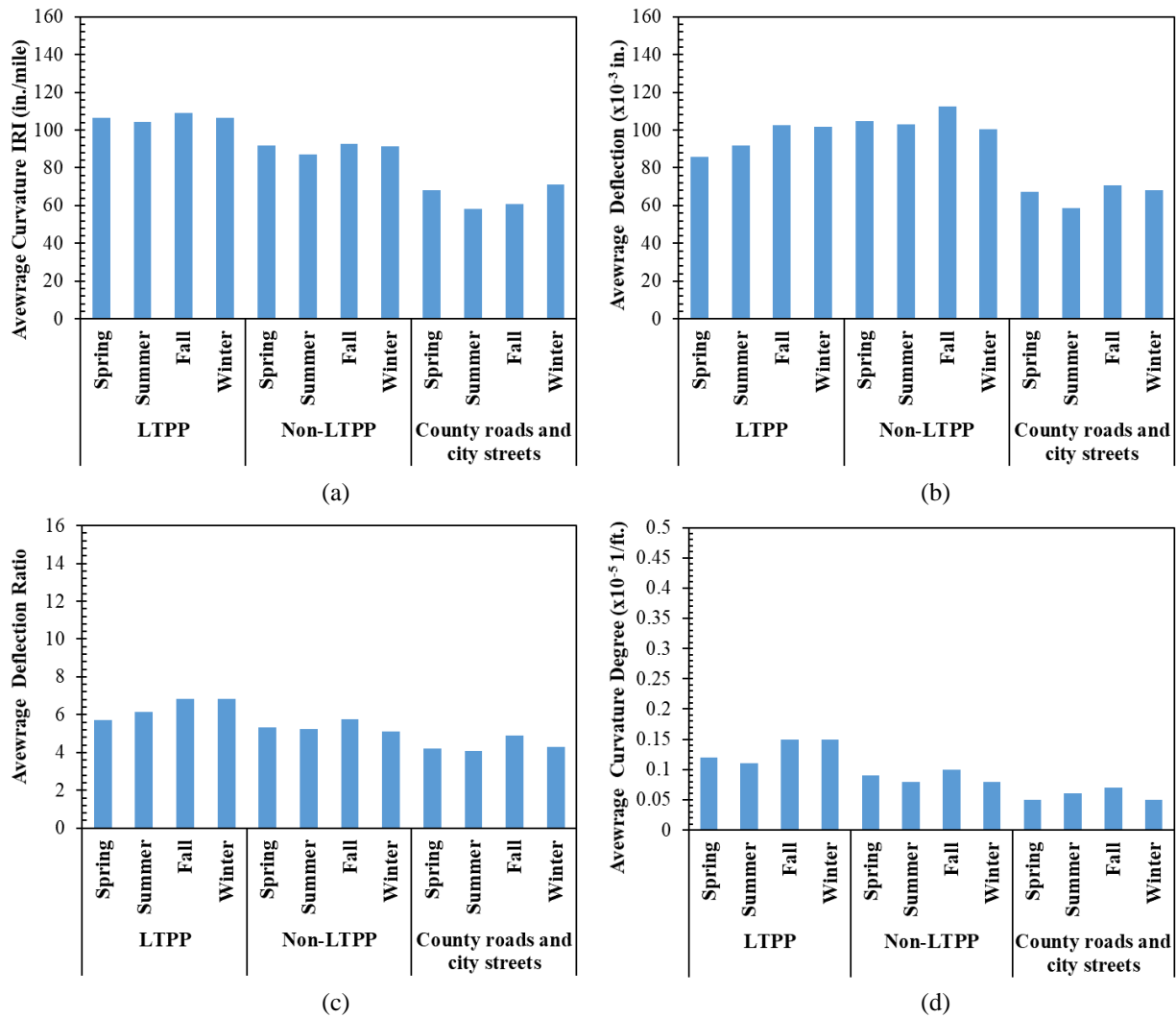


Figure 23. Summary of seasonal effects on (a) curvature IRI, (b) deflection, (c) deflection ratio, (d) degree of curvature

4.2.1.3. Diurnal Effects

During each site visit, profile data were collected at three different times of day: early morning (7:30 a.m. to 9:00 a.m. CST), noon (12:00 p.m. to 1:30 p.m. CST), and late afternoon (4:30 p.m. to 6:00 p.m. CST).

Figure 24 shows the diurnal effects on the curling and warping behavior of the LTPP sections.

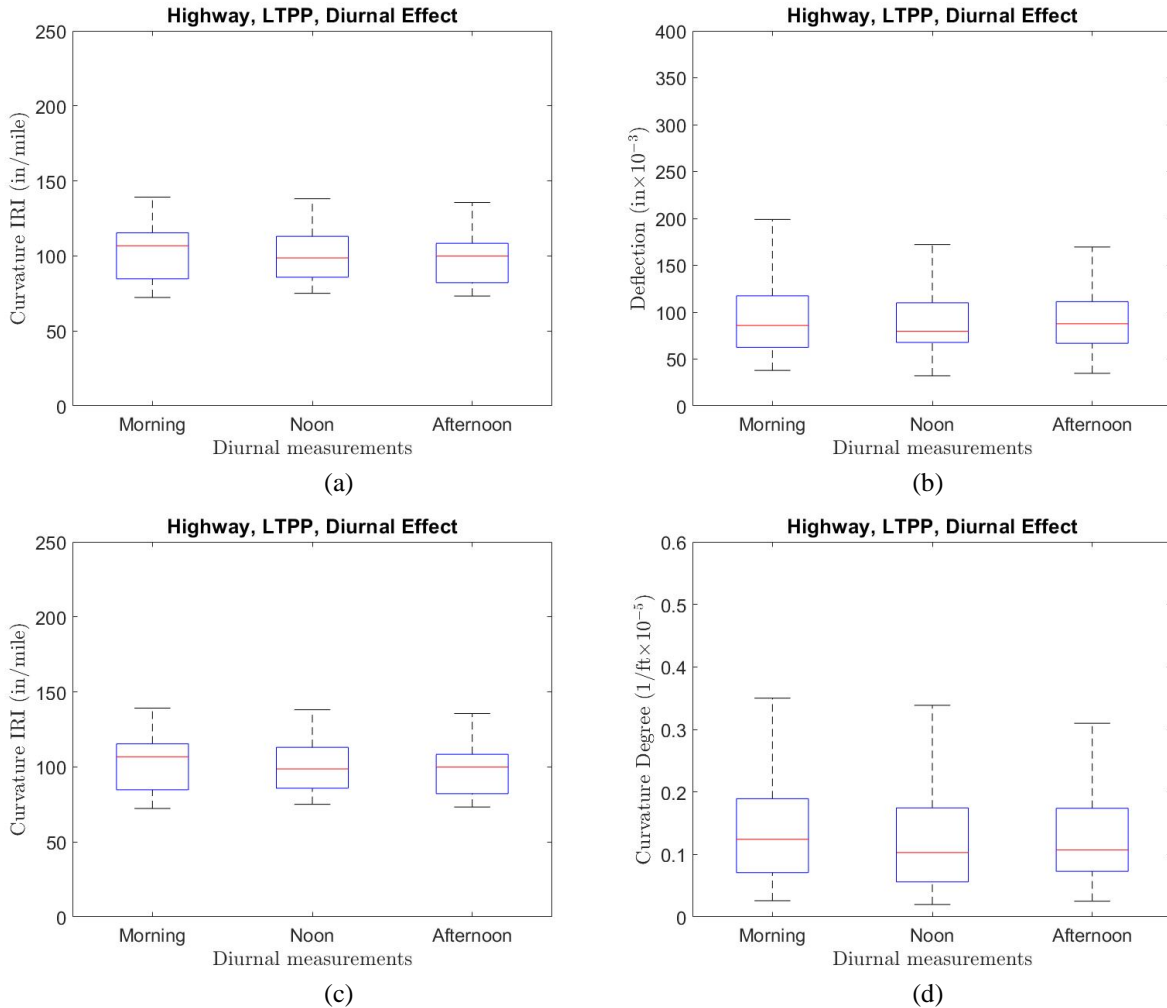


Figure 24. Diurnal effects on LTPP sections: (a) curvature IRI, (b) deflection, (c) deflection ratio, (d) degree of curvature (12 sites, 72 data points for each time)

The key findings for this group are as follows:

- For the LTPP sections, curvature IRI is in the range of 67.8 to 213.9 in./mile in the morning, 68.2 to 219.4 in./mile at noon, and 70.1 to 204.5 in./mile in the afternoon.
- For the LTPP sections, deflection is in the range of 37.9 to 209.9 $\times 10^{-3}$ in., 32.2 to 185.0 $\times 10^{-3}$ in. at noon, and 34.8 to 179.3 $\times 10^{-3}$ in. in the afternoon.
- For the LTPP sections, deflection ratio is in the range of 2.53 to 13.99 in the morning, 2.15 to 13.33 at noon, and 2.32 to 11.95 in the afternoon.
- For the LTPP sections, degree of curvature is in the range of 0.03 to 0.39 $\times 10^{-5}$ 1/ft in the morning, 0.02 to 0.34 $\times 10^{-5}$ 1/ft at noon, and 0.03 to 0.34 $\times 10^{-5}$ 1/ft in the afternoon.
- The average degree of curling/warping due to diurnal effects for the LTPP sections (Table 12) shows that curling and warping behavior is relatively higher in the early morning for all indicators.

Table 12. Summary of diurnal effects

Road Type	Time of Day	Avg. Curvature IRI (in./mile)	Avg. Deflection ($\times 10^{-3}$ in)	Avg. Deflection Ratio	Avg. Degree of Curvature ($\times 10^{-5}$ 1/ft)
LTPP	Morning	108.6	96.6	6.44	0.14
	Noon	104.7	90.2	6.01	0.12
	Afternoon	104.0	92.5	6.17	0.13
Non-LTPP	Morning	93.0	109.7	5.57	0.09
	Noon	87.4	99.3	5.04	0.08
	Afternoon	92.5	105.6	5.37	0.09
County roads and city streets	Morning	63.2	72.3	4.86	0.07
	Noon	60.8	60.5	4.13	0.06
	Afternoon	62.3	59.9	4.02	0.06

Figure 25 shows the diurnal effects on the curling and warping behavior of the non-LTPP sections.

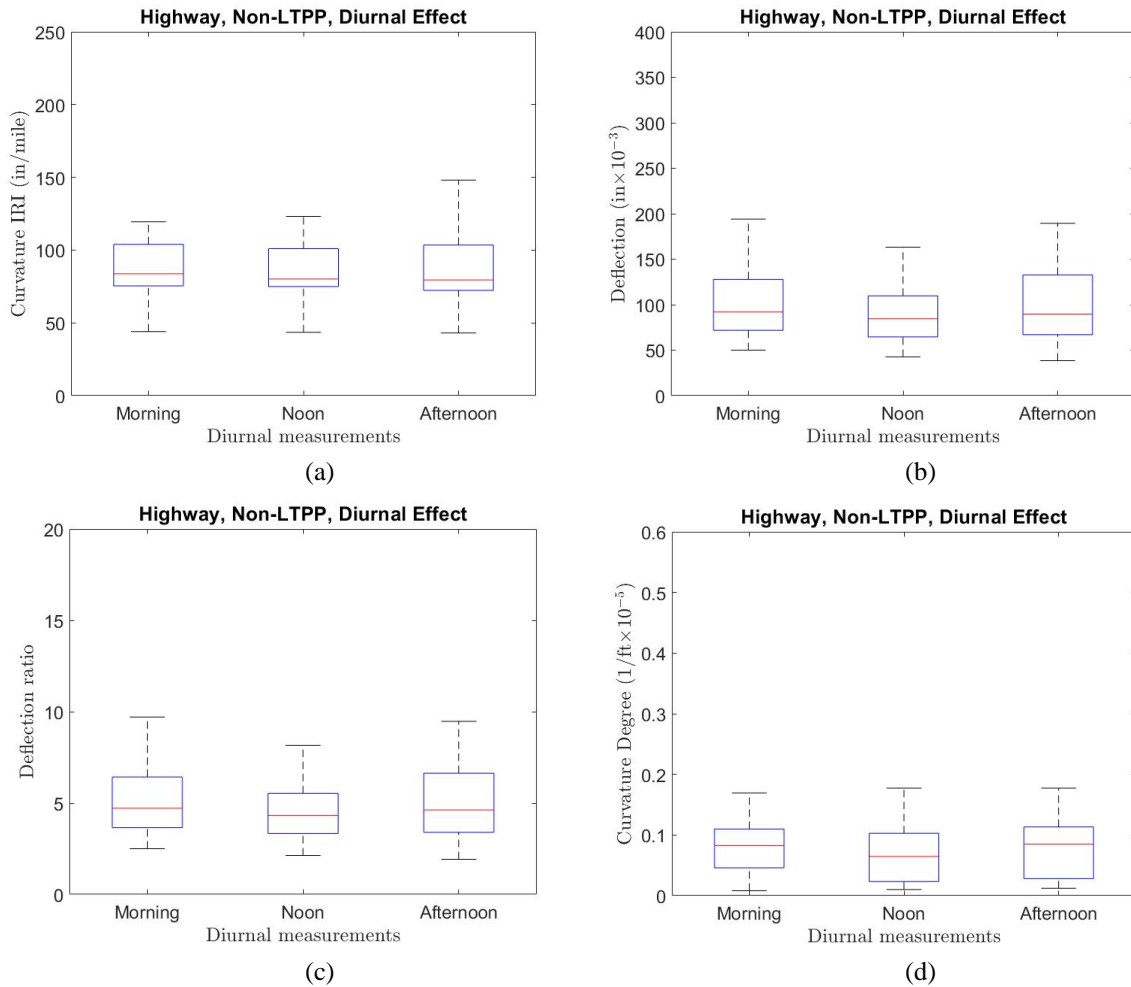


Figure 25. Diurnal effects on non-LTPP sections: (a) curvature IRI, (b) deflection, (c) deflection ratio, (d) degree of curvature (14 sites, 66 data points for each time)

The key findings for this group are as follows:

- For the non-LTPP sections, curvature IRI is in the range of 42.9 to 215.7 in./mile in the morning, 42.9 to 194.6 in./mile at noon, and 42.9 to 203.2 in./mile in the afternoon.
- For the non-LTPP sections, deflection is in the range of 50.0 to 329.2 $\times 10^{-3}$ in. in the morning, 42.6 to 304.1 $\times 10^{-3}$ in. at noon, and 38.4 to 310.8 $\times 10^{-3}$ in. in the afternoon.
- For the non-LTPP sections, deflection ratio is in the range of 2.50 to 16.46 in the morning, 2.13 to 15.21 at noon, and 1.92 to 15.54 in the afternoon.
- For the non-LTPP sections, degree of curvature is in the range of 0.01 to 0.33 $\times 10^{-5}$ 1/ft in the morning, 0.01 to 0.31 $\times 10^{-5}$ 1/ft at noon, and 0.01 to 0.27 $\times 10^{-5}$ 1/ft in the afternoon.
- As shown in the average degree of curling/warping due to diurnal effects for the non-LTPP sections (Table 12), curling and warping behavior tends to be relatively higher in the early morning for all indicators.

Figure 26 shows the diurnal effects on the curling and warping behavior of county roads and city streets.

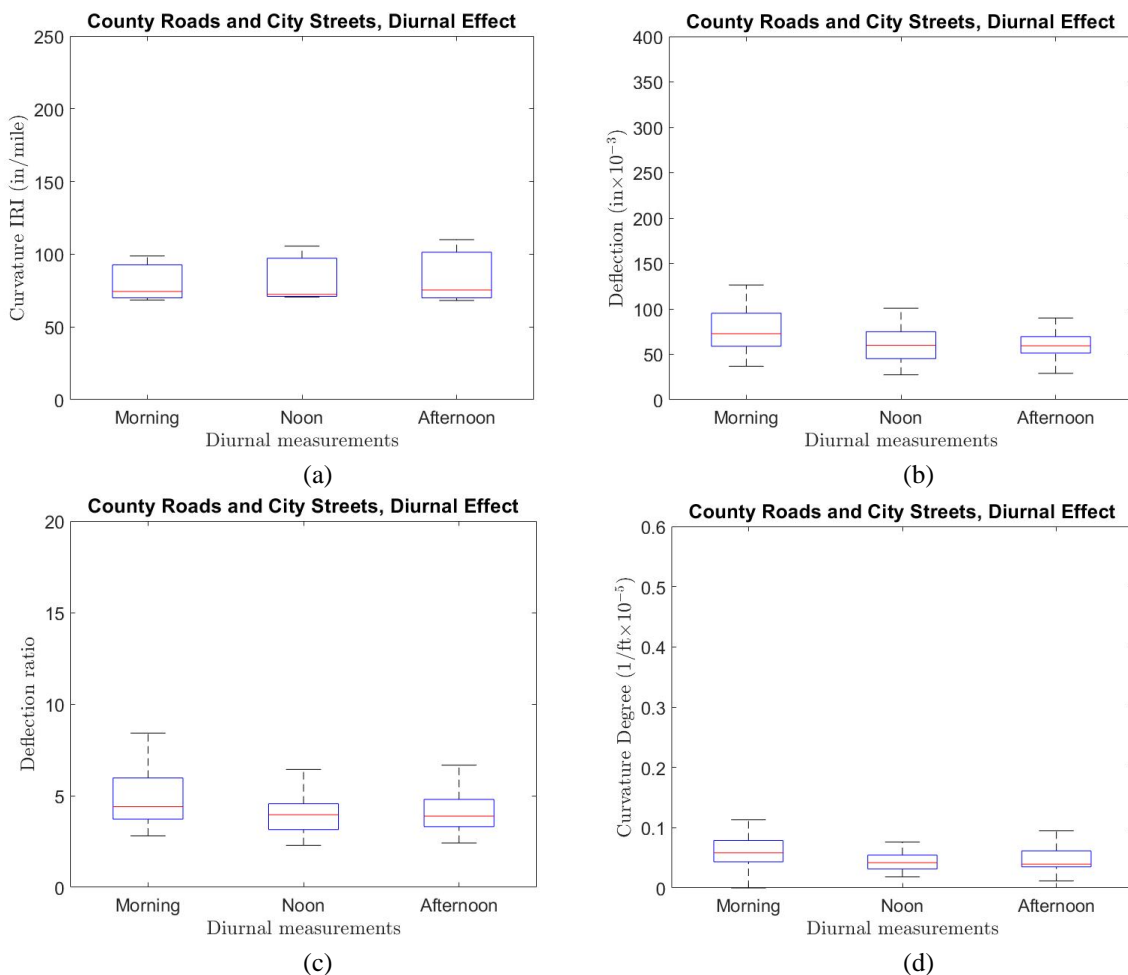


Figure 26. Diurnal effects on county roads and city streets: (a) curvature IRI, (b) deflection, (c) deflection ratio, (d) degree of curvature (7 sites, 29 data points for each time)

The key findings for this group are as follows:

- For county roads and city streets, curvature IRI is in the range of 35.3 to 102.0 in./mile in the morning, 33.9 to 105.6 in./mile at noon, and 36.2 to 110.0 in./mile in the afternoon.
- For county roads and city streets, deflections in the morning, noon, and afternoon range from 29.7 to 128.1 $\times 10^{-3}$, 27.5 to 130.1 $\times 10^{-3}$, and 29.0 to 119.0 $\times 10^{-3}$ in., respectively
- For county roads and city streets, deflection ratios in the morning, noon, and afternoon range from 2.47 to 10.68, 2.29 to 10.84, and 2.42 to 9.43, respectively.
- For county roads and city streets, degree of curvature is in the range of 0.01 to 0.29 $\times 10^{-5}$ 1/ft in the morning, 0.02 to 0.17 $\times 10^{-5}$ 1/ft at noon, and 0.01 to 0.22 $\times 10^{-5}$ 1/ft in the afternoon.
- As shown in the average degree of curling/warping due to diurnal effects for county roads and city streets (Table 12), morning shows relatively higher values of curling and warping for all indicators.

4.2.1.4. Slab Width Effects

For the LTPP sections (Figure 27), six sections (0218, 0219, 0215, 0214, 0222, and 0223) have 12 ft and six sections (0217, 0220, 0216, 0213, 0221, and 0224) have 14 ft slab widths.

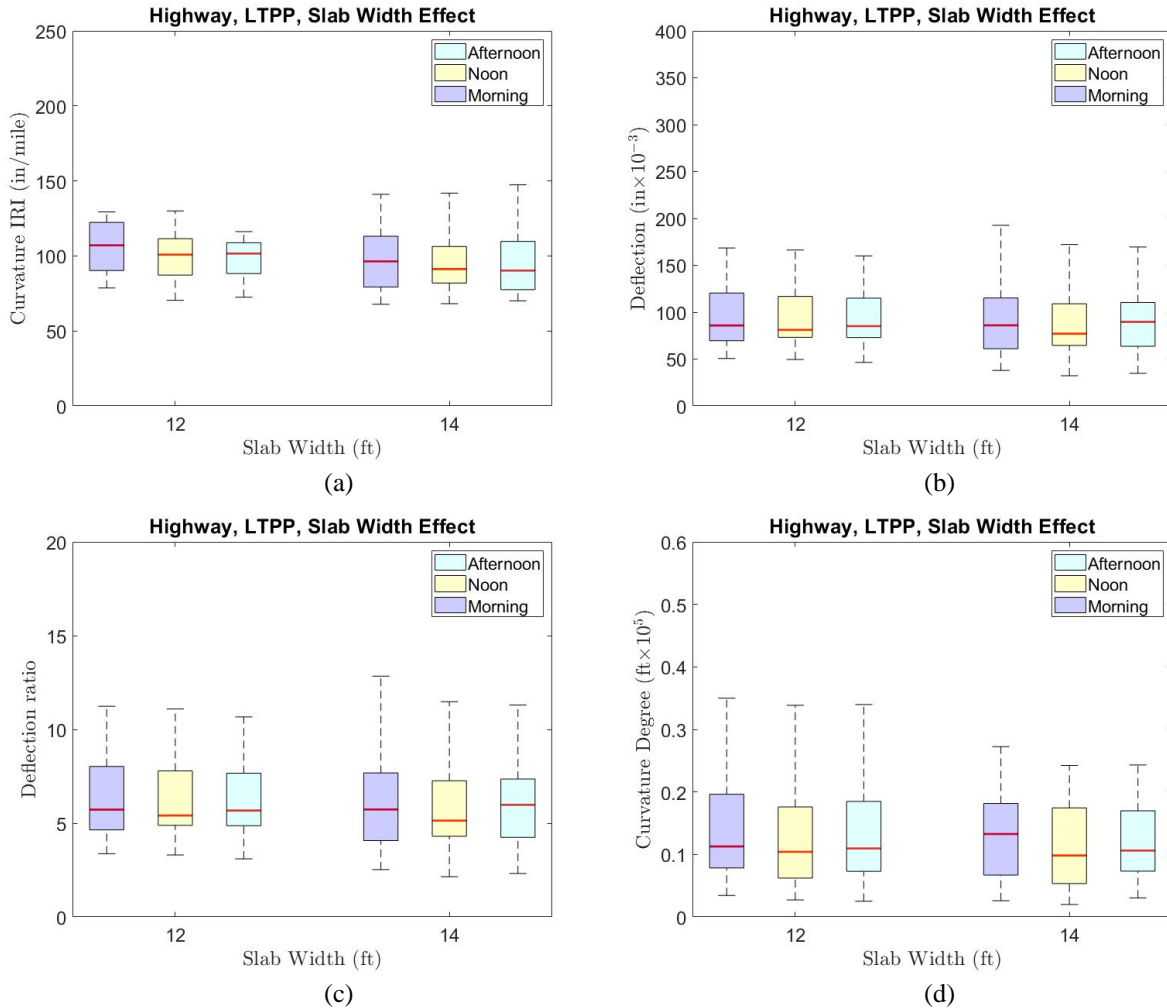


Figure 27. Slab width effects on LTPP sections: (a) curvature IRI, (b) deflection, (c) deflection ratio, (d) degree of curvature (12 ft width [6 sites, 108 data points], 14 ft width [6 sites, 108 data points])

The key findings for this group are as follows:

- For the LTPP sections, the curvature IRI is in the range of 70.5 to 219.4 in./mile for 12 ft wide slabs and 67.8 to 147.4 in./mile for 14 ft wide slabs.
- For the LTPP sections, the deflection is in the range of 46.5 to 209.9 $\times 10^{-3}$ in. for 12 ft wide slabs and 32.2 to 198.9 $\times 10^{-3}$ in. for 14 ft wide slabs.
- For the LTPP sections, the deflection ratio is in the range of 3.10 to 13.99 for 12 ft wide slabs and 2.15 to 13.26 for 14 ft wide slabs.
- For the LTPP sections, the degree of curvature ranges from 0.03 to 0.39 $\times 10^{-5}$ 1/ft for 12 ft wide slabs and 0.02 to 0.27 $\times 10^{-5}$ 1/ft for 14 ft wide slabs.
- As shown in the average degree of curling/warping due to slab width effects for the LTPP sections (Table 13), all curling and warping indicators tend to be highest for 12 ft slab widths.

Table 13. Summary of slab width effects

Road Type	Width	Avg. Curvature IRI (in./mile)	Avg. Deflection ($\times 10^{-3}$ in)	Avg. Deflection Ratio	Avg. Degree of Curvature ($\times 10^{-5}$ 1/ft)
LTPP	12 ft Width	114.1	96.5	6.40	0.14
	14 ft Width	97.4	89.7	5.98	0.12
Non-LTPP	12 ft Width	82.2	81.5	5.43	0.05
	13 ft Width	46.3	64.2	3.21	0.03
	14 ft Width	93.9	108.7	5.44	0.09
County roads and city streets	11 ft Width	54.9	65.8	4.20	0.06
	12 ft Width	68.5	61.5	4.50	0.07
	13 ft Width	68.8	64.9	4.32	0.05

The non-LTPP sections feature three different slab widths (12, 13, and 14 ft). US 63 in Wapello County was constructed with a 12 ft slab width, US 20 in Black Hawk County was built with a 13 ft slab width, and other non-LTPP highways were all constructed with a 14 ft slab width. Figure 28 shows the slab width effects on the curling and warping behavior of the non-LTPP sites.

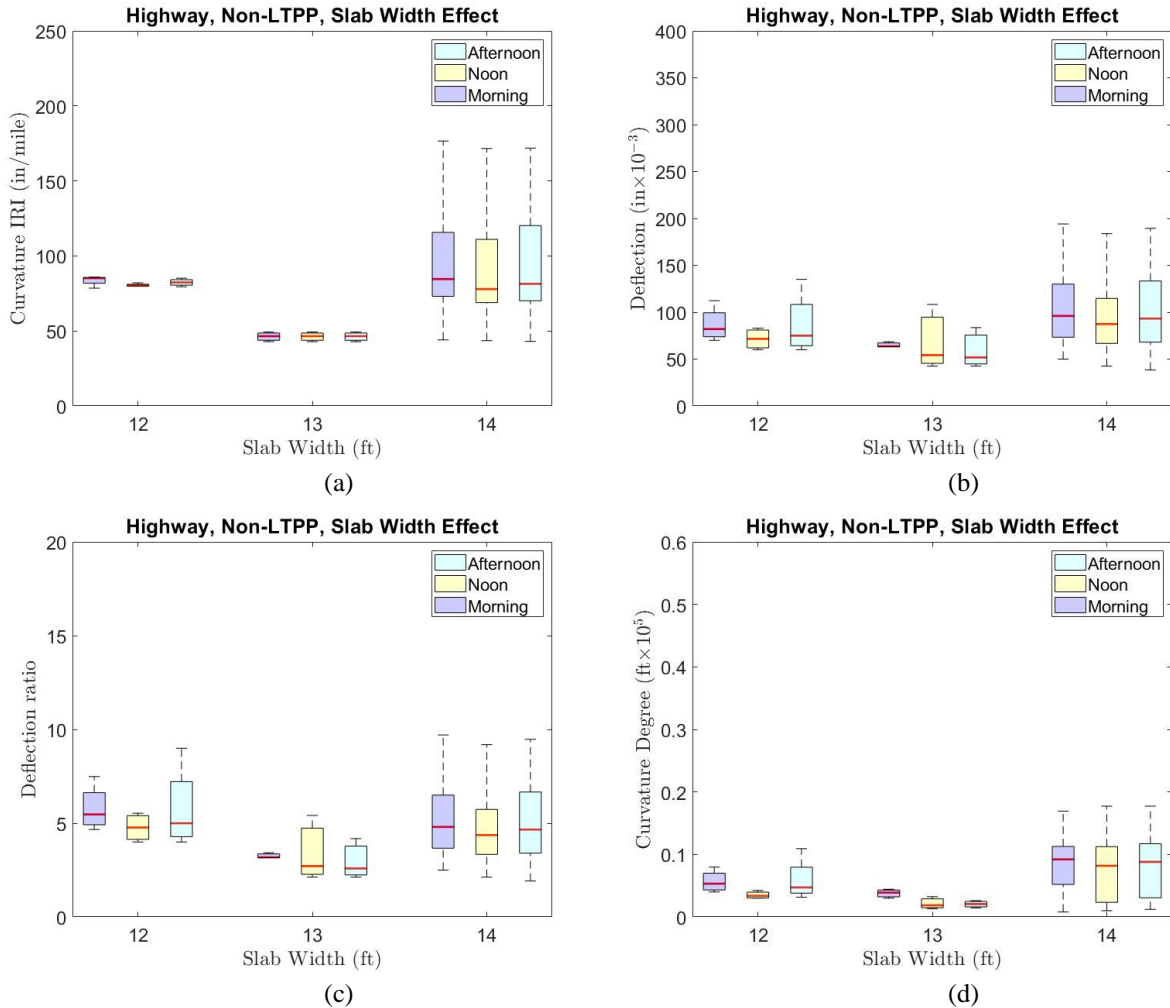


Figure 28. Slab width effects on non-LTPP sections: (a) curvature IRI, (b) deflection, (c) deflection ratio, (d) degree of curvature (12 ft slab width [1 site, 12 data points], 13 ft slab width [1 site, 9 data points], 14 ft slab width [12 sites, 174 data points])

The key findings for this group are as follows:

- For the non-LTPP sections, the curvature IRI is in the range of 78.5 to 85.9 in./mile for the 12 ft wide slab, 42.9 to 49.4 in./mile for the 13 ft wide slab, and 43.1 to 215.7 in./mile for the 14 ft wide slabs.
- For the non-LTPP sections, the deflection is in the range of 62.0 to 135.0 $\times 10^{-3}$ in. for the 12 ft wide slab, 42.6 to 108.3 $\times 10^{-3}$ in. for the 13 ft wide slab, and 38.4 to 329.2 $\times 10^{-3}$ for the 14 ft wide slabs.
- For the non-LTPP sections, the deflection ratio is in the range of 4.00 to 9.00 for the 12 ft wide slab, 2.13 to 5.41 for the 13 ft wide slab, and 1.92 to 16.46 for the 14 ft wide slabs.
- For the non-LTPP sections, the degree of curvature is in the range of 0.03 to 0.11 $\times 10^{-5}$ 1/ft for the 12 ft wide slab, 0.01 to 0.04 $\times 10^{-5}$ 1/ft for the 13 ft wide slab, and 0.01 to 0.33 $\times 10^{-5}$ 1/ft for the 14 ft wide slabs.

- As shown in the average degree of curling/warping due to slab width effects for the non-LTPP sections (Table 13), curling and warping behavior tends to be highest for 14 ft slab widths for all indicators.

The county roads and city streets include three slab widths (11, 12, and 13 ft). Figure 29 shows the slab width effects on the curling and warping behavior of county roads and city streets.

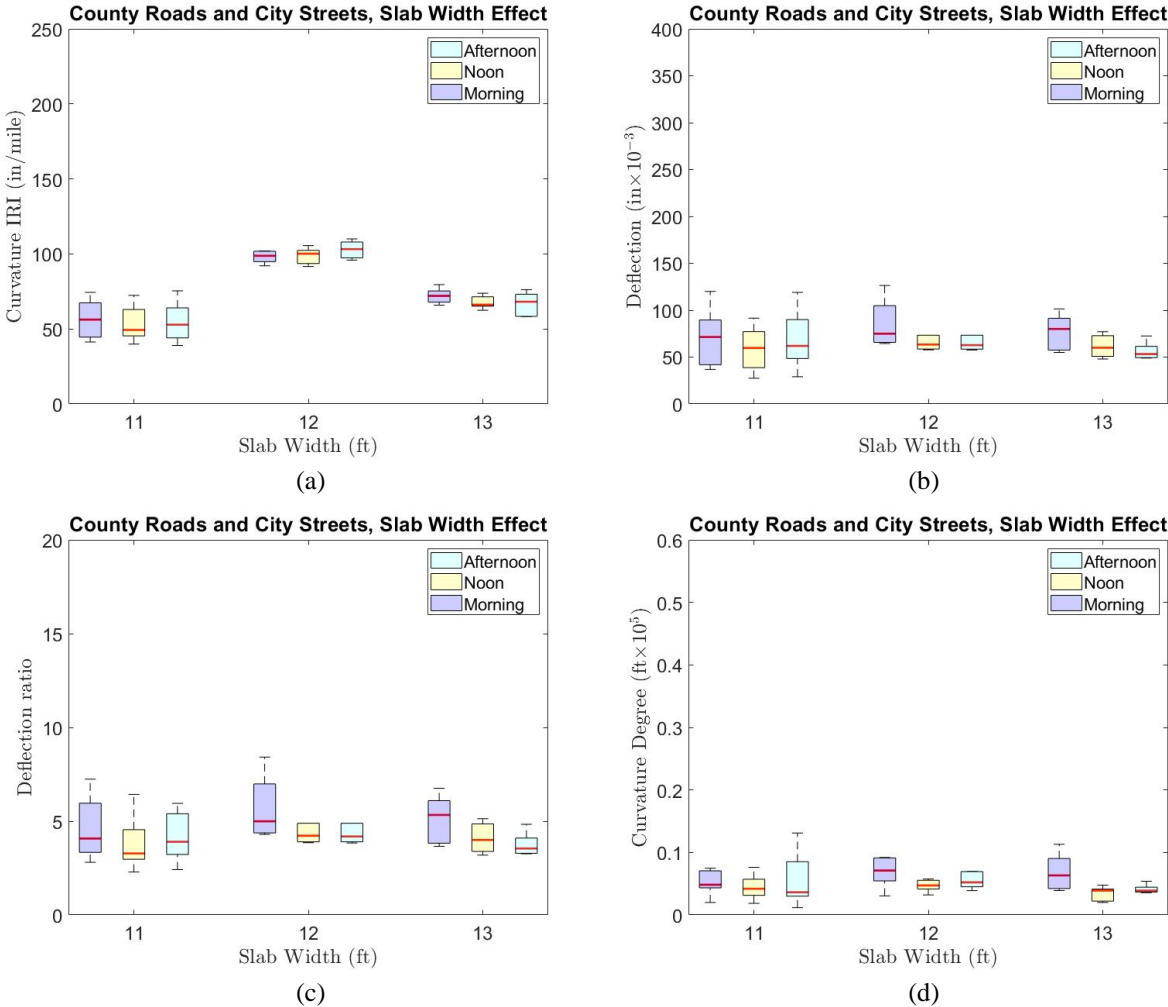


Figure 29. Slab width effects on county roads and city streets: (a) curvature IRI, (b) deflection, (c) deflection ratio, (d) degree of curvature (11 ft slab width [4 sites, 39 data points], 12 ft slab width [2 sites, 30 data points], 13 ft slab width [1 site, 15 data points])

The key findings for this group are as follows:

- For county roads and city streets, the curvature IRI ranges from 39.0 to 75.4 in./mile for the 11 ft wide slabs, 33.9 to 110.0 in./mile for the 12 ft wide slabs, and 58.2 to 79.5 in./mile for the 13 ft wide slab.

- For county roads and city streets, the deflection ranges from 27.5 to 120.0 $\times 10^{-3}$ in. for the 11 ft wide slabs, 29.5 to 130.1 $\times 10^{-3}$ in. for the 12 ft wide slabs, and 47.9 to 101.4 $\times 10^{-3}$ in. for the 13 ft wide slab.
- For county roads and city streets, the deflection ratio ranges from 2.29 to 9.43 for the 11 ft wide slabs, 2.46 to 10.84 for the 12 ft wide slabs, and 3.19 to 6.76 for the 13 ft wide slab.
- For county roads and city streets, the degree of curvature ranges from 0.01 to 0.29 $\times 10^{-5}$ 1/ft for the 11 ft wide slabs, 0.01 to 0.20 $\times 10^{-5}$ 1/ft for the 12 ft wide slabs, and 0.02 to 0.11 $\times 10^{-5}$ 1/ft for the 13 ft wide slab.
- As shown in the average degree of curling/warping due to slab width effects for the county roads and city streets (Table 13), the 12 ft wide slabs have the highest deflection ratio and degree of curvature, the 11 ft wide slabs show the highest deflection, and the 13 ft wide slab presents the highest curvature IRI values.

4.2.1.5. Slab Thickness Effects

The LTPP sections include two slab thicknesses (8 and 11 in.). Sections 0217, 0218, 0213, 0214, 0221, and 0222 were constructed with an 8 in. slab thickness. Sections 0219, 0220, 0215, 0216, 0223, and 0224 were constructed with an 11 in. slab thickness. Figure 30 shows the slab thickness effects on the curling and warping behavior of the LTPP sites.

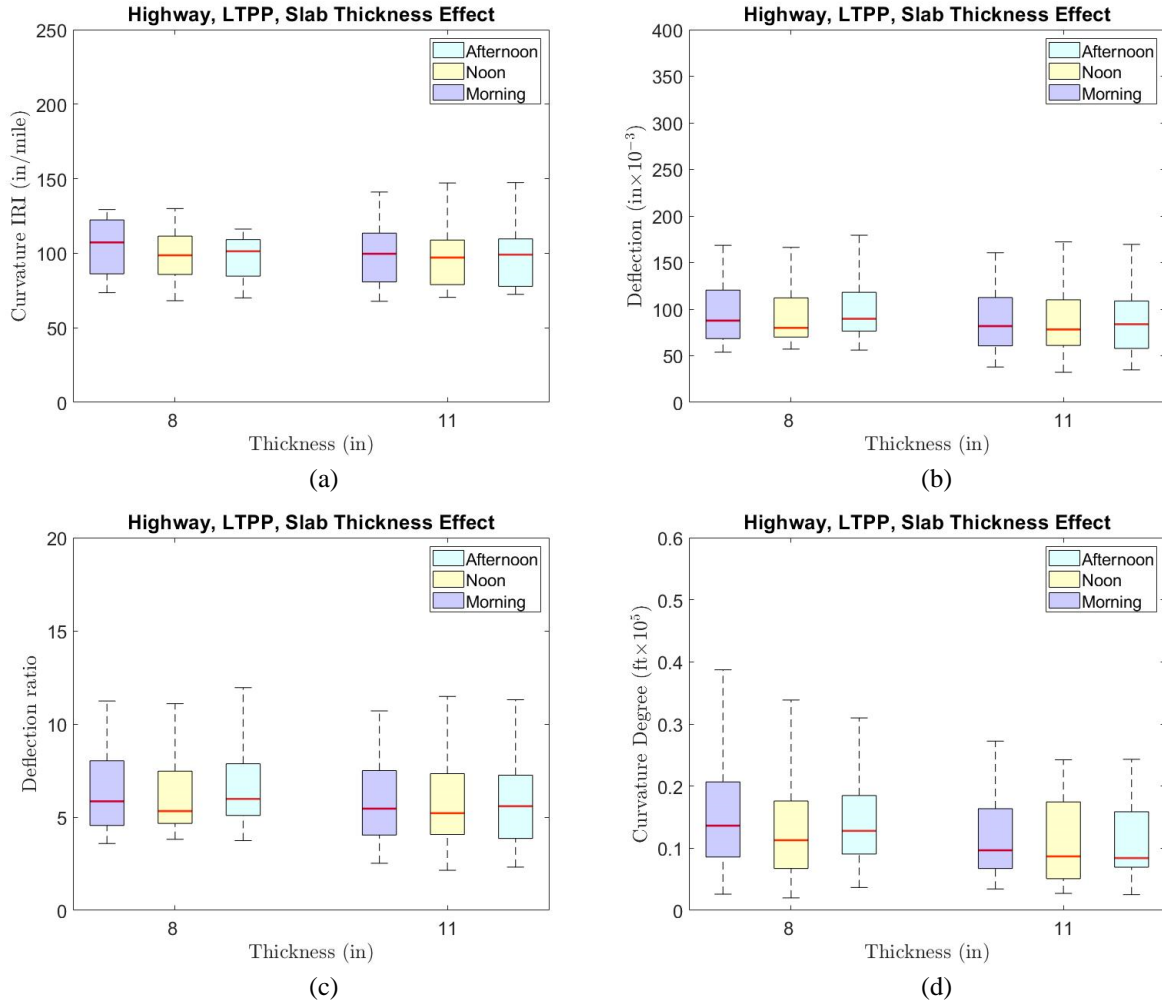


Figure 30. Slab thickness effects on LTPP sections: (a) curvature IRI, (b) deflection, (c) deflection ratio, (d) degree of curvature (8 in. thickness [6 sites, 108 data points], 11 in. thickness [6 sites, 108 data points])

The key findings for this group are as follows:

- For the LTPP sections, the curvature IRI is in the range of 68.2 to 219.4 in./mile for 8 in. thick slabs and 67.8 to 147.4 in./mile for 11 in. thick slabs.
- For the LTPP sections, the deflection is in the range of 53.8 to 209.9 $\times 10^{-3}$ in. for 8 in. thick slabs and 32.2 to 198.9 $\times 10^{-3}$ in. for 11 in. thick slabs.
- For the LTPP sections, the deflection ratio is in the range of 3.59 to 13.99 for 8 in. thick slabs and 2.15 to 13.26 for 11 in. thick slabs.
- For the LTPP sections, the degree of curvature is in the range of 0.02 to 0.39 $\times 10^{-5}$ 1/ft for 8 in. thick slabs and 0.03 to 0.27 $\times 10^{-5}$ 1/ft for 11 in. thick slabs.
- Curling and warping behavior tends to be highest in slabs with an 8 in. thickness according to the average degree of curling/warping due to slab thickness effects for the LTPP sections (Table 14).

Table 14. Summary of slab thickness effects

Road Type	Slab Thickness	Avg. Curvature IRI (in./mile)	Avg. Deflection ($\times 10^{-3}$ in)	Avg. Deflection Ratio	Avg. Degree of Curvature ($\times 10^{-5}$ 1/ft)
LTPP	8 in. Thickness	113.2	97.9	6.53	0.15
	11 in. Thickness	98.4	88.3	5.89	0.11
Non-LTPP	10 in. Thickness	106.2	122.9	6.15	0.11
	11 in. Thickness	53.8	61.9	3.10	0.02
County roads and city streets	6 in. Thickness	50.1	54.3	4.52	0.11
	8 in. Thickness	50.2	62.3	4.10	0.06
	10 in. Thickness	84.3	69.7	4.65	0.05

The non-LTPP sections include two slab thicknesses (10 and 11 in.). Ten sites were constructed with a 10 in. slab thickness, and two sites were constructed with an 11 in. slab thickness (I-35 in Story County and US 20 in Black Hawk County). Figure 31 shows the slab thickness effects on the curling and warping behavior of the non-LTPP sites.

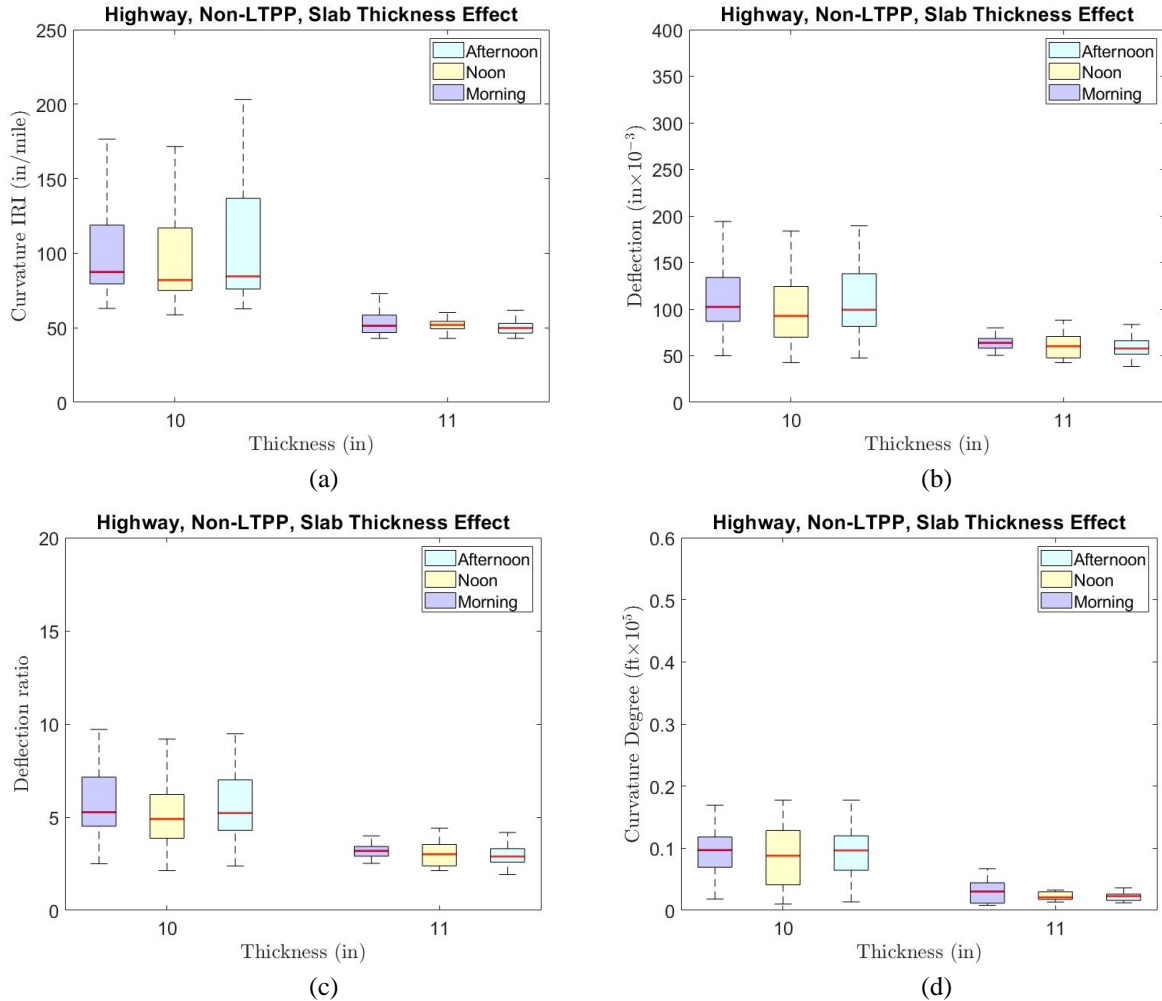


Figure 31. Slab thickness effects on non-LTPP sections: (a) curvature IRI, (b) deflection, (c) deflection ratio, (d) degree of curvature (10 in. thickness [10 sites, 138 data points], 11 in. thickness [2 sites, 33 data points])

The key findings for this group are as follows:

- For the non-LTPP sections, the curvature IRI is in the range of 58.7 to 215.7 in./mile for 10 in. thick slabs and 43.1 to 73.1 in./mile for 11 in. thick slabs.
- For the non-LTPP sections, the deflection is in the range of 42.6 to 329.2 $\times 10^{-3}$ in. for 10 in. thick slabs and 38.4 to 88.2 $\times 10^{-3}$ in. for 11 in. thick slabs.
- For the non-LTPP sections, the deflection ratio is in the range of 2.13 to 16.46 for 10 in. thick slabs and 1.92 to 4.41 for 11 in. thick slabs.
- For the non-LTPP sections, the degree of curvature is in the range of 0.01 to 0.33 $\times 10^{-5}$ 1/ft for 10 in. thick slabs and 0.01 to 0.07 $\times 10^{-5}$ 1/ft for 11 in. thick slabs.
- As shown in the average degree of curling/warping due to slab thickness effects for the non-LTPP sections (Table 14), curling and warping behavior tends to be highest in slabs with a 10 in. thickness for all indicators.

The county roads and city streets include three slab thicknesses (6, 8, 10 in.). Figure 32 shows the slab thickness effects on the curling and warping behavior of county roads and city streets.

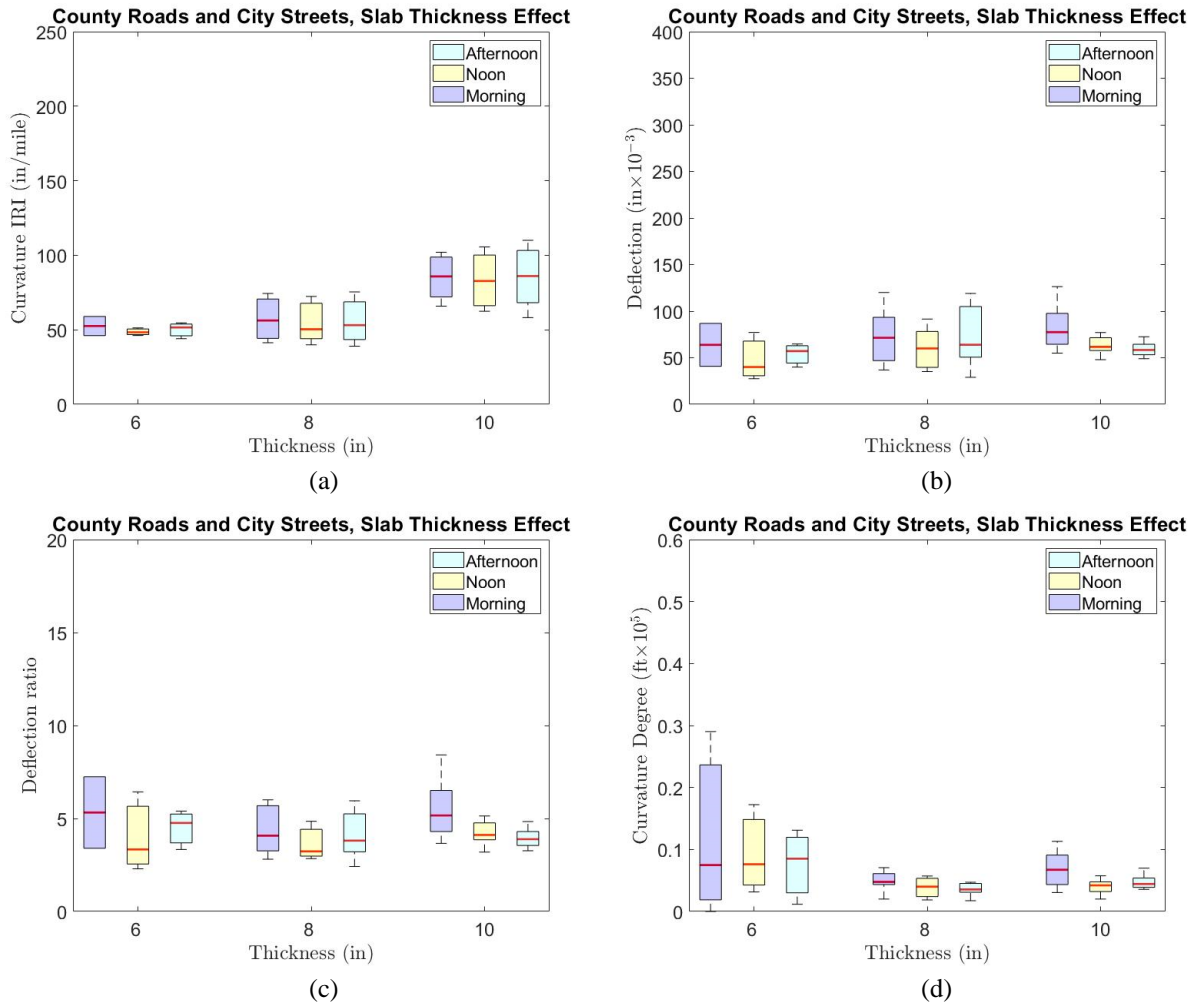


Figure 32. Slab thickness effects on county roads and city streets: (a) curvature IRI, (b) deflection, (c) deflection ratio, (d) degree of curvature (6 in. thickness [1 site, 8 data points], 8 in. thickness [4 sites, 48 data points], 10 in. thickness [2 sites, 30 data points])

The key findings for this group are as follows:

- For county roads and city streets, the curvature IRI ranges from 44.1 to 58.9 in./mile for the 6 in. thick slab, 33.9 to 75.4 in./mile for the 8 in. thick slabs, and 58.2 to 110.0 in./mile for the 10 in. thick slabs.
- For county roads and city streets, the deflection is in the range of 27.5 to 86.9 $\times 10^{-3}$ in. for the 6 in. thick slab, 29.0 to 130.1 $\times 10^{-3}$ in. for the 8 in. thick slabs, and 47.9 and 126.3 $\times 10^{-3}$ in. for the 10 in. thick slabs.
- For county roads and city streets, the deflection ratio is in the range of 2.29 to 7.24 for the 6 in. thick slab, 2.42 to 10.84 for the 8 in. thick slabs, and 3.19 to 8.24 for the 10 in. thick slabs.

- For county roads and city streets, the degree of curvature ranges from 0.01 to 0.29×10^{-5} 1/ft for the 6 in. thick slab, 0.01 to 0.22×10^{-5} 1/ft for the 8 in. thick slabs, and 0.02 to 0.11×10^{-5} 1/ft for the 10 in. thick slabs.
- As shown in the average degree of curling/warping due to slab thickness effects for county roads and city streets (Table 14), curling and warping behavior tends to be highest in slabs with a 10 in. thickness for most of the indicators except degree of curvature.

4.2.1.6. Transverse Joint Spacing Effects

All of the investigated LTPP sections have the same 15 ft joint spacing, while all of the investigated non-LTPP highways have the same 20 ft joint spacing. The county roads and city streets include three types of transverse joint spacing (12, 15, and 20 ft). Figure 33 shows the joint spacing effects on the curling and warping behavior of county roads and city streets.

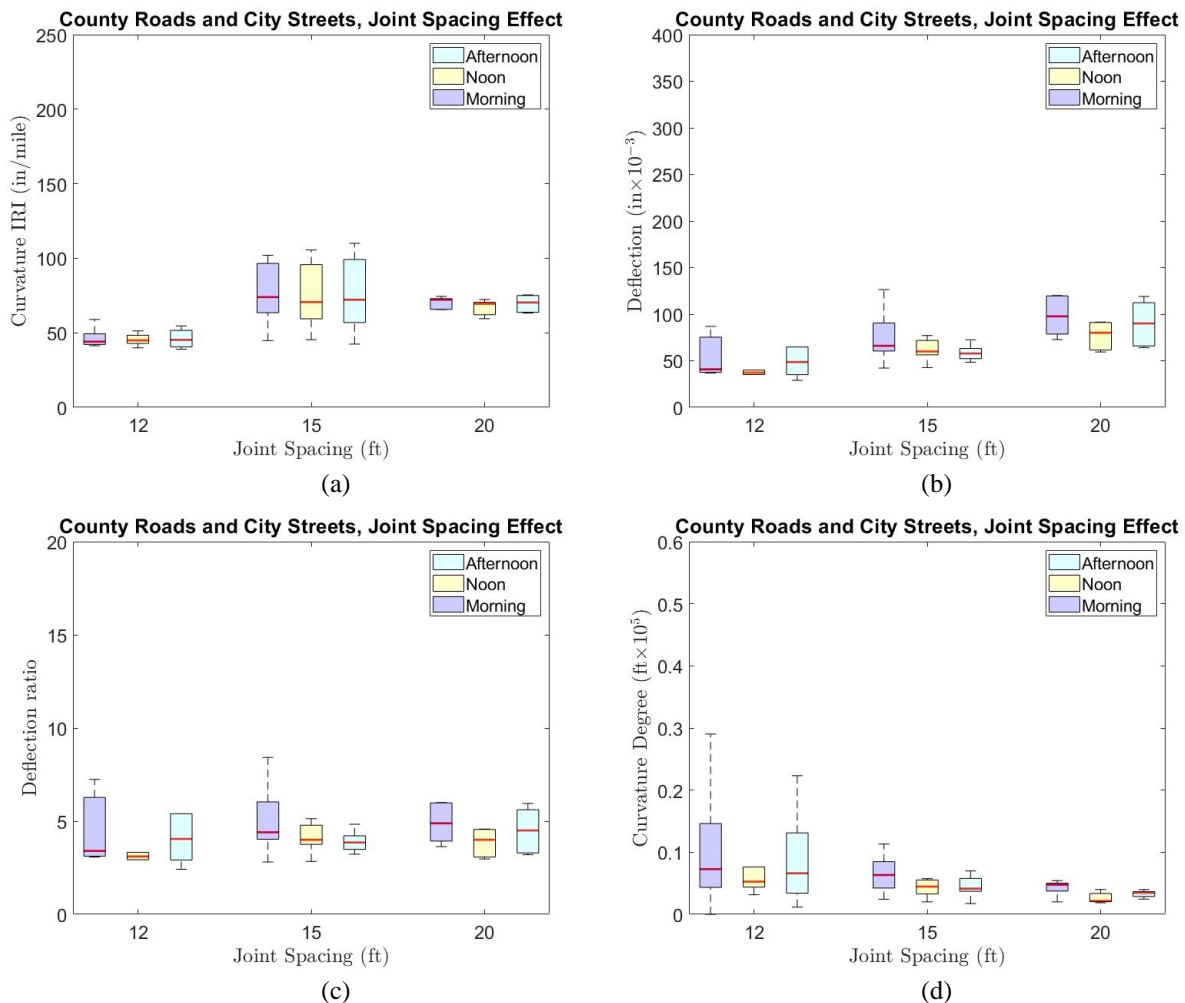


Figure 33. Transverse joint spacing effects on county roads and city streets: (a) curvature IRI, (b) deflection, (c) deflection ratio, (d) degree of curvature (12 ft joint spacing [3 sites, 32 data points], 15 ft joint spacing [3 sites, 39 data points], 20 ft joint spacing [1 site, 15 data points])

The key findings for this group are as follows:

- For county roads and city streets, curvature IRI is in the range of 33.9 to 58.9 in./mile for slabs with a 12 ft joint spacing, 42.4 to 110.0 in./mile for slabs with a 15 ft joint spacing, and 59.5 to 75.4 in./mile for the slab with a 20 ft joint spacing.
- For county roads and city streets, deflection is in the range of 27.5 to 130.1 $\times 10^{-3}$ in. for slabs with a 12 ft joint spacing, 42.2 to 126.3 $\times 10^{-3}$ in. for slabs with a 15 ft joint spacing, and 59.4 to 120.0 $\times 10^{-3}$ in. for the slab with a 20 ft joint spacing.
- For county roads and city streets, deflection ratio is in the range of 2.29 to 10.84 for slabs with a 12 ft joint spacing, 2.81 to 8.42 for slabs with a 15 ft joint spacing, and 2.97 to 6.00 for the slab with a 20 ft joint spacing.
- For county roads and city streets, degree of curvature is in the range of 0.01 to 0.29 $\times 10^{-5}$ 1/ft for slabs with a 12 ft joint spacing, 0.02 to 0.11 $\times 10^{-5}$ 1/ft for slabs with a 15 ft joint spacing, and 0.02 to 0.05 $\times 10^{-5}$ 1/ft for the slab with a 20 ft joint spacing.
- As shown in the average degree of curling/warping due to joint spacing effects for county roads and city streets (Table 15), curling and warping behavior tends to be relatively higher in slabs with a 15 ft joint spacing for all indicators except degree of curvature.

Table 15. Summary of transverse joint spacing effects

Road Type	Joint Spacing	Avg. Curvature IRI (in./mile)	Avg. Deflection ($\times 10^{-3}$ in)	Avg. Deflection Ratio	Avg. Degree of Curvature ($\times 10^{-5}$ 1/ft)
County roads	12 ft Joint Spacing	41.9	49.8	4.15	0.08
and city streets	15 ft Joint Spacing	76.1	66.6	4.44	0.05
	20 ft Joint Spacing	68.8	88.3	4.41	0.03

4.2.1.7. Dowel Bar Effects

Dowel bars carry weight while allowing horizontal joint movement due to heat-based moisture contraction and expansion. They also aid in keeping slabs aligned horizontally and vertically (Maitra et al. 2009).

The LTPP sections include two sizes of dowel bar diameter (1.25, 1.5 in.). Sections 0217, 0218, 0213, 0214, 0221, and 0222 have a 1.25 in. dowel bar diameter. Sections 0219, 0220, 0215, 0216, 0223, and 0224 have a 1.5 in. dowel bar diameter. The dowel bars in 8 in. thick slabs are usually 1.25 in. in diameter, and the dowel bars in 10/11 in. thick slabs are usually 1.5 in. in diameter. Figure 34 shows the dowel bar effects on the curling and warping behavior of the LTPP sites.

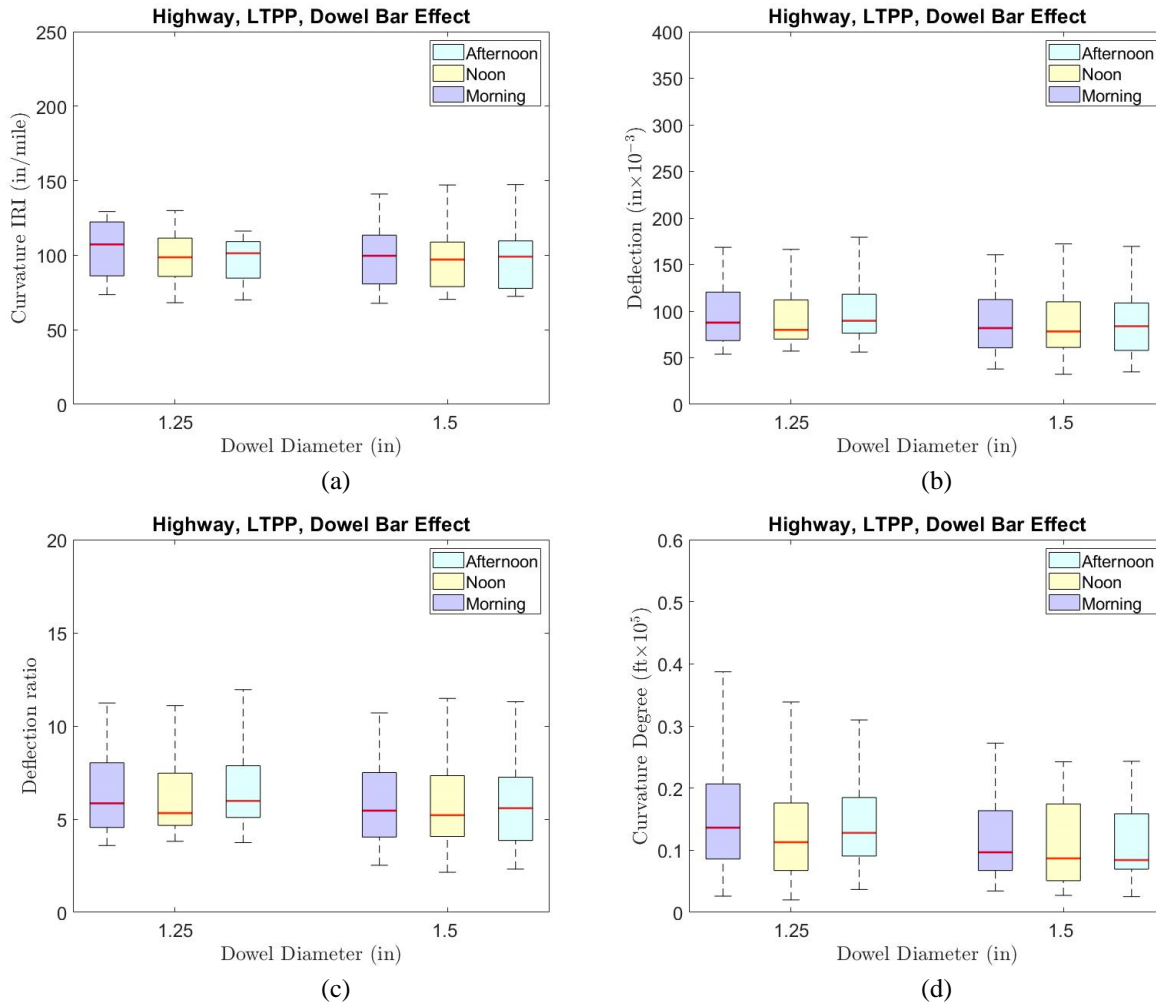


Figure 34. Dowel bar effects on LTPP sections: (a) curvature IRI, (b) deflection, (c) deflection ratio, (d) degree of curvature (1.25 in. dowel bar [6 sites, 108 data points], (1.5 in. dowel bar [6 sites, 108 data points])

The key findings for this group are as follows:

- For the LTPP sections, curvature IRI is in the range of 68.2 to 219.4 in./mile for slabs with 1.25 in. dowel bars and 67.8 to 147.4 in./mile for slabs with 1.5 in. dowel bars.
- For the LTPP sections, deflection is in the range of 53.8 to 209.9 $\times 10^{-3}$ in. for slabs with 1.25 in. dowel bars and 32.2 to 198.9 $\times 10^{-3}$ in. for slabs with 1.5 in. dowel bars.
- For the LTPP sections, deflection ratio is in the range of 3.59 to 13.99 for slabs with 1.25 in. dowel bars and 2.15 to 13.26 for slabs with 1.5 in. dowel bars.
- For the LTPP sections, degree of curvature is in the range of 0.02 to 0.39 $\times 10^{-5}$ 1/ft for slabs with 1.25 in. dowel bars and 0.03 to 0.27 $\times 10^{-5}$ 1/ft for slabs with 1.5 in. dowel bars.
- As shown in the average degree of curling/warping due to dowel bar effects for the LTPP sections (Table 16), curling and warping behavior tends to be higher in slabs with dowel bar diameters of 1.25 in. for all indicators.

Table 16. Summary of dowel bar effects

Road Type	Dowel Diameter (in.)	Avg. Curvature IRI (in./mile)	Avg. Deflection ($\times 10^{-3}$ in)	Avg. Deflection Ratio	Avg. Degree of Curvature ($\times 10^{-5}$ 1/ft)
LTPP	1.25 in.	113.2	97.9	6.53	0.15
	1.5 in.	98.4	88.3	5.89	0.11
County roads and city streets	No Dowel	50.2	61.2	4.16	0.07
	1.5 in.	84.3	69.7	4.65	0.05

All non-LTPP highways were constructed with 1.5 in. dowel bars, all county roads were constructed with no dowel bars, and all city streets were constructed with 1.5 in. dowel bars. Figure 35 shows the dowel bar effects on the curling and warping behavior of county roads and city streets.

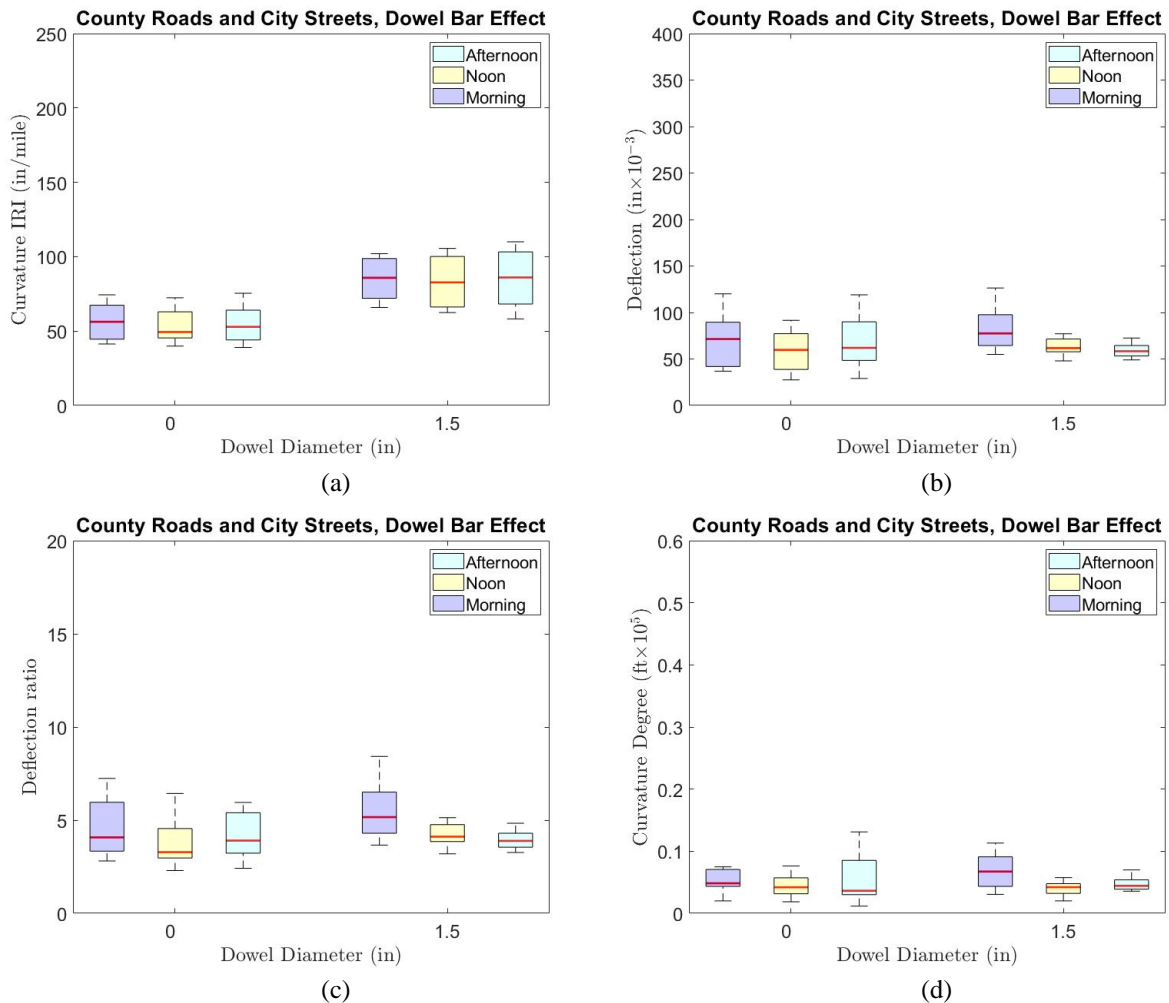


Figure 35. Dowel bar effects on county roads and city streets: (a) curvature IRI, (b) deflection, (c) deflection ratio, (d) degree of curvature (no dowel bar [4 sites, 56 data points], 1.5 in. dowel bar [2 sites, 30 data points])

The key findings for this group are as follows:

- For county roads and city streets, curvature IRI is in the range of 33.9 to 75.4 in./mile for slabs with no dowel bars and 58.2 to 110.0 in./mile for slabs with 1.5 in. dowel bars.
- For county roads and city streets, deflection is in the range of 27.5 to 130.1 $\times 10^{-3}$ in. for slabs with no dowel bars and 47.9 to 126.3 $\times 10^{-3}$ in. for slabs with 1.5 in. dowel bars.
- For county roads and city streets, deflection ratio is in the range of 2.29 to 10.84 for slabs with no dowel bars and 3.19 to 8.42 for slabs with 1.5 in. dowel bars.
- For county roads and city streets, degree of curvature is in the range of 0.01 to 0.29 $\times 10^{-5}$ 1/ft for slabs with no dowel bars and 0.02 to 0.11 $\times 10^{-5}$ 1/ft for slabs with 1.5 in. dowel bars.
- As shown in the average degree of curling/warping due to dowel bar effects for county roads and city streets (Table 16), the county roads without dowel bars have lower degrees of curling and warping compared to city streets with 1.5 in. dowel bars.

4.2.1.8. Joint Type Effects

All of the investigated LTTP sections, county roads, and city streets have rectangular joints only, while non-LTTP sections have both rectangular and skewed joints. Figure 36 shows the joint type effects on the curling and warping behavior of the non-LTTP sites.

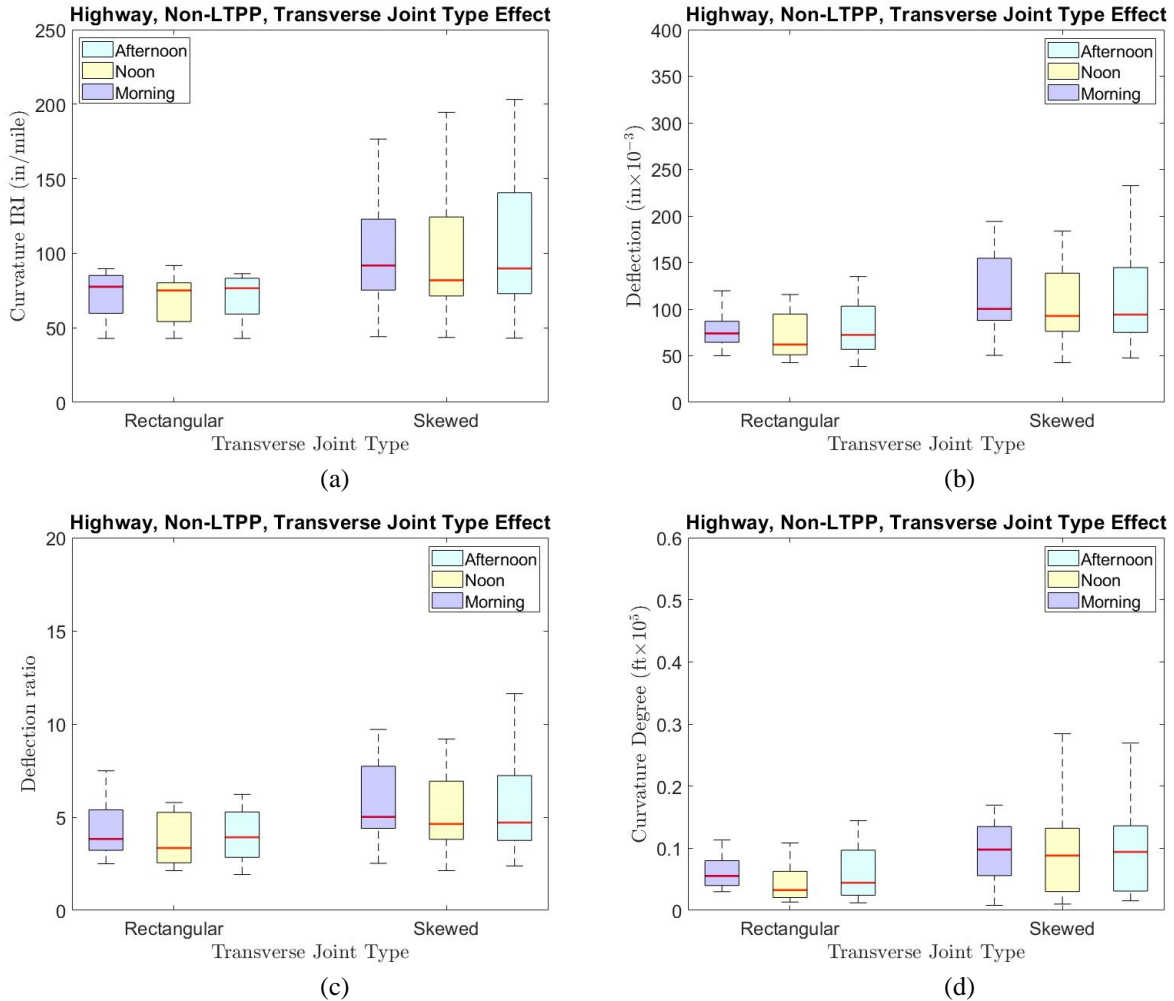


Figure 36. Joint type effects on non-LTPP sections: (a) curvature IRI, (b) deflection, (c) deflection ratio, (d) degree of curvature (rectangular joints [3 sites, 46 data points], skewed joints [9 sites, 125 data points])

The key findings for this group are as follows:

- For the non-LTPP sections, curvature IRI is in the range of 46.9 to 91.8 in./mile for slabs with rectangular joints and 43.1 to 215.7 in./mile for slabs with skewed joints.
- For the non-LTPP sections, deflection is in the range of 38.4 to 127.9 $\times 10^{-3}$ in. for slabs with rectangular joints and 42.6 to 329.2 $\times 10^{-3}$ in. for slabs with skewed joints.
- For the non-LTPP sections, deflection ratio is in the range of 1.92 to 6.40 for slabs with rectangular joints and 2.13 to 16.46 for slabs with skewed joints.
- For the non-LTPP sections, degree of curvature is in the range of 0.01 to 0.14 $\times 10^{-5}$ 1/ft for slabs with rectangular joints and 0.01 to 0.33 $\times 10^{-5}$ 1/ft for slabs with skewed joints.
- As shown in the average degree of curling/warping due to joint type effects for the non-LTPP sections (Table 17), curling and warping behavior tends to be higher with skewed joints.

Table 17. Summary of joint type effects

Road Type	Joint Type	Avg. Curvature IRI (in./mile)	Avg. Deflection ($\times 10^{-3}$ in)	Avg. Deflection Ratio	Avg. Degree of Curvature ($\times 10^5$/ft)
Non-LTPP	Rectangular	72.3	77.1	3.85	0.06
	Skewed	101.9	120.4	6.02	0.10

4.2.1.9. Shoulder Type Effects

Shoulder types include tied PCC shoulders, HMA shoulders, and granular shoulders. HMA shoulders and granular shoulders, unlike tied PCC shoulders, have no load transfer capabilities between the traffic lanes and shoulders. For this study, HMA and granular shoulders were grouped into an “untied shoulder” category.

The non-LTPP sections have both untied and PCC tied shoulders, while the LTPP sections have only untied HMA shoulders. Figure 37 shows the shoulder type effects on the curling and warping behavior of the non-LTPP sites.

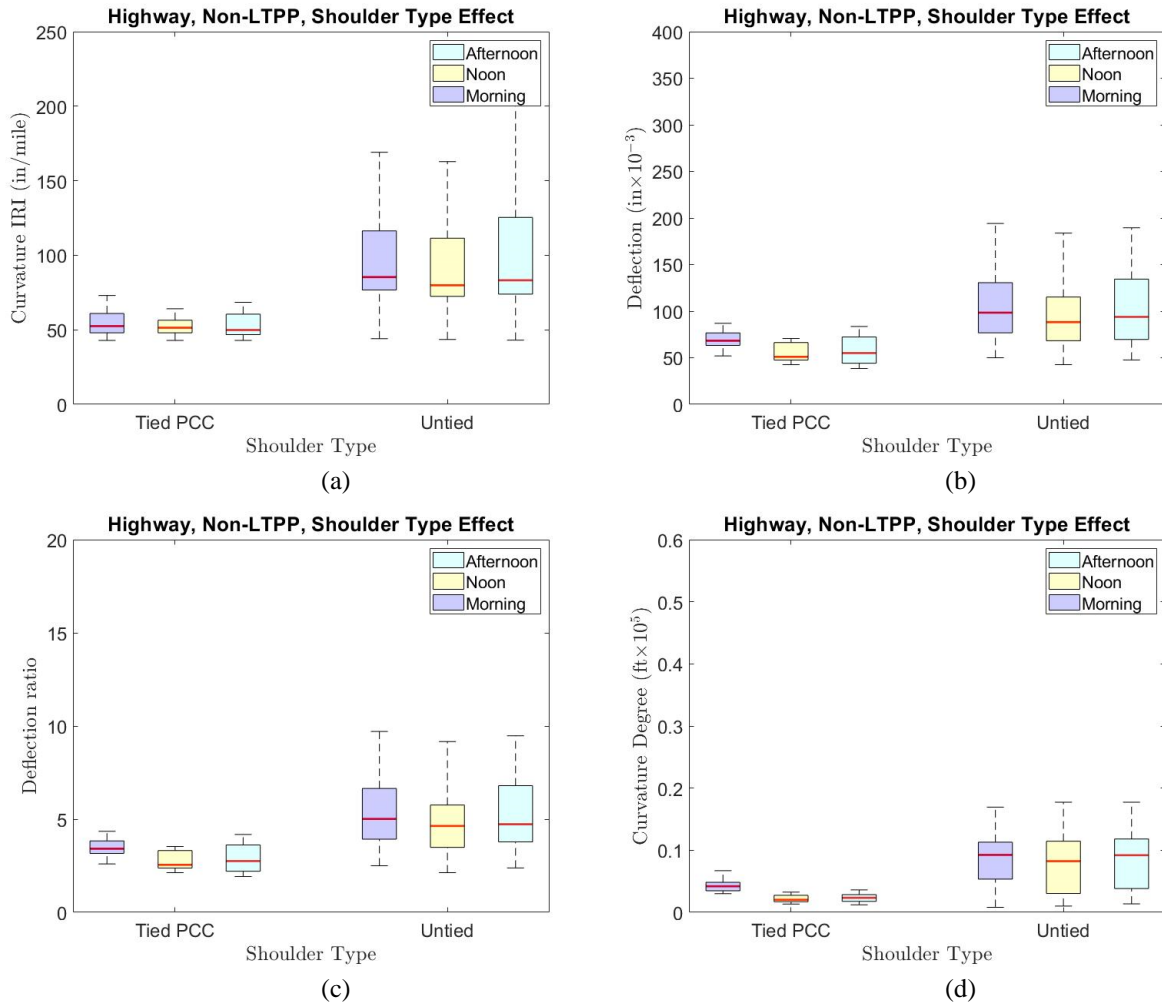


Figure 37. Shoulder type effects on non-LTPP sections: (a) curvature IRI, (b) deflection, (c) deflection ratio, (d) degree of curvature (tied PCC shoulder [1 site, 15 data points], untied shoulder [11 sites, 158 data points])

The key findings for this group are as follows:

- For the non-LTPP sections, curvature IRI is in the range of 46.9 to 73.1 in./mile for slabs with tied PCC shoulders and 58.7 to 215.7 in./mile for slabs with untied shoulders.
- For the non-LTPP sections, deflection is in the range of 38.4 to 86.9 $\times 10^{-3}$ in. for slabs with tied PCC shoulders and 46.2 to 329.2 $\times 10^{-3}$ in. for slabs with untied shoulders.
- For the non-LTPP sections, deflection ratio is in the range of 1.92 to 4.35 for slabs with tied PCC shoulders and 2.13 to 16.46 for slabs with untied shoulders.
- For the non-LTPP sections, degree of curvature is in the range of 0.01 to 0.07 $\times 10^{-5}$ 1/ft for slabs with tied PCC shoulders and 0.01 to 0.33 $\times 10^{-5}$ 1/ft for slabs with untied shoulders.
- As shown in the box plots ranges and the average degree of curling/warping due to shoulder type effects for the non-LTPP sections (Table 18), curling and warping behavior tends to be higher for slabs with untied shoulders for all indicators.

Table 18. Summary of shoulder type effects

Road Type	Shoulder Type	Avg. Curvature IRI (in./mile)	Avg. Deflection ($\times 10^{-3}$ in)	Avg. Deflection Ratio	Avg. Degree of Curvature ($\times 10^5/ft$)
Non-LTPP	Tied PCC	57.8	61.5	3.08	0.03
	Untied	106.2	122.9	6.15	0.11
County roads and city streets	Tied PCC	77.1	66.4	4.62	0.06
	Untied	50.2	62.3	4.10	0.06

The county roads had untied shoulders while the city streets had tied PCC shoulders. Figure 38 shows the shoulder type effects on the curling and warping behavior of county roads and city streets. All county roads and city streets were constructed between 2016 to 2018, and they are all newly constructed projects.

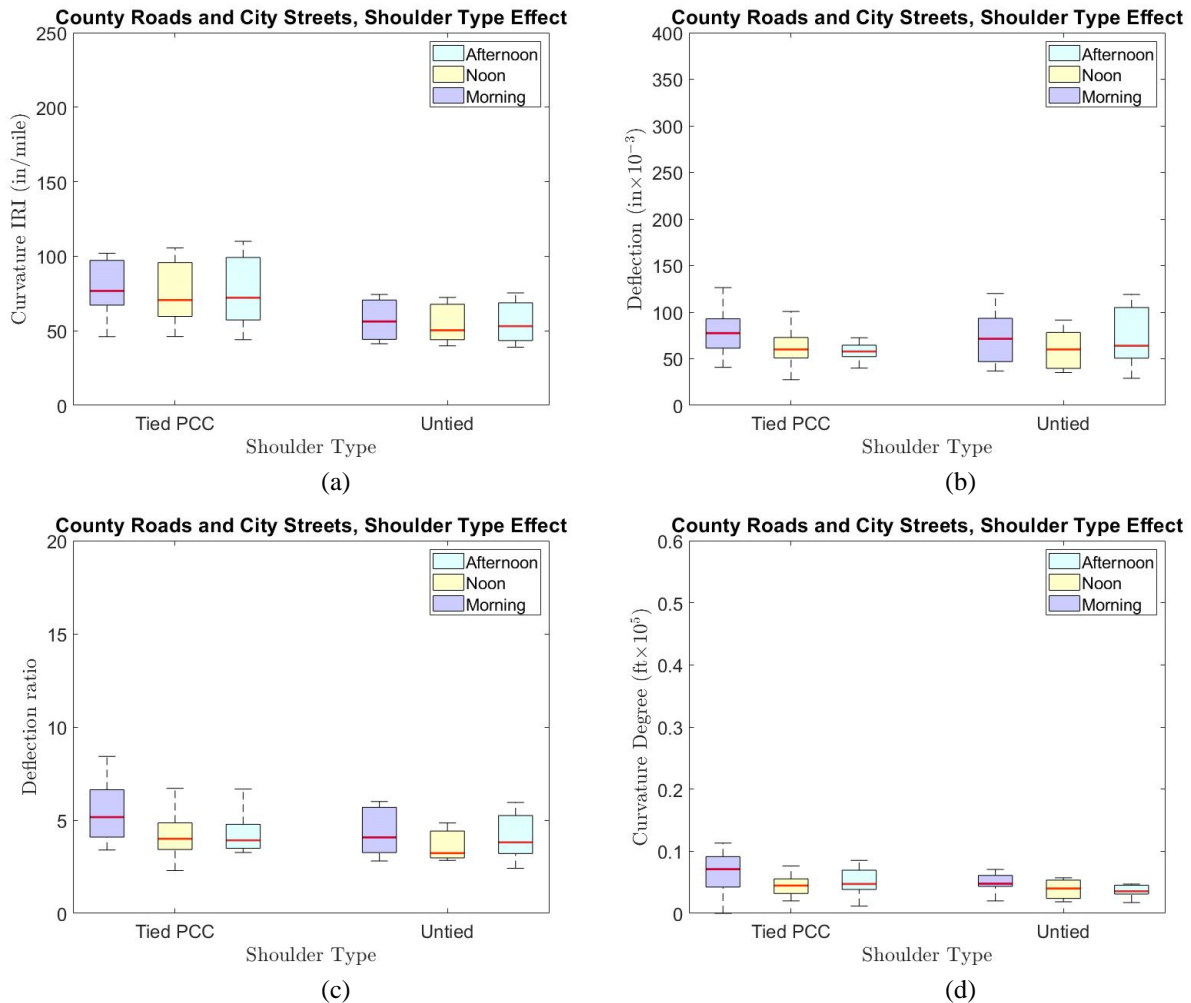


Figure 38. Shoulder type effects on county roads and city streets: (a) curvature IRI, (b) deflection, (c) deflection ratio, (d) degree of curvature (tied PCC shoulder [3 sites, 38 data points], untied shoulder [4 sites, 48 data points])

The key findings for this group are as follows:

- For county roads and city streets, curvature IRI is in the range of 44.1 to 110.0 in./mile for slabs with tied PCC shoulders and 33.9 to 75.4 in./mile for slabs with untied shoulders.
- For county roads and city streets, deflection is in the range of 27.5 to 126.3 $\times 10^{-3}$ in. for slabs with tied PCC shoulders and 29.0 to 130.1 $\times 10^{-3}$ in. for slabs with untied shoulders.
- For county roads and city streets, deflection ratio ranges from 2.29 to 8.42 for slabs with tied PCC shoulders and from 2.42 to 10.84 for slabs with untied shoulders.
- For county roads and city streets, degree of curvature is in the range of 0.01 to 0.29 $\times 10^{-5}$ 1/ft for slabs with tied PCC shoulders and 0.01 to 0.22 $\times 10^{-5}$ 1/ft for slabs with untied shoulders.
- As shown in the average degree of curling/warping due to joint type effects for county roads and city streets (Table 18), tied shoulders have a relatively higher degree of curling and warping than untied shoulders in terms of curvature IRI and deflection. In other words, the city streets have a higher degree of curling and warping behavior than the county roads.

4.2.1.10. Mix Design Effects

According to Iowa DOT technical guidance for quality management concrete (QMC), QMC describes “the design, testing, placement, and monitoring of a PCC mixture by a contractor in partnership with the owner to make a superior product while promoting innovation and understanding” (Iowa DOT 2015). QMC mix designs were implemented in the late 1990s and early 2000s.

The non-LTPP state projects investigated in this study have either pre-QMC or QMC mix designs. Pre-QMC mix designs have higher allowable w/cm ratios and lower fly ash replacement rates (frequently 15%, while most QMC mixes have a 20% replacement rate). The county roads and city streets investigated have three mix designs: C-3WR, QMC, and C-SUD (Iowa DOT 2022). The C-SUD mix design, also known as an urban durability mix for city streets, uses a basic w/cm ratio of 0.40 and may have fly ash replacement rates up to 35%, while the C-3WR mix design (which uses a 20% fly ash replacement rate and a basic w/cm ratio of 0.43) has been most often used for county pavements in recent years.

The LTPP sections investigated have two types of mixtures. Sections 0218, 0220, 0216, 0214, 0222, and 0224 were constructed with a high-strength, 900 psi mix design (0.42 w/cm ratio and 15% fly ash replacement rate), and sections 0217, 0219, 0215, 0213, 0221, and 0223 were constructed with a low-strength, 550 psi mix design (0.53 w/cm ratio and 15% fly ash replacement rate). Figure 39 shows the mix design effects on the curling and warping behavior of the LTPP sections.

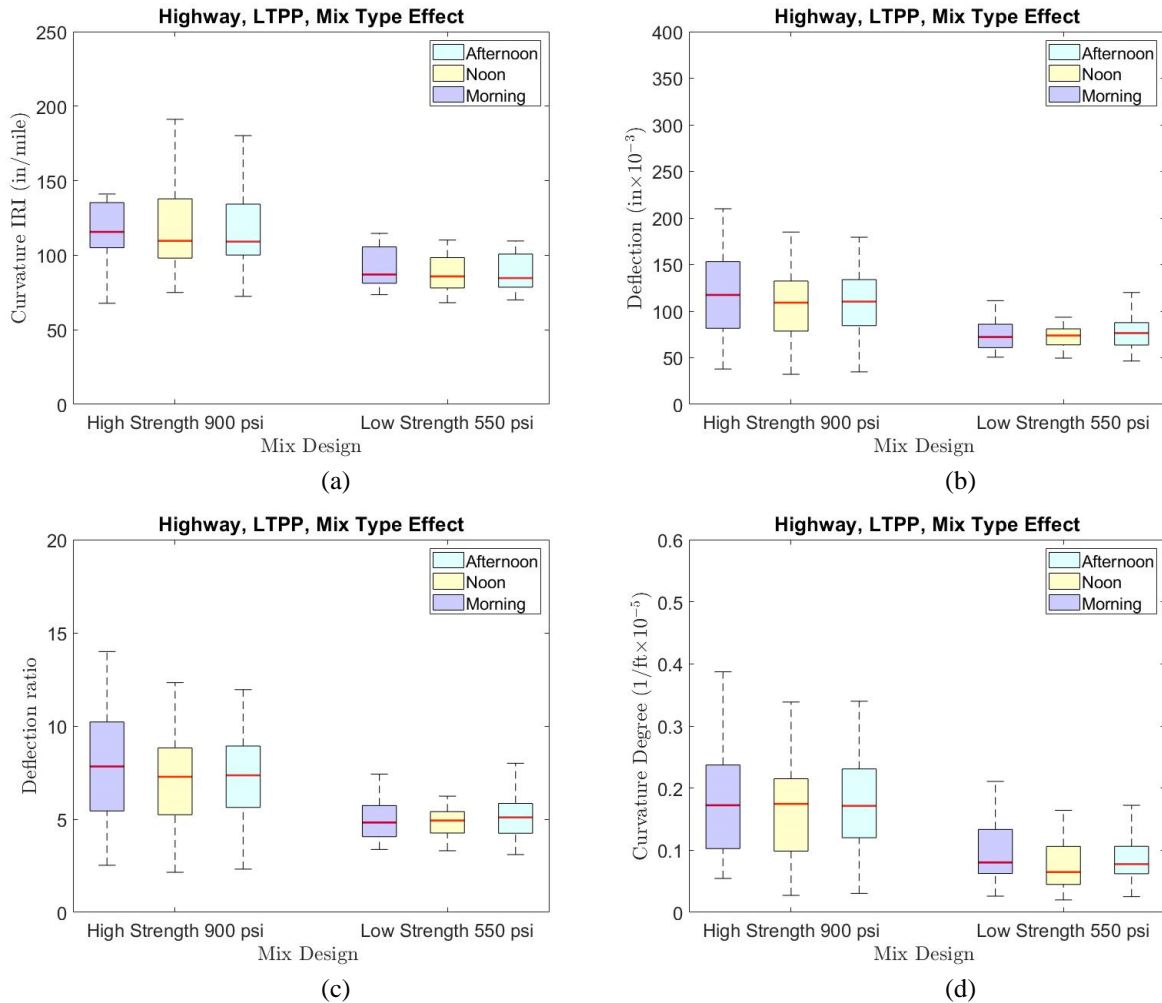


Figure 39. Mix design effects on LTPP sections: (a) curvature IRI, (b) deflection, (c) deflection ratio, (d) degree of curvature (high strength [6 sites, 72 data points], low strength [6 sites, 72 data points])

The key findings for this group are as follows:

- For the LTPP sections, curvature IRI is in the range of 67.8 to 219.4 in./mile for slabs constructed with a high-strength mix and 68.2 to 114.6 in./mile for slabs constructed with a low-strength mix.
- For the LTPP sections, deflection is in the range of 32.2 to 209.9 $\times 10^{-3}$ in. for slabs constructed with a high-strength mix and 46.5 to 120.0 $\times 10^{-3}$ in. for slabs constructed with a low-strength mix.
- For the LTPP sections, deflection ratio is in the range of 2.15 to 13.99 for slabs constructed with a high-strength mix and 3.10 to 8.00 for slabs constructed with a low-strength mix.
- For the LTPP sections, degree of curvature is in the range of 0.03 to 0.39 $\times 10^{-5}$ 1/ft for slabs constructed with a high-strength mix and 0.02 to 0.21 $\times 10^{-5}$ 1/ft for slabs constructed with a low-strength mix.

- Curling and warping behavior tends to be highest for the high-strength mix design for all indicators shown in the box plots and the average degree of curling/warping due to mix design effects for the LTPP sections (Table 19).

Table 19. Summary of mix design effects

Road Type	Mix Design	Avg. Curvature IRI (in./mile)	Avg. Deflection ($\times 10^{-3}$ in)	Avg. Deflection Ratio	Avg. Degree of Curvature ($\times 10^5$ 1/ft)
LTPP	High strength	122.0	111.3	7.42	0.17
	Low strength	89.6	75.0	5.00	0.09
Non-LTPP	Pre-QMC	110.1	130.4	6.52	0.11
	QMC	76.4	85.2	4.26	0.07
County roads and city streets	C-3WR	61.2	76.4	4.17	0.04
	C-SUD	84.3	69.7	4.65	0.05
	QMC	46.0	51.0	4.25	0.09

The non-LTPP sections have both pre-QMC and QMC mix designs. Section 0259 is constructed with a pre-QMC mix design using 0.41 w/cm ratio and a 20% fly ash replacement rate (Iowa DOT 2022). Figure 40 shows the mix design effects on the curling and warping behavior of the non-LTPP sites.

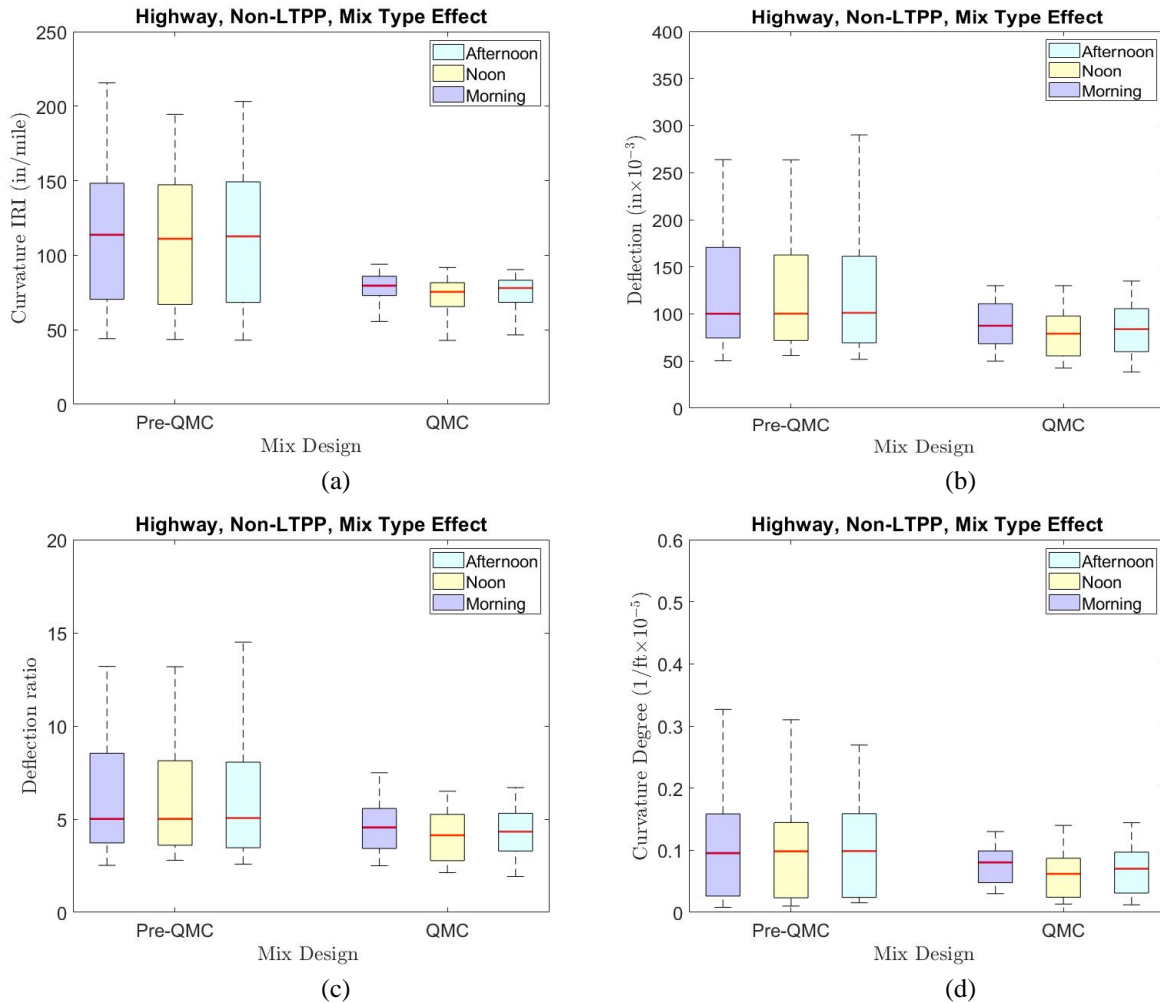


Figure 40. Mix design effects on non-LTPP sections: (a) curvature IRI, (b) deflection, (c) deflection ratio, (d) degree of curvature (pre-QMC [6 sites, 89 data points], QMC [6 sites, 82 data points])

The key findings for this group are as follows:

- For the non-LTPP sections, curvature IRI is in the range of 43.1 to 215.7 in./mile for slabs constructed with the pre-QMC mix design and 46.9 to 107.1 in./mile for slabs constructed with the QMC mix design.
- For the non-LTPP sections, deflection is in the range of 50.4 to 329.2 $\times 10^{-3}$ in. for slabs constructed with the pre-QMC mix design and 38.4 to 133.9 $\times 10^{-3}$ in. for slabs constructed with the QMC mix design.
- For the non-LTPP sections, deflection ratio is in the range of 2.52 to 16.46 for slabs constructed with the pre-QMC mix design and 1.92 to 6.69 for slabs constructed with the QMC mix design.
- For the non-LTPP sections, degree of curvature is in the range of 0.01 to 0.33 $\times 10^{-5}$ 1/ft for slabs constructed with the pre-QMC mix design and 0.01 to 0.14 $\times 10^{-5}$ 1/ft for slabs constructed with the QMC mix design.

- Curling and warping behavior tends to be higher for the pre-QMC mix design for all indicators shown in the box plots and the average degree of curling/warping due to mix design effects for the non-LTPP sections (Table 19).

County roads and city streets have C-3WR, QMC, and C-SUD mix designs. City streets adopted the urban durability mix (C-SUD), while county roads constructed in recent years typically used C-3WR (20% fly ash replacement rate, basic w/cm ratio of 0.43). Figure 41 shows the mix design effects on the curling and warping behavior of county roads and city streets.

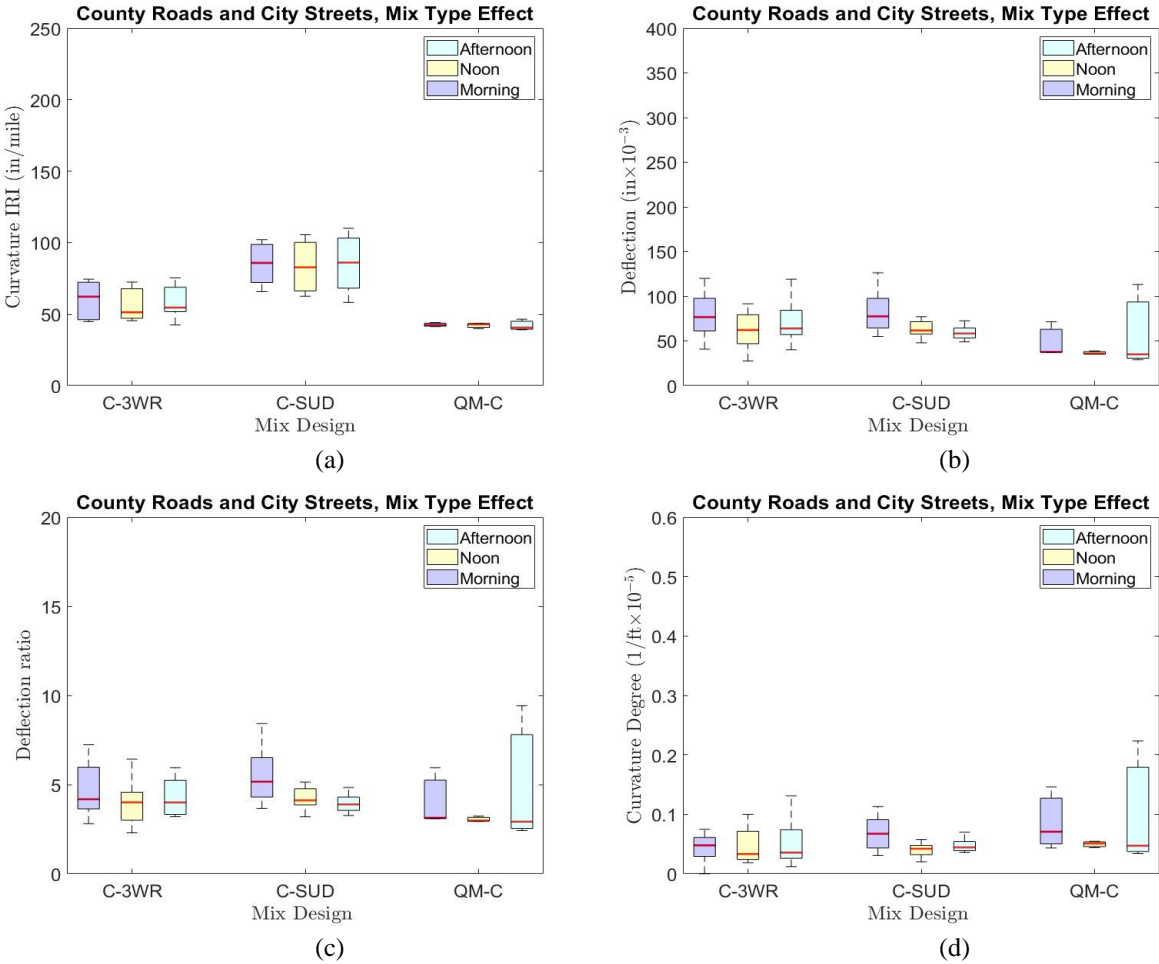


Figure 41. Mix design effects on county roads and city streets: (a) curvature IRI, (b) deflection, (c) deflection ratio, (d) degree of curvature (C-3WR [2 sites, 24 data points], C-SUD [2 sites, 30 data points], QMC [2 sites, 17 data points])

The key findings for this group are as follows:

- For county roads and city streets, curvature IRI is in the range of 42.4 to 75.4 in./mile for slabs constructed with the C-3WR mix design, 58.2 to 110.0 in./mile for slabs constructed with the C-SUD mix design, and 39.0 to 58.9 in./mile for slabs constructed with the QMC mix design.

- For county roads and city streets, deflection is in the range of 42.2 to 120.0 $\times 10^{-3}$ in. for slabs constructed with the C-3WR mix design, 47.9 to 126.3 $\times 10^{-3}$ in. for slabs constructed with the C-SUD mix design, and 27.5 to 113.1 $\times 10^{-3}$ in. for slabs constructed with the QMC mix design.
- For county roads and city streets, deflection ratio is in the range of 2.81 to 6.00 for slabs constructed with the C-3WR mix design, 3.19 to 8.42 for slabs constructed with the C-SUD mix design, and 2.29 to 9.43 for slabs constructed with the QMC mix design.
- For county roads and city streets, degree of curvature is in the range of 0.02 to 0.10 $\times 10^{-5}$ 1/ft for slabs constructed with the C-3WR mix design, 0.02 to 0.11 $\times 10^{-5}$ 1/ft for slabs constructed with the C-SUD mix design, and 0.01 to 0.29 $\times 10^{-5}$ 1/ft for slabs constructed with the QMC mix design.
- As shown in the average degree of curling/warping due to mix design effects for county roads and city streets (Table 19), the C-SUD mix design exhibits the highest curvature IRI and deflection ratio, while the C-3WR and QMC mix designs exhibit the highest deflection and degree of curvature, respectively.

4.2.1.11. Construction Season Effects

The non-LTPP sections were constructed in the spring, summer, and fall. Figure 42 shows the construction season effects on the curling and warping behavior of the non-LTPP sites.

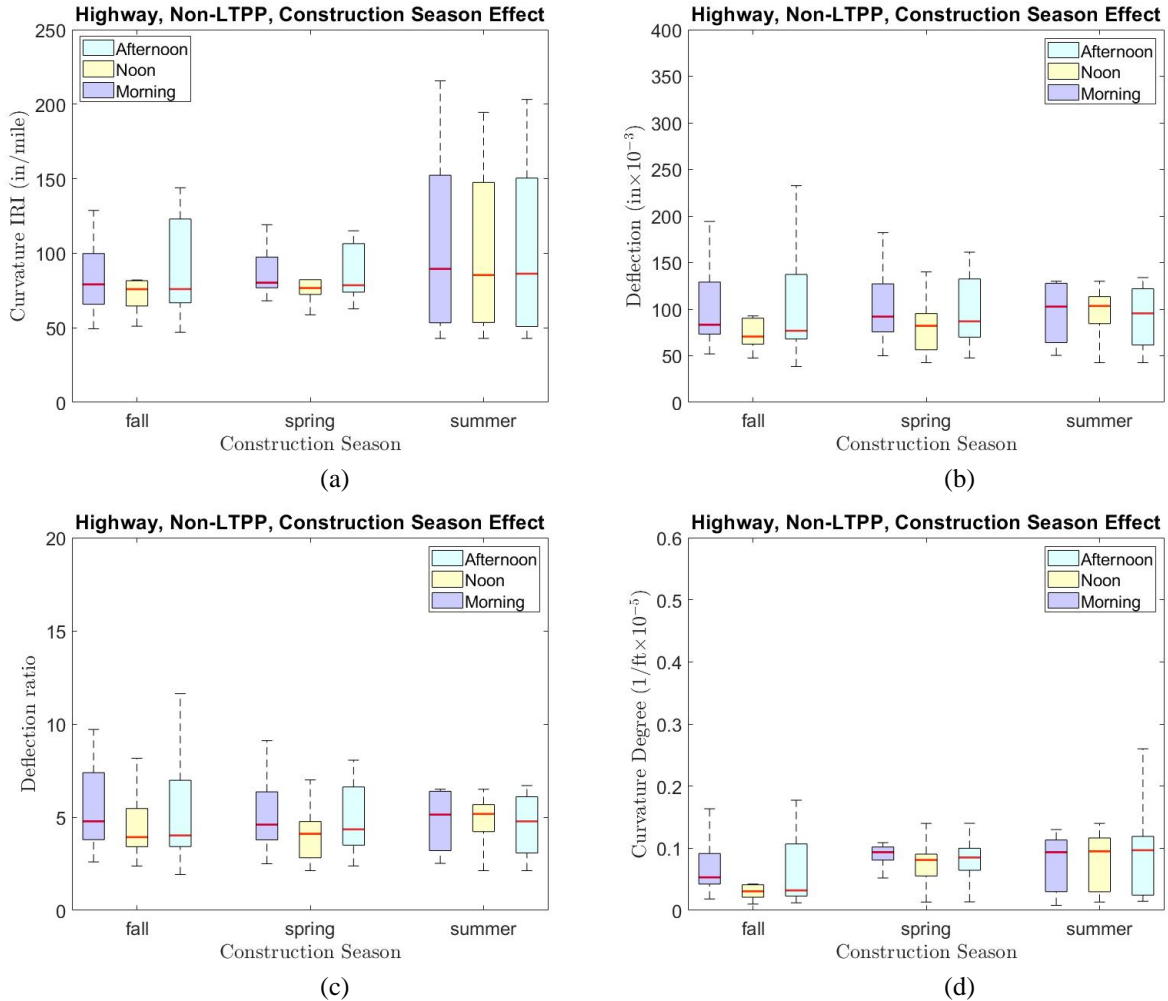


Figure 42. Construction season effects on non-LTPP sections: (a) curvature IRI, (b) deflection, (c) deflection ratio, (d) degree of curvature (spring [4 sites, 55 data points], summer [5 sites, 70 data points], fall [3 sites, 46 data points])

The key findings for this group are as follows:

- For the non-LTPP sections, curvature IRI is in the range of 58.7 to 119.1 in./mile for slabs constructed in the spring, 43.1 to 215.7 in./mile for slabs constructed in the summer, and 46.9 to 143.9 in./mile for slabs constructed in the fall.
- For the non-LTPP sections, deflection is in the range of 42.6 to 182.1 $\times 10^{-3}$ in. for slabs constructed in the spring, 50.4 to 329.2 $\times 10^{-3}$ in. for slabs constructed in the summer, and 38.4 to 232.5 $\times 10^{-3}$ in. for slabs constructed in the fall.
- For the non-LTPP sections, deflection ratio is in the range of 2.13 to 9.11 for slabs constructed in the spring, 2.52 to 16.46 for slabs constructed in the summer, and 1.92 to 11.63 for slabs constructed in the fall.
- For the non-LTPP sections, degree of curvature is in the range of 0.01 to 0.17 $\times 10^{-5}$ 1/ft for slabs constructed in the spring, 0.01 to 0.33 $\times 10^{-5}$ 1/ft for slabs constructed in the summer, and 0.01 to 0.18 $\times 10^{-5}$ 1/ft for slabs constructed in the fall.

- As shown in the average degree of curling/warping due to construction season effects for the non-LTPP sections (Table 20), sites paved in the spring exhibit the lowest degrees of curling/warping for all indicators except degree of curvature. This suggests that paving during the spring rather than during other seasons might decrease curling and warping.

Table 20. Summary of construction season effects

Road Type	Construction Season	Avg. Curvature IRI (in./mile)	Avg. Deflection (x10⁻³ in)	Avg. Deflection Ratio	Avg. Degree of Curvature (x10⁵1/ft)
Non-LTPP	Spring	84.8	94.8	4.74	0.09
	Summer	107.2	124.9	6.25	0.11
	Fall	84.8	100.8	5.04	0.06
County roads and city streets	Summer	56.7	68.5	4.33	0.07
	Fall	76.1	66.6	4.44	0.05

County roads and city streets were constructed in the summer and fall. Figure 43 shows the construction season effects on the curling and warping behavior of county roads and city streets.

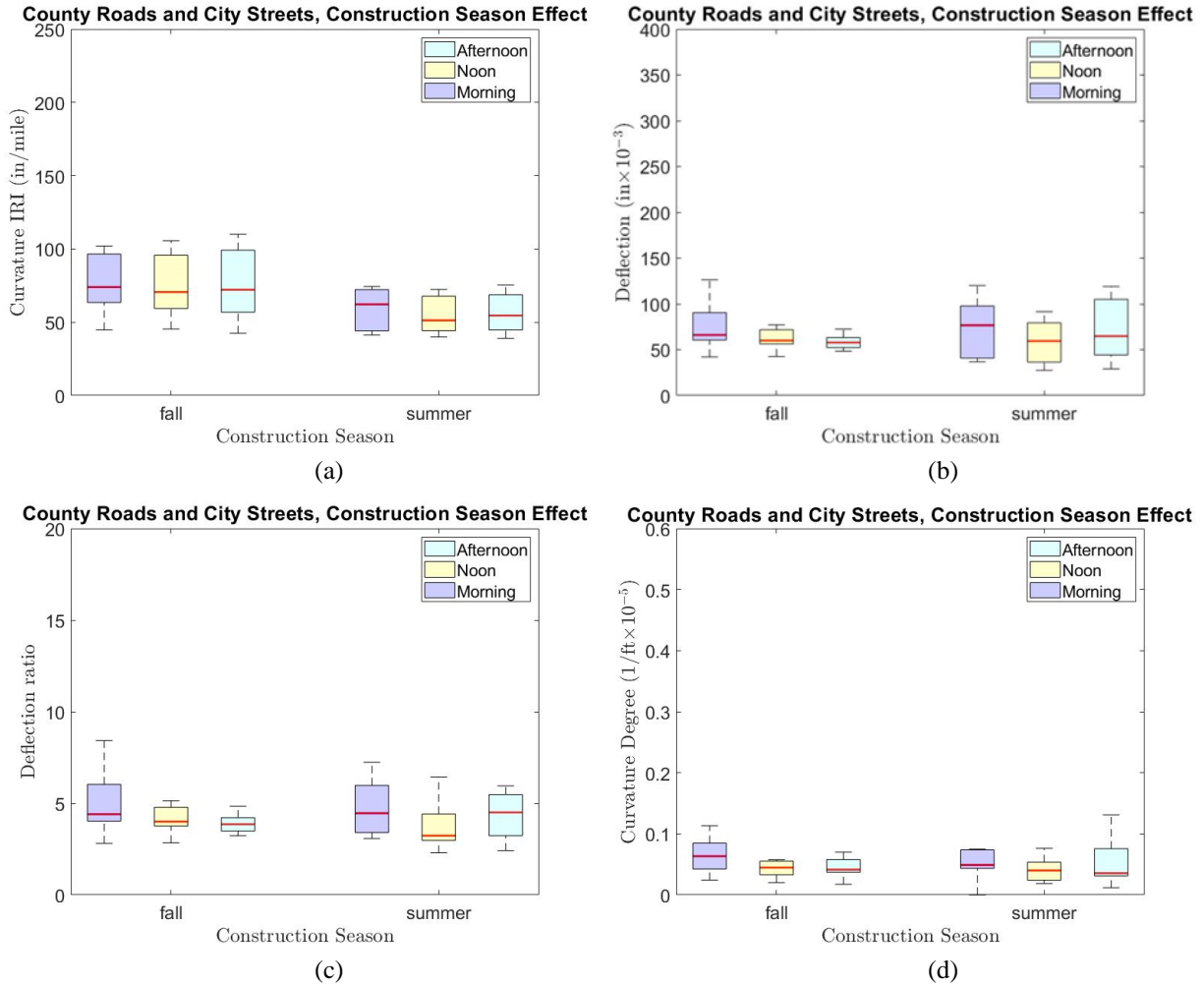


Figure 43. Construction season effects on county roads and city streets: (a) curvature IRI, (b) deflection, (c) deflection ratio, (d) degree of curvature (summer [3 sites, 11 data points], fall [1 site, 6 data points])

The key findings for this group are as follows:

- For county roads and city streets, curvature IRI is in the range of 39.0 to 75.4 in./mile for slabs constructed in the summer and 42.4 to 110.0 in./mile for slabs constructed in the fall.
- For county roads and city streets, deflection is in the range of 27.5 to 120.0 $\times 10^{-3}$ in. for slabs constructed in the summer and 42.2 to 126.3 $\times 10^{-3}$ in. for slabs constructed in the fall.
- For county roads and city streets, deflection ratio is in the range of 2.29 to 9.43 for slabs constructed in the summer and 2.81 to 8.42 for slabs constructed in the fall.
- For county roads and city streets, degree of curvature is in the range of 0.01 to 0.29 $\times 10^{-5}$ 1/ft for slabs constructed in the summer and 0.02 to 0.11 $\times 10^{-5}$ 1/ft for slabs constructed in the fall.
- As shown in the average degree of curling/warping due to construction season effects for county roads and city streets (Table 20), projects constructed in the summer demonstrate a

higher deflection and degree of curvature, while projects constructed in the fall show a higher curvature IRI and deflection ratio.

4.2.1.12. Statistical Analysis Results

Table 21 shows the results of the one-way ANOVA for the LTPP sections. Dowel bar diameter, seasonal effects, diurnal effects, mix type, slab width, and slab thickness have different impacts on the different curling and warping indicators.

Table 21. One-way ANOVA results for LTPP sections

Factor	Curvature IRI	Deflection	Deflection Ratio	Degree of Curvature
Dowel Bar Diameter	<0.001	0.054	0.054	0.001
Seasonal Effect	0.871	0.021	0.021	0.002
Diurnal Effect	0.669	0.567	0.567	0.391
Slab Width	<0.001	0.171	0.171	0.169
Slab Thickness	<0.001	0.005	0.001	<0.001
Mix Type	<0.001	<0.001	<0.001	<0.001

Table 22 shows the results of the one-way ANOVA for the non-LTPP sections. Construction season, seasonal effects, diurnal effects, slab width, thickness, joint type, mix type, and shoulder type exhibit different impacts on the different curling and warping indicators.

Table 22. One-way ANOVA results for non-LTPP sections

Factor	Curvature IRI	Deflection	Deflection Ratio	Degree of Curvature
Construction Season	0.016	0.029	0.054	0.002
Seasonal Effect	0.777	0.776	0.725	0.557
Diurnal Effect	0.648	0.590	0.572	0.630
Mix Type	<0.001	<0.001	<0.001	<0.001
Slab Width	<0.001	0.025	0.073	0.003
Slab Thickness	<0.001	<0.001	<0.001	<0.001
Joint Type	<0.001	<0.001	<0.001	<0.001
Shoulder Type	<0.001	<0.001	<0.001	<0.001

Table 23 shows the results of the one-way ANOVA for county roads and city streets. Similar to the other two groups, the listed variables exhibit different impacts on the different curling and warping indicators.

Table 23. One-way ANOVA results for county roads and city streets

Factor	Curvature IRI	Deflection	Deflection Ratio	Degree of Curvature
Construction Season	<0.001	0.748	0.730	0.236
Dowel Bar Diameter	<0.001	0.157	0.209	0.200
Seasonal Effect	0.246	0.319	0.341	0.357
Diurnal Effect	0.920	0.140	0.132	0.264
Mix Type	<0.001	0.002	0.417	<0.001
Joint Spacing	<0.001	<0.001	0.760	<0.001
Slab Width	0.012	0.790	0.770	0.440
Slab Thickness	<0.001	0.269	0.370	0.005
Shoulder Type	<0.001	0.478	0.160	0.553

The results from Table 21 to Table 23 show that there was no single factor in common among the three groups that significantly influenced all four curling/warping indicators. Figure 44 summarizes the variables evaluated for each group.

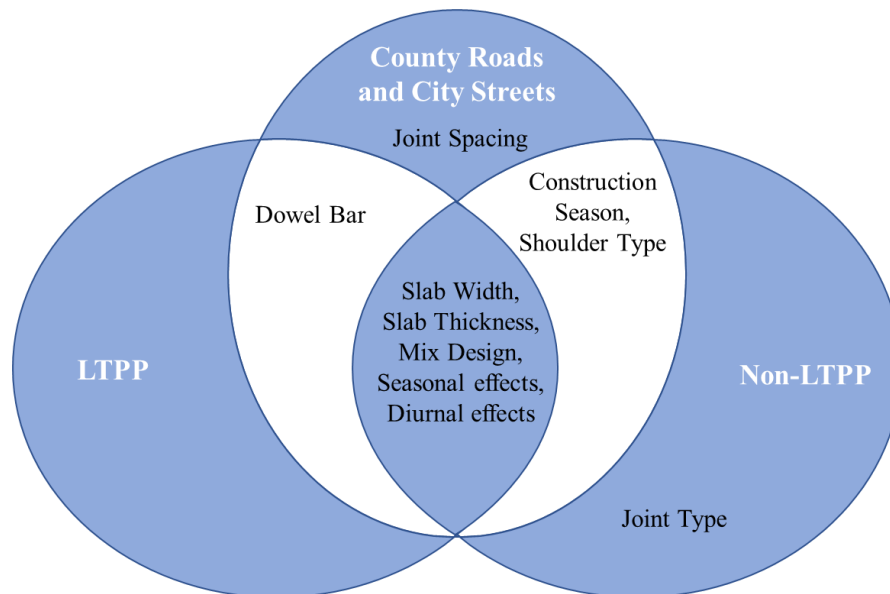


Figure 44. Variables for three groups

The correlation between the groups is not strong, so combining them does not yield a consistent conclusion. In the following discussion, multiple linear regression models were used to determine the engineering factors that most influence curling and warping behavior and the trends for each group. Multiple linear regression analysis is used to evaluate which variables are significant.

The general multiple linear regression model was chosen in this study to predict the curling and warping behaviors for each site group. In this investigation, models were developed for each of the three groups: LTPP highways, non-LTPP highways, and county roads and city streets. The R^2 value and root mean squared error (RMSE) value for each curling and warping indicator were utilized to evaluate the accuracy of the regression models. Higher R^2 values were expected

because they indicate less variance. The RMSE represents the difference between the actual and anticipated values. The lower the RMSE value, the more accurate the prediction and the greater the model's quality. A summary of the model results for all three groups is shown in Table 24.

Table 24. Model results summary

Road Type	Curvature IRI		Deflection		Deflection Ratio		Degree of Curvature	
	R ²	RMSE	R ²	RMSE	R ²	RMSE	R ²	RMSE
Highways (LTPP only)	0.36	26.59	0.32	30.44	0.32	2.03	0.21	0.06
Highways (non-LTPP)	0.59	24.66	0.37	46.73	0.36	2.35	0.37	0.05
County Roads and City Streets	0.95	4.83	0.38	19.72	0.12	1.38	0.28	0.04

In this study, multiple linear regression models were built for each group to test the prediction models' effectiveness in predicting curling and warping behavior.

The prediction equations for the LTPP group are shown in equations (14) to (17) (all variables refer to Table 7).

$$\begin{aligned} \text{Curvature IRI} = & 197.1634 + 0.7597 * \text{Visit Season} - 2.2979 * \text{Visit Time} - 4.9335 \\ & * \text{Slab Thickness} - 8.3531 * \text{Slab Width} + 0.0925 * \text{Mix} \end{aligned} \quad (14)$$

$$\begin{aligned} \text{Deflection} = & 81.2648 + 7.0085 * \text{Visit Season} - 2.0317 * \text{Visit Time} - 3.1809 \\ & * \text{Slab Thickness} - 3.4035 * \text{Slab Width} + 0.1037 * \text{Mix} \end{aligned} \quad (15)$$

$$\begin{aligned} \text{Deflection Ratio} = & 5.4177 + 0.4672 * \text{Visit Season} - 0.1354 * \text{Visit Time} - 0.2121 \\ & * \text{Slab Thickness} - 0.2269 * \text{Slab Width} + 0.0069 * \text{Mix} \end{aligned} \quad (16)$$

$$\begin{aligned} \text{Degree of Curvature} = & 0.1501 + 0.0157 * \text{Visit Season} - 0.0087 * \text{Visit Time} - 0.0109 \\ & * \text{Slab Thickness} - 0.0092 * \text{Slab Width} + 0.0003 * \text{Mix} \end{aligned} \quad (17)$$

The results of the multiple linear regression analysis between the measured and predicted degrees of curling and warping for the LTPP sections (N = 194, S = 13) are demonstrated in Figure 45.

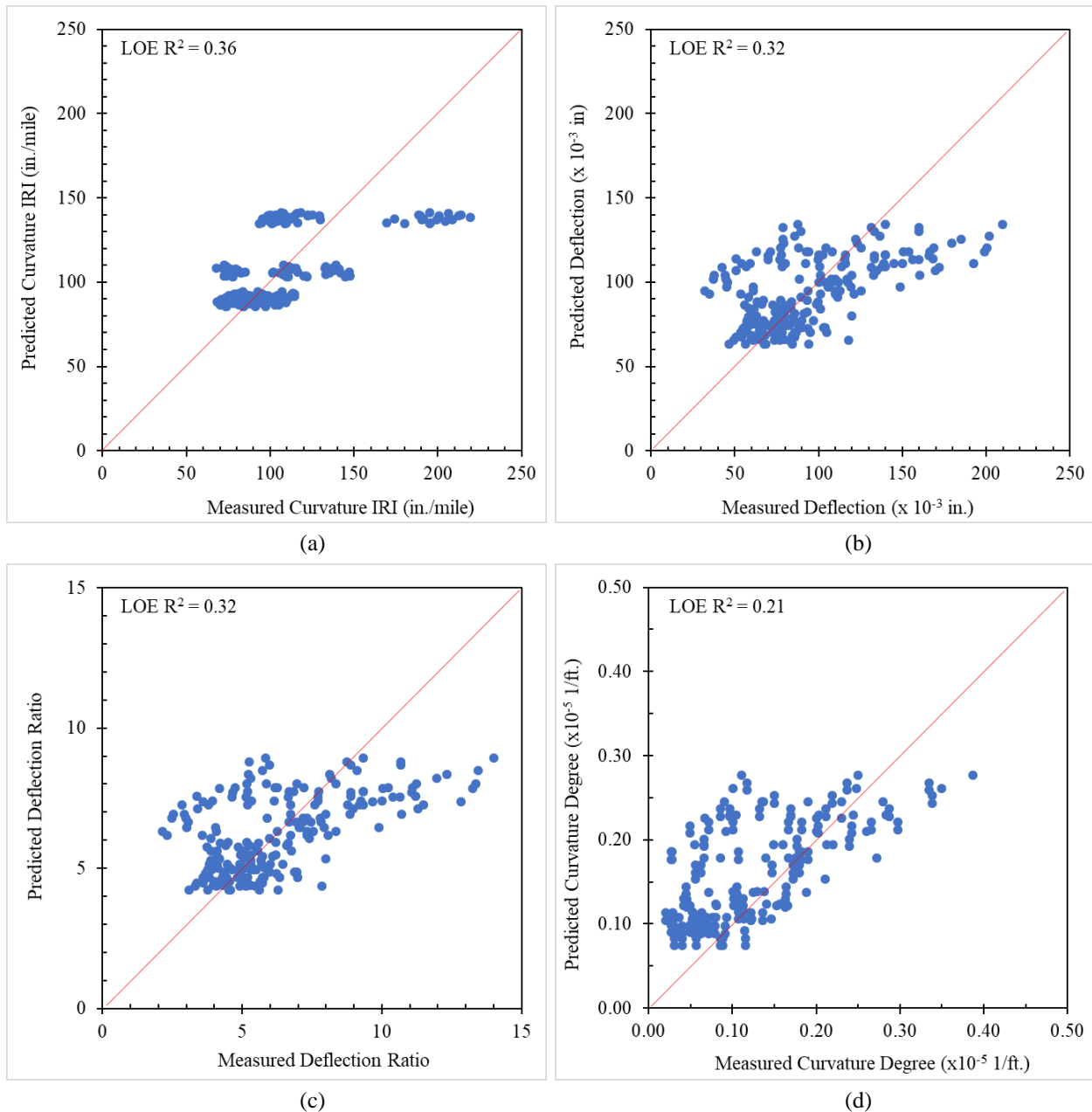


Figure 45. Multiple linear regression models’ prediction results for LTTP sections: (a) curvature IRI, (b) deflection, (c) deflection ratio, (d) degree of curvature

The analysis shows that all prediction models for the LTTP group exhibit a line of equality (LOE) R^2 above 0.2, and the regression model for each indicator is statistically significant (p-value less than 0.05). As slab width or thickness increases, curling and warping behavior will decrease. A high-strength mix will result in higher degrees of curling and warping than a low-strength mix. A low-strength mix has a lower total cementitious content and higher w/cm ratio than a high-strength mix. In summary, the prediction models for the four indicators of curling and warping behavior for the LTTP sections do not show a high correlation.

The multiple linear regression equations for the non-LTPP highways are shown in equations (18) to (21) (all variables refer to Table 7).

$$\begin{aligned} \text{Curvature IRI} &= 925.6805 - 1.4745 * \text{Visit Season} + 0.0198 * \text{Visit Time} - 4.6607 \\ &* \text{Construction Season} - 76.4013 * \text{Slab Thickness} + 0.1619 * \text{Joint Type} - 2.0183 \\ &* \text{Slab Width} - 47.6565 * \text{Mix} + 53.2612 * \text{Shoulder Type} \end{aligned} \quad (18)$$

$$\begin{aligned} \text{Deflection} &= 1015.5978 - 1.5998 * \text{Visit Season} - 1.7110 * \text{Visit Time} - 4.2000 \\ &* \text{Construction Season} - 86.8947 * \text{Slab Thickness} + 10.4472 * \text{Joint Type} - 1.1650 \\ &* \text{Slab Width} - 55.5177 * \text{Mix} + 68.7407 * \text{Shoulder Type} \end{aligned} \quad (19)$$

$$\begin{aligned} \text{Deflection ratio} &= 58.3168 - 0.0760 * \text{Visit Season} - 0.0859 * \text{Visit Time} - 0.1292 \\ &* \text{Construction Season} - 4.3240 * \text{Slab Thickness} + 0.4899 * \text{Joint Type} - 0.5998 \\ &* \text{Slab Width} - 2.7033 * \text{Mix} + 3.0776 * \text{Shoulder Type} \end{aligned} \quad (20)$$

$$\begin{aligned} \text{Degree of Curvature} &= 1.1992 - 0.0019 * \text{Visit Season} - 0.0026 * \text{Visit Time} - 0.0145 \\ &* \text{Construction Season} - 0.1146 * \text{Slab Thickness} + 0.0073 * \text{Joint Type} + 0.0053 \\ &* \text{Slab Width} - 0.0534 * \text{Mix} + 0.0831 * \text{Shoulder Type} \end{aligned} \quad (21)$$

The difference between measured and predicted curling and warping for the non-LTPP sections is shown in Figure 46.

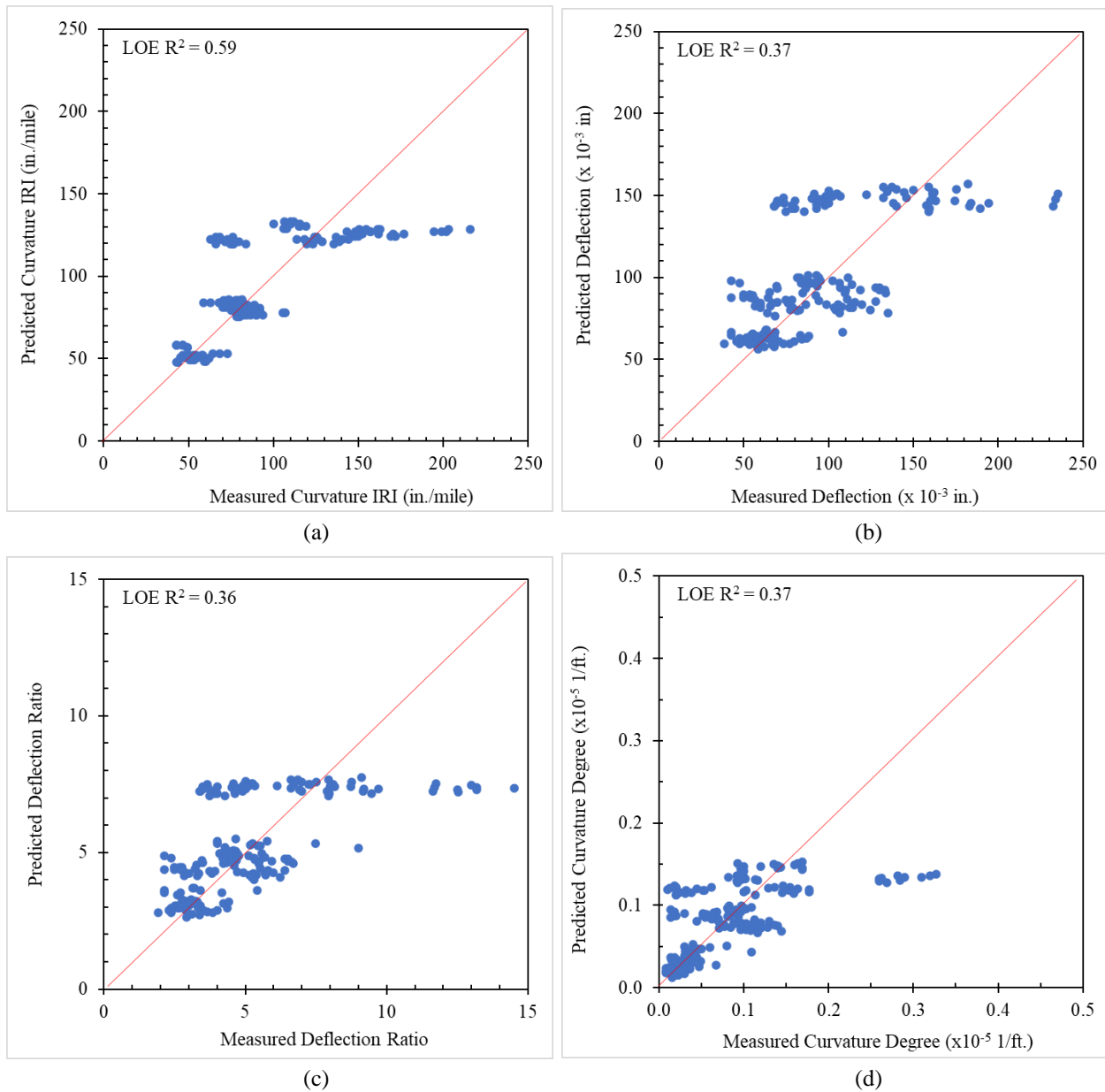


Figure 46. Multiple linear regression models' prediction results for non-LTPP sections: (a) curvature IRI, (b) deflection, (c) deflection ratio, (d) degree of curvature

All four models exhibit p-values less than 0.05, indicating their statistical significance. As slab thickness or width increases, curling and warping behavior will decrease. Similarly, using the QMC mix type will result in lower curling and warping behavior. Pavements constructed with untied shoulders will exhibit higher degrees of curling and warping.

The multiple linear regression models for county roads and city streets are presented in equations (22) to (25) (all variables refer to Table 7).

$$\begin{aligned} \text{Curvature IRI} &= 150.1452 + 2.0016 * \text{Visit Season} - 0.2002 * \text{Visit Time} + 17.8647 \\ &* \text{Slab Thickness} + 4.035 * \text{Spacing} - 31.0213 * \text{Slab Width} - 2.9201 * \text{Mix} + 43.5649 \\ &* \text{Shoulder Type} \end{aligned} \quad (22)$$

$$\begin{aligned} \text{Deflection} &= 44.6894 + 3.5052 * \text{Visit Season} - 4.6293 * \text{Visit Time} + 3.8939 \\ &* \text{Slab Thickness} + 6.3145 * \text{Spacing} - 9.6653 * \text{Slab Width} - 5.2756 * \text{Mix} + 14.4169 \\ &* \text{Shoulder Type} \end{aligned} \quad (23)$$

$$\begin{aligned} \text{Deflection ratio} &= 7.2473 + 0.2317 * \text{Visit Season} - 0.2901 * \text{Visit Time} + 0.2445 \\ &* \text{Slab Thickness} + 0.1267 * \text{Spacing} - 0.6444 * \text{Slab Width} - 0.3110 * \text{Mix} + 1.0320 \\ &* \text{Shoulder Type} \end{aligned} \quad (24)$$

$$\begin{aligned} \text{Degree of Curvature} &= 0.2848 + 0.0041 * \text{Visit Season} - 0.0094 * \text{Visit Time} - 0.0061 \\ &* \text{Slab Thickness} - 0.0038 * \text{Spacing} - 0.0096 * \text{Slab Width} - 0.0076 * \text{Mix} + 0.0186 \\ &* \text{Shoulder Type} \end{aligned} \quad (25)$$

Figure 47 depicts the relationship between measured and predicted degrees of curling and warping for county roads and city streets.

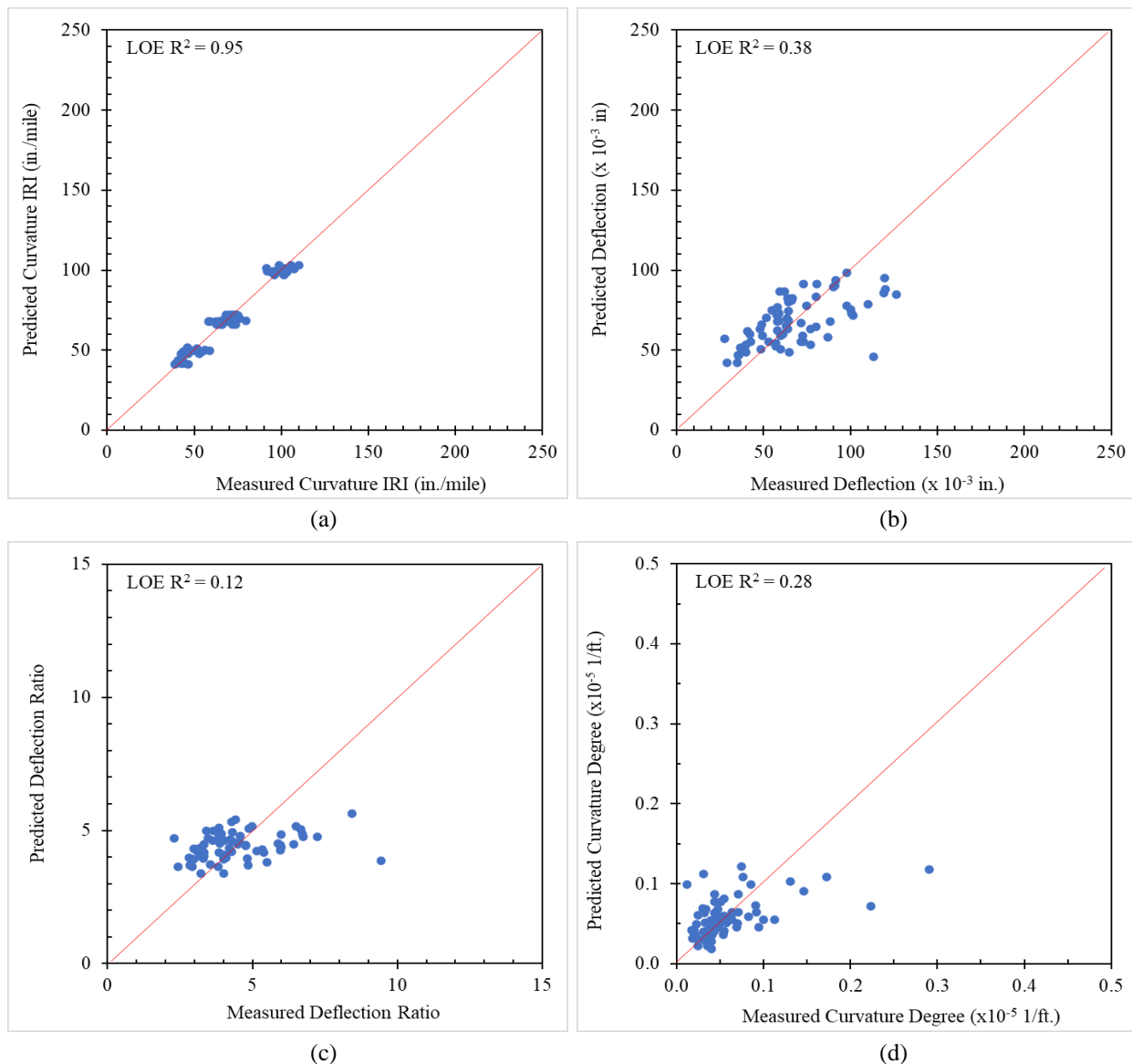


Figure 47. Multiple linear regression model's prediction results for county roads and city streets: (a) curvature IRI, (b) deflection, (c) deflection ratio, (d) degree of curvature

The analysis shows that as slab width increases, curling and warping behavior will decrease. In contrast, increased slab thickness and joint spacing could result in elevated degrees of curling and warping. Using the C-3WR mix type and tied shoulders will reduce the degrees of curling and warping. In summary, except for the model for deflection ratio, the prediction models for county roads and city streets are assessed as statistically significant.

The results of the multiple linear regression analysis show that mix type and slab thickness are significant variables for the LTPP group. For the non-LTPP group, slab thickness, shoulder type, and mix type can significantly impact the predicted curling and warping behavior. The county roads and city streets group differs from the other two groups in that joint spacing is a significant variable in the model for predicting curvature IRI.

According to the LOE R^2 values, correlations between the predicted and actual measurements are not as good as expected, possibly for the following reasons:

- Several significant variables were removed from the multiple linear regression analysis due to the requirements of the method (e.g., the data must obey a normal distribution and a linear correlation must exist between the dependent and independent variables).
- The effects of otherwise insignificant variation accumulated.
- Some potential factors such as temperature and moisture gradients could affect the correlations.
- Construction information was lacking for several sites (e.g., base type).
- The whole database lacks data points with well-controlled variables.
- Measurement accuracy and operation are affected by various weather conditions.

4.2.2. Curled Down Sites

Curled-down sites were analyzed separately from curled-up sites in this study. The hourly equivalent temperature differences for the JPCP slabs at three curled-down sites (D20 in Hamilton County, F67 in Iowa County, and G26 in Washington County) were extracted from PMED, and the shrinkage and overall equivalent temperature differences were calculated by following Equations 10 through 14. Figure 48, Figure 49, and Figure 50 show the hourly, shrinkage, and overall equivalent temperature differences, respectively, for these sites. The effective permanent curling/warping temperature difference was 44°F.

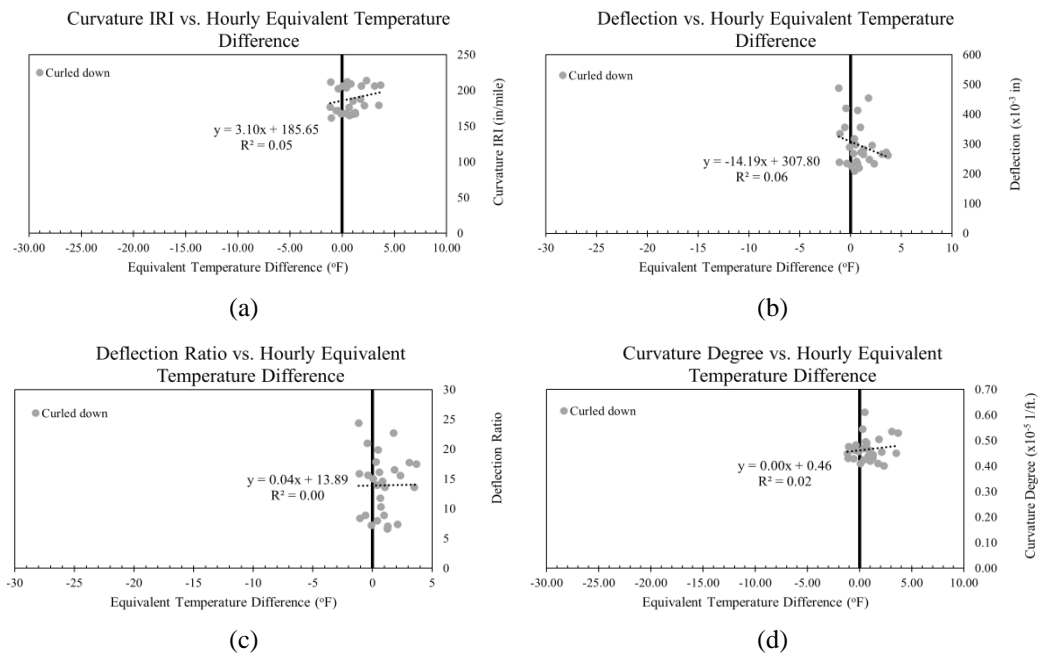


Figure 48. Hourly equivalent temperature difference versus (a) curvature IRI, (b) deflection, (c) deflection ratio, (d) degree of curvature

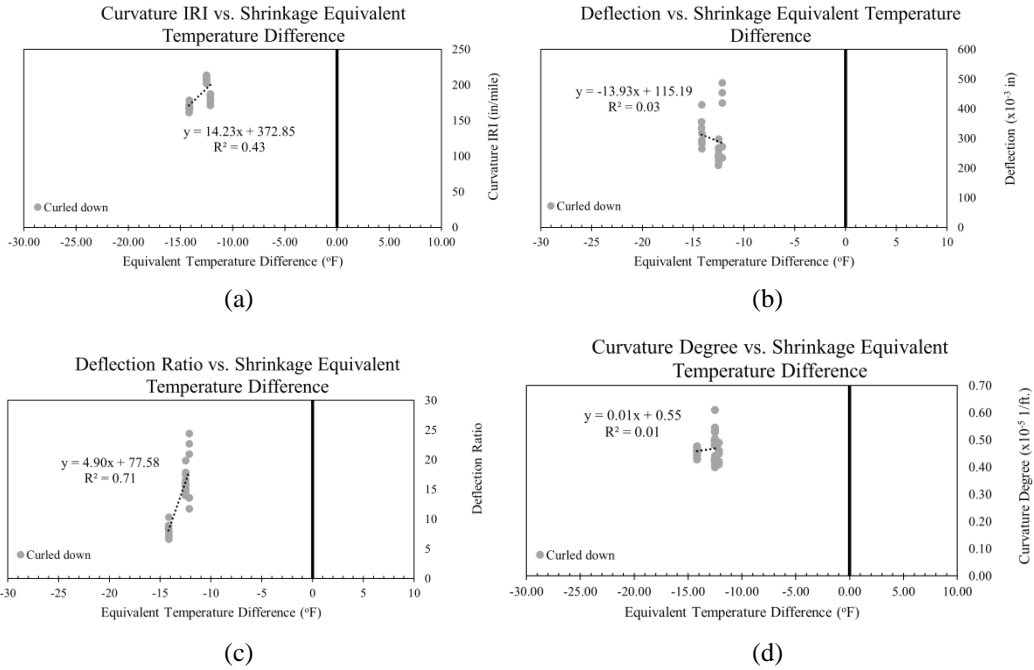


Figure 49. Shrinkage equivalent temperature difference versus (a) curvature IRI, (b) deflection, (c) deflection ratio, (d) degree of curvature

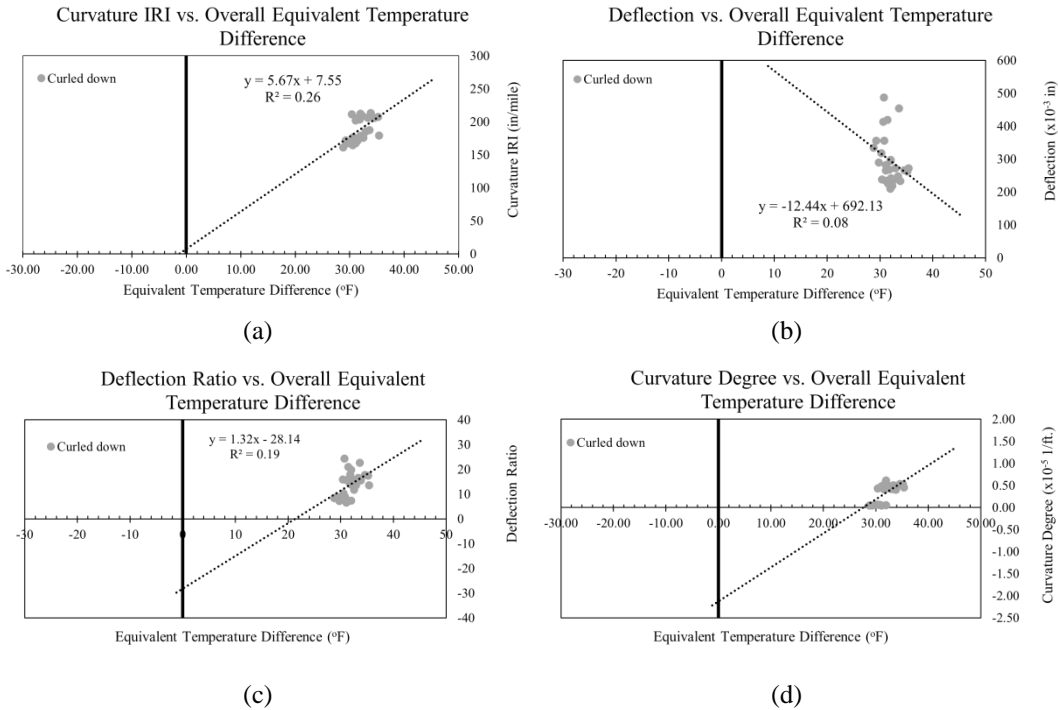


Figure 50. Overall equivalent temperature difference versus (a) curvature IRI, (b) deflection, (c) deflection ratio, (d) degree of curvature

With the hypothesis that 15°F to 44°F is the effective permanent curling/warping temperature differential, most curling and warping indicators are around zero, with the trendline extending to zero. The following assumptions apply to curled-down sites:

- The curled-down sites were all constructed between the 1970s and the 1990s (i.e., they are old construction).
- The curled-down sites are 6 to 7 in. thick, thinner than the curled-up/flat sites (8 to 11 in.), and the slabs are easier to bend. Another possible reason the slabs curled down could be the long joint spacing (40 ft) at the curled-down sites.
- According to the Iowa bedrock map, the curled-down sites are all located near Mississippian-age limestones, which might explain why the pavements' foundations are so fragile.
- Mississippian-age limestones are soluble (i.e., will dissolve) under the right conditions, which means they can be easily eroded by water moving through the ground.

4.3. Summary

In this study, the analysis of pavements within the three groups (LTPP highways, non-LTPP highways, and county roads and city streets) showed a consistent seasonal effect on curling and warping behavior; fall typically exhibited the highest average values for four indicators of the degree of curling/warping, while spring and summer exhibited the lowest values. Compared to measurements taken at noon and in the late afternoon, morning measurements reflected a relatively higher degree of curing and warping for all three groups (LTPP highways, non-LTPP highways, and county roads and city streets) based on the average degree of curling/warping.

A number of variables related to pavement design and pavement structure were evaluated in this study. For the LTPP sections, the sites with a 12 ft width had higher curling and warping than those with 14 ft width based on the average degree of curling/warping. Most non-LTPP highways with a 14 ft width exhibited higher curling and warping behavior based on the average degree of curling/warping. County roads/city streets did not show a clear trend related to slab width, and the highest degree of curling and warping varied with the various indicators.

For the LTPP sections and the non-LTPP highways, thicker slabs exhibited lower curling and warping based on the box plot ranges and the average degree of curling/warping. County roads/city streets exhibited the opposite result, with thicker slabs exhibiting greater curling and warping based on the average degree of curling/warping. Other factors, such as mix design, may have resulted in higher curling and warping behavior for thicker slabs in the county roads and city streets group.

The shorter transverse joint spacing in the county roads and city streets group produced relatively lower curling and warping based on the ranges of the box plots and the average degree of curling/warping.

The use of a larger dowel bar diameter lowered curling and warping behavior for the LTPP sections based on the average degree of curling/warping. While a larger dowel bar diameter

could improve load transfer efficiency and help reduce curling and warping, two city streets with 1.5 in. dowel bars demonstrated higher curling and warping than county roads without dowel bars. Further research is needed to examine other influencing factors.

For the non-LTPP sites, rectangular joints exhibited relatively lower curling and warping for all indicators, and slabs constructed with tied PCC shoulders significantly decreased all four indicators of curling and warping behavior compared to slabs with untied (HMA and gravel) shoulders based on the box plot ranges and the average degree of curling/warping.

City street projects had higher curling and warping behavior than county highway projects.

For the LTPP sections, a high-strength mixture tended to produce higher curling and warping behavior than a low-strength mixture based on the box plot ranges and the average degree of curling/warping. A low-strength mix has a lower total cementitious content (408 lbs) than a high-strength mix (850 lbs), while a low-strength mix has a higher w/cm ratio (0.53) than a high-strength mix (0.42). For the non-LTPP highways and county roads and city streets, the QMC mix lowered all curling and warping indicators more than the other mixes based on the box plot ranges and the average degree of curling/warping. The pre-QMC and C-SUD mix designs exhibited the greatest curling and warping tendencies.

Regarding the effects of construction season, this study found that non-LTPP highways paved during the spring might exhibit decreased curling and warping behavior compared to highways in the same group paved during other seasons based on the four indicators of the average degree of curling/warping. For county roads and city streets, projects constructed in the summer demonstrated a slightly higher average degree of curling/warping than projects constructed in the fall for all indicators.

It should be noted that LTPP section 0259 was categorized in the non-LTPP group because it is very different from the other LTPP sections. Those differences (especially in terms of mix design) most likely dominate other factors because the section was meant to be representative of a typical Iowa DOT concrete pavement at the time of construction, while the other LTPP sections contained many design variables according to the goals and objectives of Specific Pavement Study 2 (SPS-2). Notable differences include that LTPP section 0259 was constructed with an Iowa DOT mix similar to the pre-QMC mix used in other projects in this study, while the other 12 LTPP sections used various mix designs such as low-strength and high-strength mixes. LTPP section 0259 was also constructed over a standard Iowa DOT subbase like most of the non-LTPP projects, while the other LTPP sections were constructed with a variety of subbase layers in accordance with the goals of SPS-2. LTPP section 0259 was found to have significantly less curling and warping behavior than the other LTPP sections.

In the end, the multiple linear regression analysis showed that shorter and thicker slabs can reduce curling and warping. The findings are consistent with the recommendations made in the Phase I study and are summarized in Table 25 and Table 26.

Table 25. Comparison between literature review and findings for highways investigated in the study

Factor	Literature Review	This Study (Highways)	Match
Slab Thickness	A thicker slab can lower curling and warping (Wei et al. 2017).	A thicker slab resulted in lower curling and warping.	Yes
Transverse Joint Spacing	A shorter slab length can result in lower curling and warping (Roesler et al. 2012).	N/A	N/A
Slab Width	Slab width affects the curling stresses at the slab corners. To avoid excessive upward built-in curling, widened slabs should be no wider than 14 ft wide (Yu et al. 1998).	Slabs with 14 ft widths showed lower curling and warping behavior than slabs with 12 ft width for the LTPP sections.	N/A
Joint Type	Skewed joints can increase curling and warping behavior (Rasmussen et al. 2007).	Rectangular joints reduced curling and warping behavior compared to skewed joints.	Yes
Shoulder Type	Granular or HMA shoulders increase curling and warping behavior (Yang et al. 2018).	Tied shoulders showed lower curling and warping behavior.	Yes
Construction Season	Paving in the late fall season can minimize curling (Hansen et al. 2006, Kasu et al. 2021).	Paving in the spring or fall season reduced curling and warping behavior.	Yes
Dowel Bar Diameter	Dowel bars can restrain vertical curling deflection at joints but can also decrease curling and warping stresses by restraining vertical deflection (Ceylan et al. 2016a).	A larger dowel bar diameter could result in lower curling and warping behavior for the LTPP sections.	Yes

Table 26. Comparison between literature review and findings for county roads and city streets investigated in the study

Factor	Literature Review	This Study (County Roads and City Streets)	Match
Transverse Joint Spacing	A shorter slab length can result in lower curling and warping (Roesler et al. 2012).	A shorter slab length resulted in lower curling and warping.	Yes
Construction Season	Paving in the late fall season can minimize curling (Hansen et al. 2006, Kasu et al. 2021).	Paving in the fall season reduced curling and warping behavior.	Yes

5. ANALYSIS OF LIDAR SCANNING ON CONCRETE SLABS

5.1. Overview of LiDAR

A stationary light detection and ranging (LiDAR) system is a laser-based optical remote-sensing instrument that can measure a three-dimensional (3D) profile of the surface of an object. It can construct a high-resolution 3D geo-referenced point cloud (i.e., x, y, z coordinates) through physical scanning on the selected target. This advanced technology has been widely utilized in many applications, such as earth surveying, geodesy, geomatics, archaeology, geography, geology, forestry, atmospheric physics, and so on.

For pavement inspection and evaluation, the LiDAR system offers the possibility of collecting a high-resolution point cloud for pavement surfaces to measure slab curling and warping behavior. Unlike a high-speed profiler, which only provides profiles extracted from the wheel paths and centerline, a LiDAR scanner can cover the entire slab surface and offer multiple line paths, including a diagonal profile. Figure 51 demonstrates a typical field scan using the LiDAR system and a 3D view of the resulting slab profile.

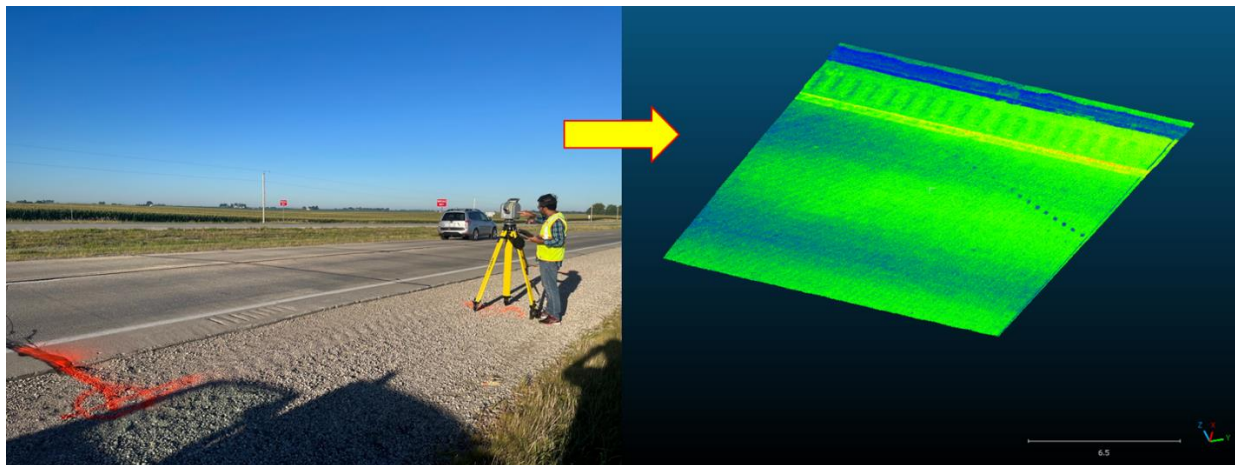


Figure 51. Field LiDAR scanning and 3D slab profile

Recent studies have investigated the use of LiDAR in pavement profiling. Chang et al. (2006) assessed 3D laser scanning technology to measure pavement roughness and recommended it for construction quality control and quality assurance (QC/QA). Chin and Olsen (2015) investigated the use of a LiDAR system for pavement roughness measurement and concluded that the measurements were comparable to those of other Class 1 profilometers. Yang et al. (2022) validated the accuracy and reliability of LiDAR through laboratory and field scanning and compared it to a reference device, a Class 1 walking profiler.

In the Phase I study (Ceylan et al. 2016a), a Leica ScanStation C10 LiDAR device was utilized to document the diurnal variations in slab profiles at six PCC sites; these sites are also included in the site list for this Phase II study. The first LiDAR scanning for the six sites was performed in

October and November 2015. For this Phase II study, three of the Phase I sites were rescanned to evaluate changes in curling and warping behavior, and one additional site was scanned.

5.2. Field LiDAR Data Collection and Processing

This Phase II study executed the field data collection using a Trimble SX10 LiDAR system for three Phase I sites located on US 30 and one Phase II site on D20 in Hamilton County. Table 27 lists the four sites scanned in the Phase II study, along with the scanning dates.

Table 27. Selected sites for LiDAR scanning

Site Code	Site Location	Route	Direction	Station	Construction Year	Phase I Scanning Date	Phase II Scanning Date
A	Ames, Story County	US 30	EB	1422	2013	10/28/2015	08/16/2022
B	Nevada, Story County	US 30	WB	2207	1995	10/28/2015	08/17/2022
C	Toledo, Tama County	US 30	EB	113	2005	11/10/2015	10/17/2022
D	Webster City, Hamilton County	D20	WB	N/A	1984	N/A	08/12/2022

One slab was selected for profile data collection and analysis at each site, with one scan at 7:30 a.m. (morning) and another at 3:00 p.m. (afternoon) performed separately on the same day. The three US 30 sites were each curled up with a 20 ft joint spacing, a 14 ft slab width, and a 10 in. thickness. Full details for these projects are presented in Table 2. D20 in Hamilton County was curled down with a 15 ft joint spacing, an 11 ft slab width, and a 6 in. thickness. Full details for this project are shown in Table 5.

Figure 52 illustrates the schematic diagram of directions for the PCC slabs investigated in this study. To make the results comparable with the findings from the Phase I study, this Phase II study followed the method executed in the Phase I study and extracted two diagonal profiles (D1 and D2) and one longitudinal profile (L) from the point cloud collected through the LiDAR system. Based on this method, the 2D slab profiles along the D1, D2, and L directions were extracted separately for further analysis.

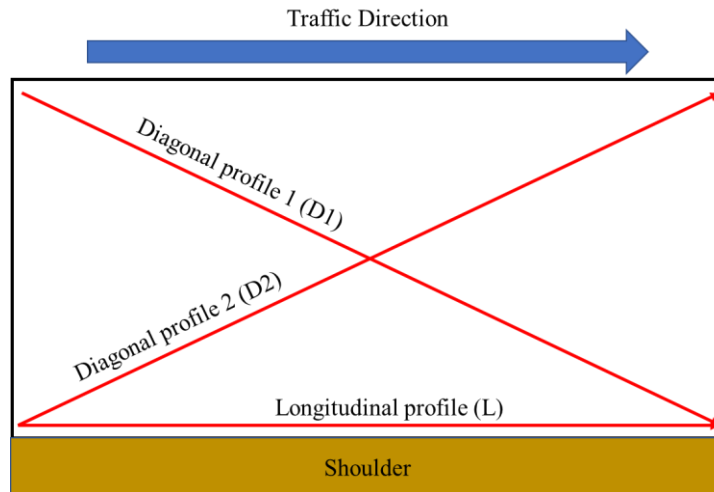


Figure 52. Schematic diagram of directions for a PCC slab

Figure 53 exhibits the general procedure for LiDAR data processing. This study utilized the CloudCompare software program for LiDAR data analysis. Since the raw scanning data typically include a lot of noise and unwanted data points (from the shoulder, adjacent slabs, joints, etc.), the first step was to segment the selected slab and eliminate unnecessary areas. The next step involved selecting the polyline paths. As demonstrated in Figure 52, D1, D2, and L were the three polylines selected in the 3D point cloud. The next step was to extract and output the 2D slab profile data points along these selected polylines. The remaining steps were similar to those described in Figure 11. The slab grade was removed from the extracted slab profile, and the profile was then filtered through the second polynomial fitting model to obtain a smooth curve shape. The last step was to level the fitted slab shape in the 2D coordinate system to determine the relative deflection, which is the curling and warping indicator utilized in the Phase I study.

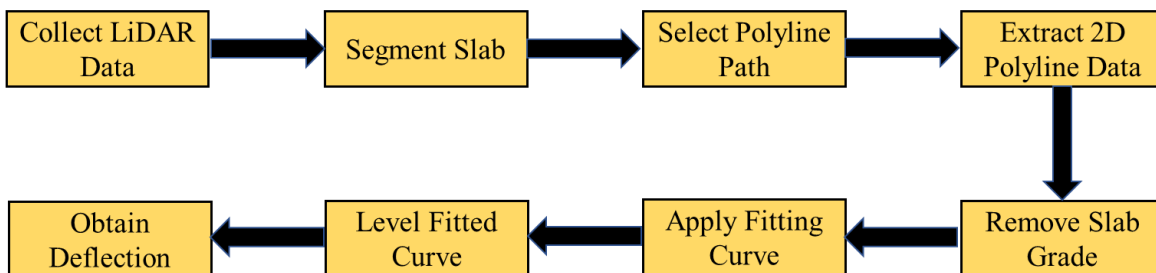


Figure 53. Flowchart of the LiDAR data processing procedure

5.3. Results and Discussion

Table 28 lists the surface temperatures during LiDAR scanning in the field. It should be noted that Slab C in Tama County was not scanned in the afternoon in 2015. Although Slab D in Hamilton County was not included in the Phase I study, its morning and afternoon profiles were well documented in the summer of 2022. Additionally, the Phase I data were collected in the fall of 2015, while the Phase II data were collected mainly in the summer of 2022. Data collection in

different seasons led to differences in the surface temperatures measured in Slabs A and B in Story County between 2015 and 2022. Slab C was measured in the same season in both years, October 2015 and October 2022. However, the surface temperature of Slab C in the fall of 2022 was significantly lower than that measured in 2015.

Table 28. Measured surface temperatures at the investigation sites

Slab Code	Site Location	Route	Direction	2015		2022	
				Morning	Afternoon	Morning	Afternoon
A	Ames, Story County	US 30	EB	46.9°F	47.6°F	62.9°F	85.3°F
B	Nevada, Story County	US 30	WB	43.7°F	36.6°F	64.5°F	83.9°F
C	Toledo, Tama County	US 30	EB	46.1°F	N/A	30.2°F	42.8°F
D	Webster City, Hamilton County	D20	WB	N/A	N/A	69.0°F	79.7°F

Figure 54 through Figure 57 illustrate the slab profiles extracted from the Phase II data collection activities, including the morning and afternoon profile shapes along the D1, D2, and L directions.

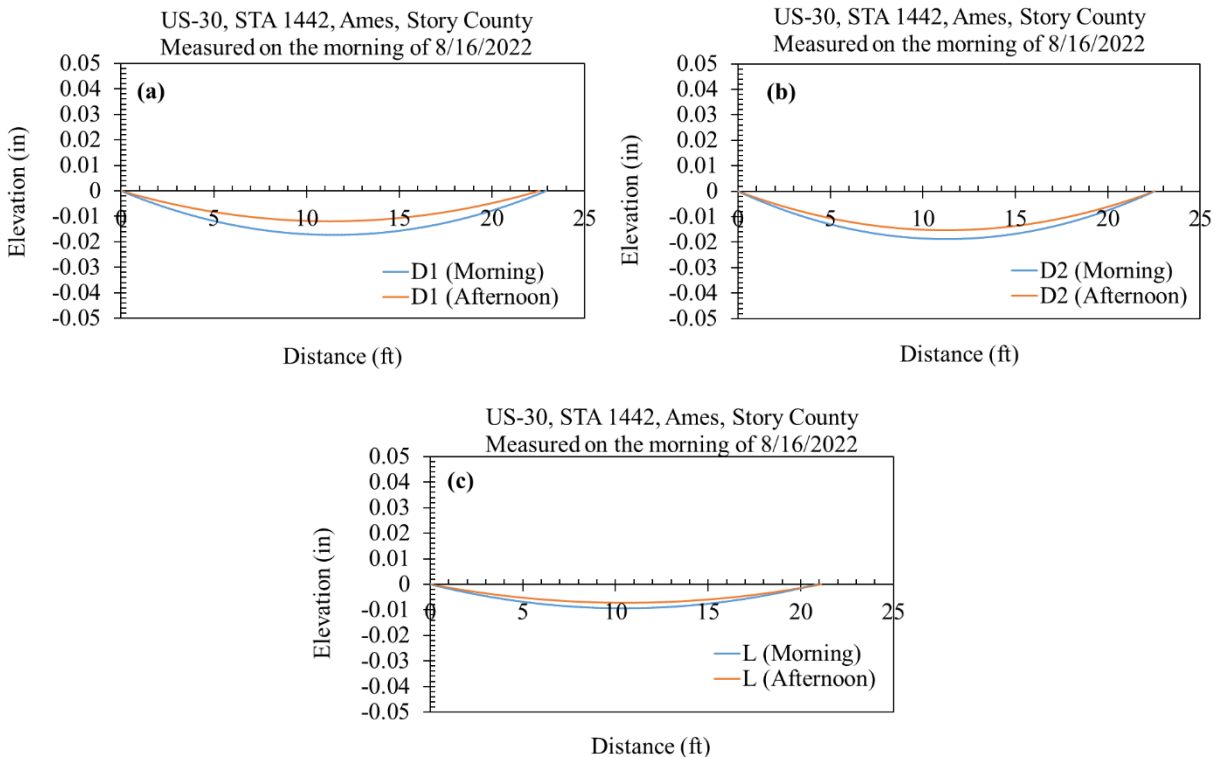


Figure 54. Profiles at Slab A along the directions of (a) D1, (b) D2, and (3) L

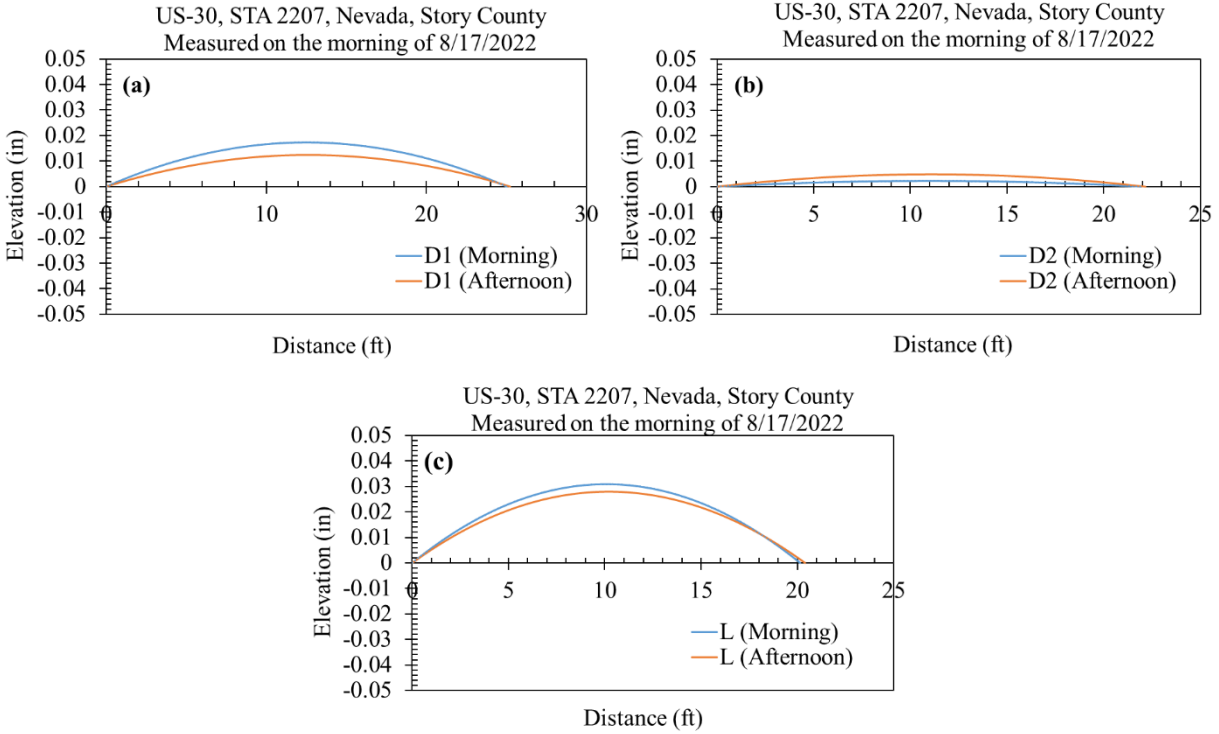


Figure 55. Profiles at Slab B along the directions of (a) D1, (b) D2, and (3) L

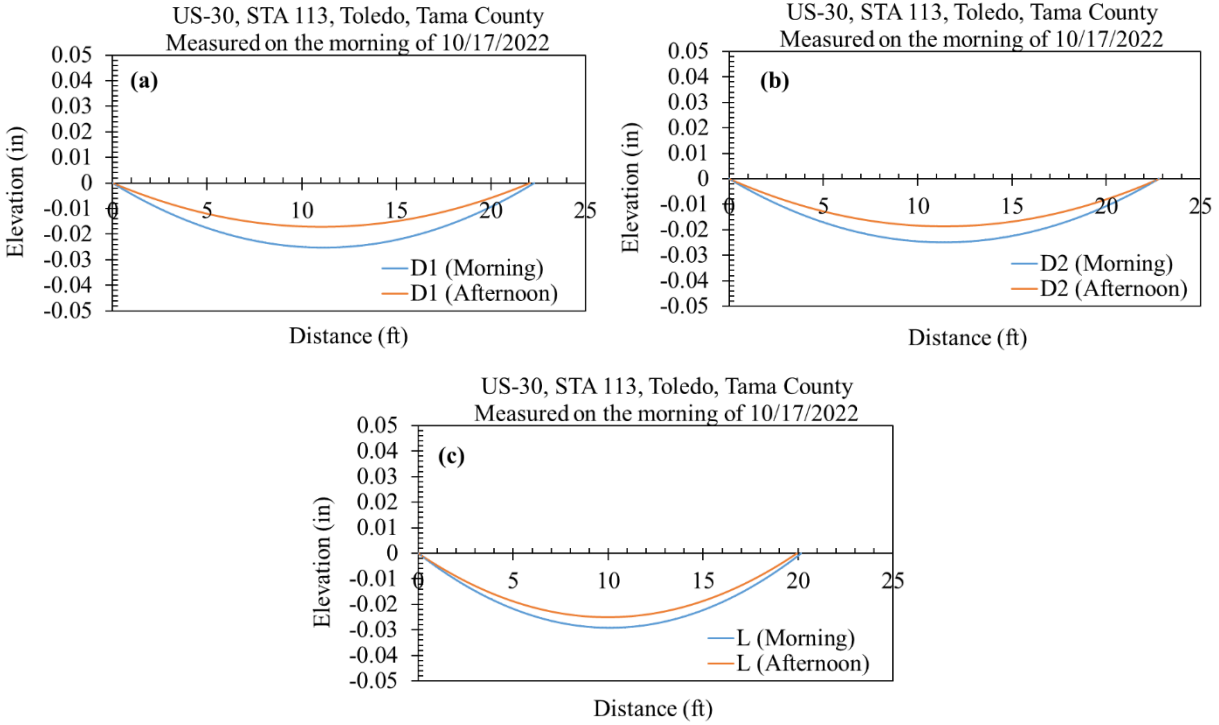


Figure 56. Profiles at Slab C along the directions of (a) D1, (b) D2, and (3) L

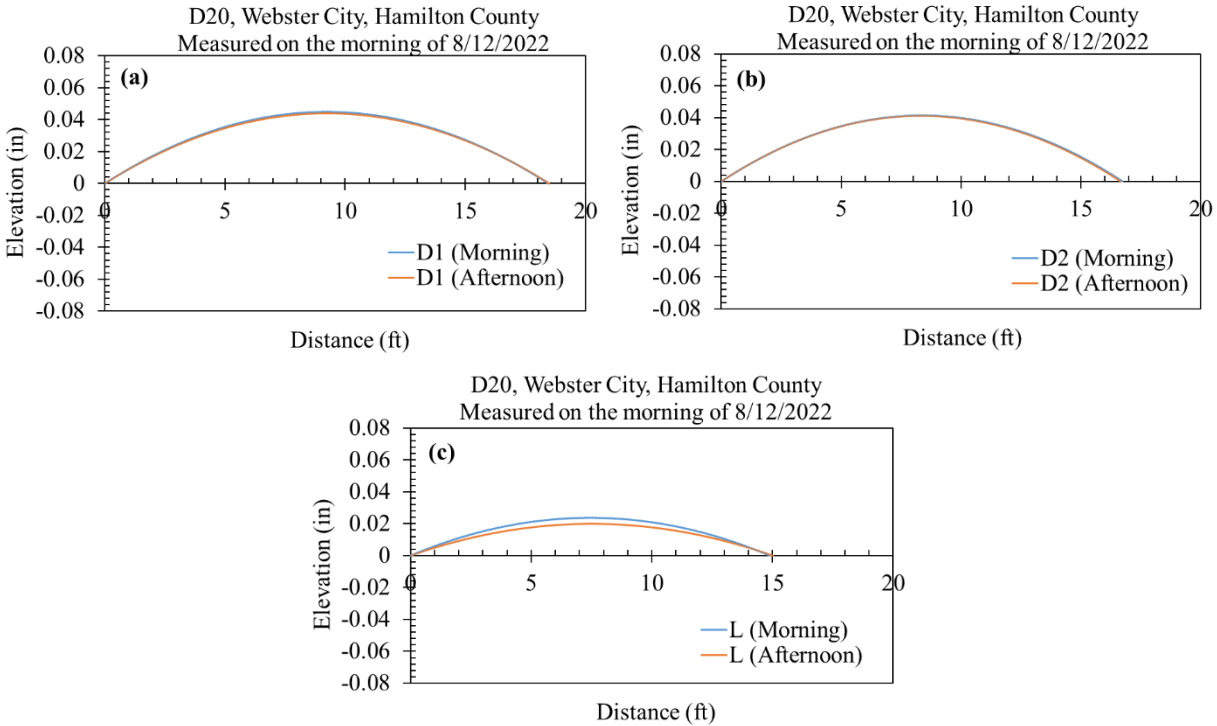


Figure 57. Profiles at Slab D along directions of (a) D1, (b) D2, and (c) L

Slabs A and C showed upward curling, while Slabs B and D curled down in all directions. As mentioned previously, mix design can influence curling and warping behavior. A QMC mix design was typically used for the sites constructed after 2000, while a pre-QMC mix design was widely used before 2000. The mix design information used for D20 was unavailable due to a lack of records.

Table 29 presents the detailed mix design information for the three Phase I sites. The influence of mix design on curling and warping was summarized in the Phase I study (Ceylan et al. 2016a).

Table 29. Mix design at the investigation sites

Slab Code	Site Location	Cement (lb/yd ³)	Fly Ash (lb/yd ³)	Coarse Agg. (lb/yd ³)	Fine Agg. (lb/yd ³)	Water (lb/yd ³)	w/c	air (%)
A	Ames, Story County	448	112	1,403	1,307	225	0.40	7.2
B	Nevada, Story County	457	114	1,653	1,446	250	0.44	7.8
C	Toledo, Tama County	448	112	1,446	1,272	224	0.40	6.0
D	Webster City, Hamilton County	N/A	N/A	N/A	N/A	N/A	N/A	N/A

Figure 58 depicts the relative deflections measured in 2015 and 2022. It should be noted that in the Phase I findings the profiles of D1 and L at Slab B showed upward curling while the profile

of D2 showed downward curling. In Phase II, the latest LiDAR scanning found that all three profiles showed upward curling.

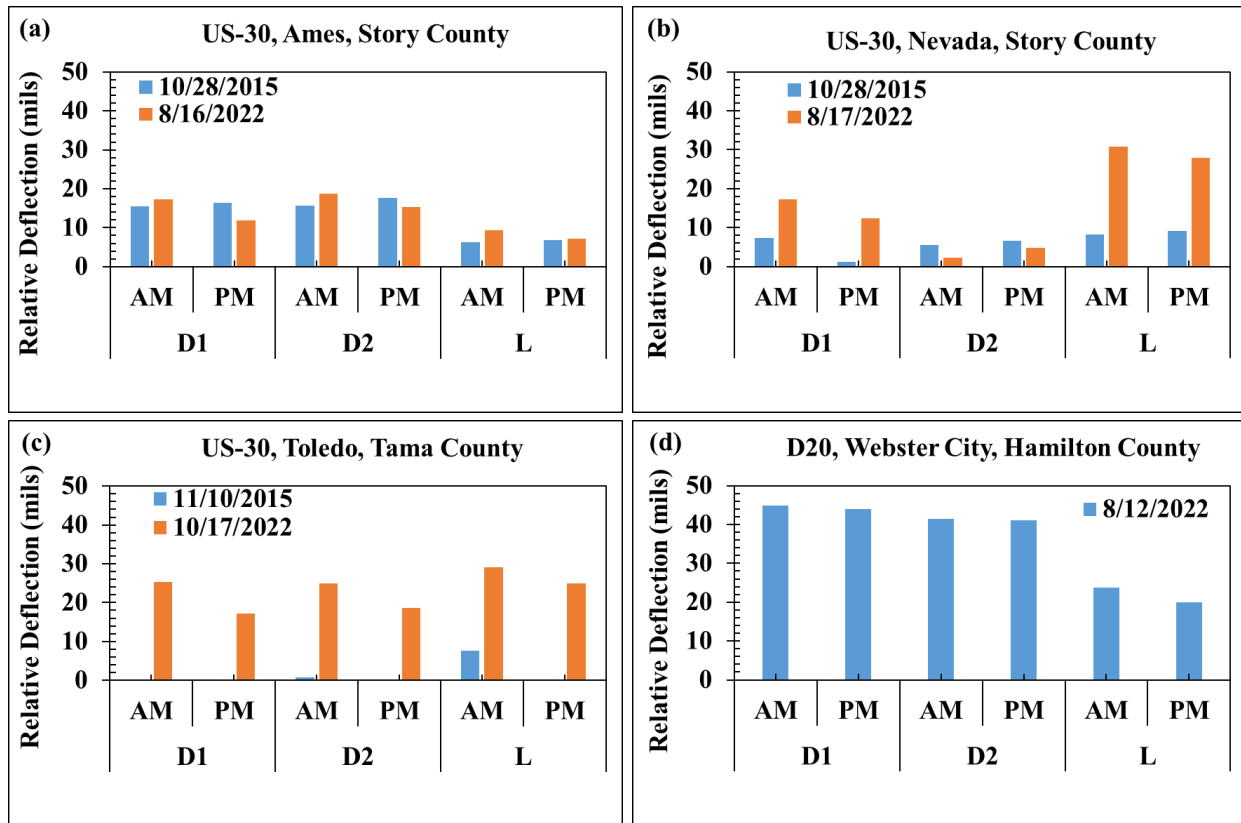


Figure 58. Absolute values of relative deflection for (a) Slab A, (b) Slab B, (c) Slab C, and (d) Slab D

The key findings after comparing the 2015 and 2022 data are as follows:

- Curled-up Slab A exhibited a relative deflection in the range of 7.2 mils to 18.8 mils, similar to the measurements taken in 2015.
- The profiles measured at Slab B showed significant changes after seven years. The direction of curling changed from upward to downward, with the D1 and L profiles showing changes of 24.7 and 39.1 mils, respectively.
- Slab C also exhibited a significant increase in relative deflection between 2015 and 2022, ranging from 17.1 to 25.0 mils.
- Slab D, a skewed slab with downward curling and warping, exhibited a relative deflection ranging from 19.9 to 44.9 mils.
- Morning measurements typically exhibited a higher relative deflection than afternoon measurements, which is consistent with the data collected using a high-speed profiler.
- For Slabs B and C, deflection in the diagonal direction was lower than in the longitudinal direction. However, Slabs A and D exhibited the reverse.

5.4. Summary

LiDAR scanning was performed at three Phase I sites and one Phase II site in 2022.

The findings indicate that after seven years, the profile for Slab A on US 30 near Ames was relatively unchanged, while the profile for Slab C on US 30 in Tama County exhibited a significant increase in curling and warping. For Slab B, the notable result is that its curling direction changed from upward to downward. The high-speed profiler scanning along the slab's L profile showed that the overall curling direction at that site on US 30 near Nevada is upward curling. This result indicates that a PCC site can exist that has both curled-up and curled-down slabs and that a slab can exist that shows different curling directions along different profile lines. For Slab D on D20 in Hamilton County, both LiDAR scanning and high-speed profiler scanning clearly indicated downward curling and showed a much higher degree of curling than at other sites.

The results did not indicate any consistent trends between curling in any direction and slab shape (i.e., skewed versus rectangular), mix design, or any other factors that were considered in the analysis of the high-speed profiler data.

6. CONCLUSIONS AND RECOMMENDATIONS

6.1. General Summary

The primary goal of this study was to identify the impacts of various design factors on the degree of curling and warping in Iowa concrete pavements by investigating the parameters that most significantly affect the curling and warping behavior of Iowa's highways, county roads, and city streets. The impact of seasonal and diurnal variations on the severity/magnitude of curling and warping in concrete slabs was also evaluated. This study investigated a number of indicators of pavement curling and warping, including curvature IRI, deflection, deflection ratio, and degree of curvature.

Thirty-six concrete pavement sections in Iowa were evaluated using a high-speed profiler at different times of day (early morning, noon, and late afternoon) and during each season (spring, summer, fall, and winter), and four of these sites were also assessed using a LiDAR device. A MATLAB algorithm was developed to analyze the raw profile data collected using an SSI high-speed profiler. This algorithm utilizes 2GCI-based and second-order polynomial-based models to compute four indicators of pavement curling and warping behavior. The LiDAR data were processed through the CloudCompare software program and compared with the data collected during the Phase I study in 2015.

Locations near MERRA climate stations were chosen to compute the equivalent temperature difference using PMED in order to test the algorithms and investigate the curling and warping behavior attributable to temperature gradient and moisture gradient.

A statistical study investigated general trends among the parameters that affect curling and warping, including slab geometry, shoulder type, mix type, and construction season, among others. One-way ANOVA was used to identify which variables significantly influenced curling and warping behavior. Finally, multiple linear regression models were created using various parameters to predict curling and warping behavior and analyze the parameters' impacts on curling and warping. Since four different indicators of the degree of curling and warping were assessed in this study, it is a good sign that the parameters generally agreed with each other in terms of the direction of the identified trends and statistical significance.

6.2. Algorithm Development and Data Processing

This study developed an advanced MATLAB-based algorithm for identifying the curling and warping behavior of PCC slabs using raw profile data collected from a high-speed profiler. The algorithm successfully integrates a joint detection function and 2GCI and second-order polynomial fitting curve models for characterizing four curling and warping indicators, including curvature IRI, deflection, deflection ratio, and degree of curvature. The algorithm was validated in the field with different profilers and demonstrated sufficient accuracy and repeatability for pavement profile data analysis.

The outputs from the algorithm are as follows:

- 2GCI fitting model:
 - PSG
 - Radius of relative stiffness (l)
 - Curvature and non-curvature profile
 - Curvature and non-curvature IRI
 - Deflection
 - Deflection ratio
- Second-order polynomial fitting model:
 - Degree of curvature
 - Curvature profile
 - Deflection
 - Deflection ratio

As the list of outputs shows, this algorithm uses raw profile data to compute several different measurements of the slab profile. It is easy to operate and can process large amounts of profile data. The benefits of this MATLAB-based algorithm are summarized as follows:

- After the profile data file is loaded and the joint spacing and curling direction are input, the algorithm can automatically process the data and save the results, with a progress bar to monitor the progress of the data analysis.
- The algorithm can process any profile data as long as the data are provided in *.erd format.
- The algorithm can process multiple raw data files at the same time.
- The integrated 2GCI algorithm and second-order polynomial algorithm can remove the slab grade before curve fitting and then re-apply the slab grade after fitting each slab.
- Removal and re-application of the slab grade has only a slight impact on curvature IRI. This process can generate continuous slab profiles with construction slopes. The resulting fitted and filtered profile is close to the actual pavement profile.
- The algorithm can output several results, including curvature IRI, deflection, curvature-related profile, non-curvature-related profile, deflection, deflection ratio, and degree of curvature. Users can choose the outputs based on their research needs.

Although the algorithm provides powerful functionality, two limitations should be pointed out. The first limitation is that the user needs to visually verify the curling direction from the raw profile plot before running the algorithm, and sometimes it is not easy to discern whether the pavement is curling up or down because the surface is too flat. The second limitation is the accuracy of the joint detection process. Surface distress, non-straight driving paths, sealed joints, and other factors may interfere with the accurate detection of joint locations, and this can sometimes result in a 2 to 3 ft error range. Finding multiple joint locations in the field (by placing more safety cones) and manually correcting the joint index in the output file are two potential solutions to this issue.

6.3. Key Findings

Temperature and moisture variations in slabs cause slab curling and warping. The effects of temperature gradients on slab deformation have been extensively investigated, and moisture gradients are typically converted to temperature gradients in analyses of slab deformation. This study successfully predicted the temperature differences between the top and bottom of the slab at curled-up PCC sites near reliable climatic stations using PMED. The key findings related to temperature and moisture variations are summarized as follows:

- For curled-up sites near reliable MERRA climate stations, the results indicated that curling and warping behavior decreases as the overall equivalent temperature difference increases.
- Using -10°F as the default effective permanent curling/warping temperature difference in PMED is a reasonable assumption because in this study when the extended trendlines of three curling/warping indicators (curvature IRI, deflection, and deflection ratio) practically approached zero, their overall equivalent temperature differences approached 0°F .
 - For the hourly component, ΔT_{Hourly} at noon always had positive values, while ΔT_{Hourly} in the morning and afternoon exhibited both negative and positive values. The scattered distribution indicated that the hourly temperature difference is not as significant as other variables for curling and warping behavior.
 - The shrinkage equivalent temperature difference had a more significant effect on curling and warping behavior than the hourly equivalent temperature difference and the total equivalent temperature difference.
- This study found that curling and warping behavior was greater in the morning than at noon or in the afternoon, which is consistent with previous studies that found that the diurnal temperature effect had a maximum impact during the nighttime and in the morning of the following day (Masad et al. 1996).
- The seasonal equivalent temperature difference was not evaluated using PMED due to the lack of winter data because when this study was conducted MERRA had not yet released climatic data for winter 2021.

Four indicators, including curvature IRI, deflection, deflection ratio, and degree of curvature, were obtained as outputs from the MATLAB algorithm to evaluate the curling and warping behavior of Iowa concrete pavements by analyzing these four indicators' relationships with different design, construction, and environmental factors. The key findings are summarized as follows:

- The results show that, in general, county roads and city streets exhibited relatively lower degrees of curling and warping than highway sections.
- For all groups, the fall season typically exhibited the highest average values for all indicators of curling/warping, while the spring and summer seasons had the lowest average values.
- Compared to measurements taken at noon and in the late afternoon, morning measurements reflect relatively higher average values for all four curing and warping indicators across all three roadway types (LTPP highways, non-LTPP highways, and county roads and city streets).

- The following results were found for the design factors affecting curling and warping behavior:
 - LTPP sections where larger diameter dowel bars were used exhibited less curling and warping behavior based on all indicators. However, LTPP sections with larger diameter dowel bars are typically associated with thicker slabs, which could also affect curling/warping behavior.
 - For the non-LTPP sites, rectangular joints exhibited much lower average values than skewed joints for all four curling and warping indicators.
 - For the non-LTPP sites, projects constructed with tied PCC shoulders exhibited significantly less curling and warping than projects constructed with untied (HMA and gravel) shoulders across all four indicators.
 - For the LTPP sections, projects constructed with high-strength mixes exhibited higher curling and warping behavior than projects constructed with low-strength mixes according to all four indicators. For the non-LTPP sites, projects constructed with the QMC mix exhibited less curling and warping than projects built using pre-QMC mixes across all four indicators.
 - For the non-LTPP highways, sites paved during the spring exhibited the lowest average values for all curling and warping indicators except degree of curvature, indicating that paving during the spring may result in lower curling and warping than paving during other seasons. For county roads and city streets, projects constructed in the summer demonstrated a slightly higher average degree of curling and warping than those constructed in the fall season. Paving during hot weather can lead to a large temperature gradient when the concrete sets at an early age.

A LiDAR device was utilized in this study to evaluate changes in curling and warping behavior over time for three sites from the Phase I study and one site from the Phase II study. The key findings are as follows:

- A curled-up slab on US 30 highway near Ames exhibited a similar deflections in 2015 and 2022.
- One diagonal and one longitudinal profile of a slab on US 30 near Nevada exhibited significant changes after seven years. The curling direction was upward in 2015 and downward in 2022.
- A slab on US 30 in Tama County also exhibited a significant increase in deflection after seven years.
- The LiDAR results for D20 in Hamilton County showed consistency with the results obtained from a high-speed profiler. Both sets of results indicated a high level of downward curling.
- LiDAR measurements taken in the morning typically exhibited a higher relative deflection than measurements taken in the afternoon, which is consistent with data collected using a high-speed profiler.

This study also analyzed the statistical impacts of different variables on curling and warping through one-way ANOVA and multiple linear regression prediction models. Different significant parameters were identified for each roadway type, and the findings are summarized as follows:

- According to the statistical analysis of curled-up sites, the relationships between curling and warping behavior and design, construction, and environmental variables matched those found in the literature review, as summarized in Table 25 and Table 26.
- The one-way ANOVA results indicated that the degree of curling and warping for the LTPP sections is highly influenced by mix type and slab thickness for all indicators.
- The one-way ANOVA results indicated that mix type, slab thickness, joint type, and shoulder type significantly influence the curvature IRI, deflection, and degree of curvature for the non-LTPP highways.
- The one-way ANOVA results indicated that the variables for county roads and city streets, such as mix type and joint spacing, significantly impact all curling and warping indicators except for the deflection ratio.
- Due to the limited number of data points and the lack of well-controlled sites, some factors (e.g., slab width, transverse joint spacing) did not show the expected trends summarized in Table 25.
- The effects of the design and construction parameters showed more significance than the effects of the seasonal and diurnal environmental parameters in this study. One limitation of these findings is that, due to safety considerations, data were not collected at night, which may have limited the ability to perceive maximum differences in curling behavior related to daily temperature changes.
- The multiple linear regression analyses for the three roadway types (i.e., LTPP sites, non-LTPP highways, and county roads and city streets) considered the effects of different variables on curling and warping behavior. However, the prediction models did not show very high R^2 values due to the limited number of data points.

6.4. Recommendations

Based on the field data collection, algorithm processing, and statistical analysis activities undertaken in this research, several recommendations can be advanced.

6.4.1. Recommendations for Computing the Degree of Curling and Warping

The recommendations regarding data collection using the high-speed profiler and data processing through the developed algorithm can be summarized as follows:

- Among the four proposed indicators of the degree of curling and warping, the deflection ratio and degree of curvature are theoretically the most useful measures because they reflect the unit slab curvature. Curvature IRI is a computational output reflecting the roughness caused by slab curvature, while deflection is a direct measure but not comparable among slabs with various joint spacings.
- The high-speed profiler can be used for profile data collection without the traffic control needed for other types of devices like the walking profiler. The accuracy and reliability of the high-speed profiler were validated in this study by comparing its results with those of a Class I walking profiler at the Reimen Garden parking lot site.
- For better measurement accuracy, rainy and snow days should be avoided for data collection.

- Concrete pavement that is relatively flat and/or exhibits a significant amount of cracking can be challenging to analyze. This is because in some cases cracks (especially transverse cracks) can be mistakenly recognized as joints in the joint detection algorithm, and a flat slab profile can cause difficulty in identifying curling direction and peaks (e.g., joint locations).
- Based on the experience collecting data using a high-speed profiler in this study, failure to calibrate the high-speed profiler's sensor will lead to poor quality data. It is recommended that the high-speed profiler be calibrated before collecting field data.
- Placing safety cones at different joint locations along the PCC pavement is recommended. The electrical eye of the high-speed profiler can detect the joints where the safety cones have been placed, and these known joint locations can help users manually correct other joint locations and obtain reliable slab profiles for data analysis.
- Before analyzing a site's profile data in MATLAB, it is best to select different sections of the site's raw data profile to judge the curling direction. If the curling direction is difficult to identify, try identifying upward curling first.

6.4.2. Design Recommendations for Minimizing Curling and Warping in Iowa Concrete Pavements

From a pavement design perspective, the following are some recommendations for minimizing curling and warping behavior in Iowa concrete pavements:

- The QMC mix design is recommended because it can reduce curling and warping compared to other mix design types.
- Pavements constructed with rectangular joints can effectively decrease curling and warping behavior compared to pavements constructed with skewed joints.
- The use of tied PCC shoulders can effectively reduce curling and warping behavior.

6.4.3. Recommendations for Future Research

The following list includes recommendations for future research to address some of the study's drawbacks and improve the results obtained from this study:

- Once the 2022 data are available for the MERRA climate stations used in this study, continue to analyze temperature and moisture gradients for winter data.
- The effects of slab width on curling and warping behavior could not be determined in this study due to a lack of data points. These effects could be the subject of a potential future study.
- The effects of transverse joint spacing on curling and warping behavior could not be determined for the non-LTPP highway sites since they have only one type of joint spacing (i.e., 20 ft). A future study could be undertaken to evaluate the effects of different (i.e., 15 ft, 17 ft, etc.) joint spacings for non-LTPP highway sites as recently implemented in Iowa.
- The limited information on mix design, such as cementitious content, fly ash content, aggregate gradation, w/cm ratio, and water content, for many pavements in this study made it challenging to draw a clear conclusion regarding the effects of mix design on curling and

warping behavior. The selection of PCC sites with a well-documented mix design and construction season and date is strongly recommended for future research.

- Long-term observation to track variations in curling and warping behavior, preferably beginning site monitoring during construction, is recommended.
- The MATLAB-based algorithm for data analysis can be improved in future research by allowing for the immediate use of the *.rsd files generated by the SSI software (the software bundled with the SSI high-speed profiler). The current algorithm can only recognize *.erd files, which means that the user has to convert *.rsd files to *.erd format first.
- Joint detection accuracy can also be improved by increasing the number of known joint locations during data collection. This recommendation suggests that the user should identify multiple transverse joints in the field (i.e., by placing a safety cone at the side of multiple joints), not only the start and end joints. Afterward, the user can utilize the “event” function integrated into the SSI high-speed profiler to mark such “events” (joints) during profile data collection. Such operations could be used to manually correct the results of joint detection in the algorithm and improve the accuracy of the analysis.
- Since the multiple linear regression model described in this study is based on a limited number of sites and a small amount of data, further improvement of the model in future research is recommended to better predict curling and warping behavior.
- The use of a LiDAR device for pavement inspection can be investigated in a future study, and the degree of curling and warping could be calculated along the longitudinal, transverse, and diagonal directions.
- To address the limited availability of construction information in this study, future exploration could focus more on the effects of construction season and paving time on curling and warping behavior. Sites should be selected with known construction seasons, dates, times, temperatures, and moisture contents.

REFERENCES

- AASHTO. 1993. *AASHTO Guide for Design of Pavement Structures*. American Association of State Highway and Transportation Officials, Washington, DC.
- AASHTO. 2002. *AASHTO Mechanistic-Empirical Pavement Design Guide*. American Association of State Highway and Transportation Officials, Washington, DC.
- ACI Committee 302. 2016. *Concrete Q&A: Concrete Slab Curling Over Vapor Retarders*. American Concrete Institute, Farmington Hills, MI.
- Ahammed, M. A., and Tighe, S. L. 2008. Statistical Modeling in Pavement Management: Do the Models Make Sense? *Transportation Research Record: Journal of the Transportation Research Board*, Vol. 2084, No. 1, pp. 3–10.
- Arora, J., S. Nazarian, and V. Tandon. 2007. *Continuous Deflection Testing of Texas Pavements*. University of Texas at El Paso (UTEP), El Paso, TX.
- Asadi, I., P. Shafiq, Z. F. B. A. Hassan, and N. B. Mahyuddin. 2018. Thermal Conductivity of Concrete: A Review. *Journal of Building Engineering*, Vol. 20, pp. 81–93.
- Asbahan, R. E. 2009. Effects of the Built-In Construction Gradient and Environmental Conditions on Jointed Plain Concrete Pavements. PhD dissertation. University of Pittsburgh, Pittsburgh, PA.
- Asbahan, R. E., and J. M. Vandenbossche. 2011. Effects of Temperature and Moisture Gradients on Slab Deformation for Jointed Plain Concrete Pavements. *Journal of Transportation Engineering*, Vol. 137, No. 8, pp. 563–570.
- Bischoff, D. L. 1996. *Random Skewed Joints with and Without Dowels*. Wisconsin Department of Transportation, Madison, WI.
- Byrum, C. R. 2001. A High-Speed Profiler-Based Slab Curvature Index for Jointed Concrete Pavement Curling and Warping Analysis. PhD dissertation. University of Michigan, Ann Arbor, MI.
- Byrum, C. R. 2005. The Effect of Slab Curvature on IRI Values for Jointed Concrete Pavements. *International Journal of Pavement Engineering*, Vol. 1, No. 1, pp. 23–32.
- Byrum, C. R. 2009. Measuring Curvature in Concrete Slabs and Connecting the Data to Slab Modeling Theory. *Transportation Research Record: Journal of the Transportation Research Board*, Vol. 2094, No. 1, pp. 79–88.
- Ceylan, H., D. Turner, R. O. Rasmussen, G. K. Chang, J. Grove, S. Kim, and C. S. Reddy. 2005. *Impact of Curling, Warping, and Other Early-Age Behavior on Concrete Pavement Smoothness: Early, Frequent, and Detailed (EFD) Study*. National Concrete Pavement Technology Center, Ames, IA.
- Ceylan, H., S. Yang, K. Gopalakrishnan, P. Taylor, S. Kim, and A. Alhasan. 2016a. *Impact of Curling and Warping on Concrete Pavement*. National Concrete Pavement Technology Center, Ames, IA.
- Ceylan, H., R. F. Steffes, K. Gopalakrishnan, S. Kim, S. Yang, and K. Zhuang. 2016b. *Development and Evaluation of a Portable Device for Measuring Curling and Warping in Concrete Pavements*. Institute for Transportation, Ames, IA.
- Chang, J., K. Chang, and D. Chen. 2006. Application of 3D Laser Scanning on Measuring Pavement Roughness. *Journal of Testing and Evaluation*, Vol. 34, No. 2, pp. 1–9. <https://doi.org/10.1520/JTE13178>.

- Chang, G. K., S. M. Karamihas, R. O. Rasmussen, D. Merritt, and M. Swanlund. 2008. Quantifying the Impact of Jointed Concrete Pavement Curling and Warping on Pavement Unevenness. 6th Symposium on Pavement Surface Characteristics (SURF), October 3–5, Potoroz, Slovenia.
- Chin, A., and M. J. Olsen. 2015. Evaluation of Technologies for Road Profile Capture, Analysis, and Evaluation. *Journal of Surveying Engineering*, Vol. 141, No. 1, pp. 1–13. [https://doi.org/10.1061/\(ASCE\)SU.1943-5428.0000134](https://doi.org/10.1061/(ASCE)SU.1943-5428.0000134).
- Choi, S., and M. C. Won. 2009. Design of Tie Bars in Portland Cement Concrete Pavement Considering Nonlinear Temperature Variations. *Transportation Research Record: Journal of the Transportation Research Board*. No. 2095.1, pp. 24–33.
- Choubane, B., and M. Tia. 1992. Nonlinear Temperature Gradient Effect on Maximum Warping Stresses in Rigid Pavements. *Transportation Research Record: Journal of the Transportation Research Board*, Vol. 1370, No. 1, pp. 11–19.
- Chung, Y. 2012. Thermal Stress Analysis of Jointed Plain Concrete Pavements Containing Fly Ash and Slag. PhD dissertation. Louisiana State University, Baton Rouge, LA.
- Dempsey, B. J. 1969. A Heat-Transfer Model for Evaluating Frost Action and Temperature-Related Effects in Multilayered Pavement Systems. PhD dissertation. University of Illinois at Urbana-Champaign, Urbana, IL.
- Eisenmann, J., and G. Leykauf. 1990. Simplified Calculation Method of Slab Curling Caused by Surface Shrinkage. *Proceedings of the 2nd International Workshop on Theoretical Design of Concrete Pavements*, Ede, Netherlands, pp. 185–197.
- FHWA. 2020. Highway Statistics Series. Federal Highway Administration. <https://www.fhwa.dot.gov/policyinformation/statistics/2019/hm51.cfm>.
- Grasley, Z. C., D. A. Lange, and M. D. D'Ambrosia. 2006. Internal Relative Humidity and Drying Stress Gradients in Concrete. *Materials and Structures*, Vol. 39, No. 9, pp. 901–909.
- Hajibabae, A., and M. T. Ley. 2016. The Impact of Wet Curing on Curling in Concrete Caused by Drying Shrinkage. *Materials and Structures*, Vol. 49, No. 5, pp. 1629–1639.
- Harr, M. E. 1958. Warping Stresses and Deflections in Concrete Slabs. PhD dissertation. Purdue University. West Lafayette, IN.
- Hasan, M. A., and R. A. Tarefder. 2018. Development of Temperature Zone Map for Mechanistic Empirical (ME) Pavement Design. *International Journal of Pavement Research and Technology*, Vol. 11, No. 1, pp. 99–111.
- Ioannides, A. M., and R. A. Salsilli-Murua. 1989. Temperature Curling in Rigid Pavements. An Application of Dimensional Analysis. *Transportation Research Record: Journal of the Transportation Research Board*, Vol. 1227, pp. 1–11.
- Iowa DOT. 2015. *DS-15031. Developmental Specifications for Quality Management Concrete (QM-C)*. Iowa Department of Transportation, Ames, IA. https://iowadot.gov/specifications/dev_specs/2015/DS-15031.pdf.
- Iowa DOT. 2022. *Materials IM 529. Portland Cement (PC) Concrete Proportions*. Iowa Department of Transportation, Ames, IA. <https://iowadot.gov/erl/current/IM/content/529.htm>.
- Johnson, A. M., B. C. Smith, W. H. Johnson, and L. W. Gibson. 2010. *Evaluating the Effect of Slab Curling on IRI for South Carolina Concrete Pavements*. FHWA-SC-10-04. South Carolina Department of Transportation, Columbia, SC.

- Karamihas, S. 1999. *Guidelines for Longitudinal Pavement Profile Measurement*. University of Michigan. Transportation Research Institute, Ann Arbor, MI.
- Karamihas, S., and K. Senn. 2012. *Curl and Warp Analysis of the LTPP SPS-2 Site in Arizona*. FHWA-HRT-12-068. Turner-Fairbank Highway Research Center, McLean, VA.
- Karamihas, S. M., R. O. Rasmussen, and G. K. Chang. 2008. Development of a Second-Generation Index to Describe Concrete Pavement Slab Curvature. 87th Annual Meeting of the Transportation Research Board, January 13-17, Washington, DC.
- Kasu, S. R., S. Patel, A. R. Muppireddy. 2021. Field Experiments and Numerical Analysis of Curling Behavior of Cast-in-Situ Short Paneled Concrete Pavement on Lean Concrete Base. *International Journal of Pavement Engineering*, Vol. 23, No. 11, pp. 1–14.
- Khazanovich, L., R. Bartlett, T. McPeak, and M. Darter. 1998. *Common Characteristics of Good and Poorly Performing PCC Pavements*. FHWA-RD-97-131. Turner-Fairbank Highway Research Center, McLean, VA.
- Olidis, C., and D. Hein. 2004. Guide for the Mechanistic-Empirical Design of New and Rehabilitated Pavement Structures Materials Characterization: Is Your Agency Ready? Annual Conference of the Transportation Association of Canada, September 19–22, Quebec, Canada.
- Kim, K., S. Chun, B. Park, and S. Han. 2021. Precast Prestressed Concrete Pavement (PPCP): Effect of Thermal Gradient on Curling Deflection and Stress. *Construction and Building Materials*, Vol. 274, No. 8.
- Lang, F. C. 1942. Temperature and Moisture Variations in Concrete Pavements. *Highway Research Board Proceedings, December 2–5, 1941, Baltimore, MD*, Vol. 21.
- Lederle, R. E., R. W. Lothschutz, and J. E. Hiller. 2011. *Field Evaluation of Built-In Curling Levels in Rigid Pavements*. MN/RC 2011-16. Minnesota Department of Transportation, St Paul, MN.
- Lee, C. J., D. A. Lange, and Y. S. Liu. 2011. Prediction of Moisture Curling of Concrete Slab. *Materials and Structures*, Vol. 44, No. 4, pp. 787–803.
- Lee, D. H., K. H. Kim, S. Y. Jang, and G. Zi. 2017. Deformation and Stress Distribution of Discontinuous Precast Concrete Track Slab: I. Initial and Temperature Deformation. *Journal of the Korean Society for Railway*, Vol. 20, No. 5, pp. 625–636.
- Lee, H. S., S. W. Haider, K. Chatti, and N. Buch. 2020. Effect PCC Slab Curling and Warping on Pavement Roughness. 12th International Conference on Concrete Pavements, September 27–October 1, Minneapolis, MN.
- Mackiewicz, P., A. Szydło, and B. Krawczyk. 2018. Influence of the Construction Technology on the Texture and Roughness of Concrete Pavements. *Roads and Bridges (Drogi i Mosty)*, Vol. 17, No. 2, pp. 111–126.
- Maitra, S. R., K. S. Reddy, and L. S. Ramachandra. 2009. Load Transfer Characteristics of Dowel Bar System in Jointed Concrete Pavement. *Journal of Transportation Engineering*, Vol. 135, No. 11, pp. 813–821.
- Masad, E., R. Taha, and B. Muhunthan. 1996. Finite-Element Analysis of Temperature Effects on Plain-Jointed Concrete Pavements. *Journal of Transportation Engineering*, Vol. 122, No. 5, pp. 388–398.
- Mateos, A., J. Harvey, J. Bolander, R. Wu, J. Paniagua, and F. Paniagua. 2020. Structural Response of Concrete Pavement Slabs under Hygrothermal Actions. *Construction and Building Materials*, Vol. 243.

- McCracken, J. K. K. 2008. Seasonal Analysis of the Response of Jointed Plain Concrete Pavements to FWD and Truck Loads. PhD dissertation. University of Pittsburgh. Pittsburgh, PA.
- Mesinger, F., G. DiMego, E. Kalnay, K. Mitchell, P. C. Shafran, W. Ebisuzaki, D. Jović, J. Woollen, E. Rogers, and E. H. Berbery. 2006. North American Regional Reanalysis. *Bulletin of the American Meteorological Society*, Vol. 87, No. 3, pp. 343–360.
- Můčka, P. 2017. International Roughness Index Specifications around the World. *Road Materials and Pavement Design*, Vol. 18, No. 4, pp. 929–965.
- Nassiri, S. 2011. Establishing Permanent Curl/Warp Temperature Gradient in Jointed Plain Concrete Pavements. PhD dissertation. University of Pittsburgh, Pittsburgh, PA.
- Nantung, E. T. 2011. *High-Performance Concrete Pavement in Indiana*. FHWA/IN/JTRP-2011/20. Joint Transportation Research Program, Indiana Department of Transportation, West Lafayette, IN.
- Perera, R. W., C. Byrum, and S. D. Kohn. 1998. *Investigation of Development of Pavement Roughness*. FHWA-RD-97-147. Turner-Fairbank Highway Research Center, McLean, VA.
- Perera, R. W., S. D. Kohn, and S. Tayabji. 2005. *Achieving a High Level of Smoothness in Concrete Pavements without Sacrificing Long-Term Performance*. FHWA-HRT-05-068. Turner-Fairbank Highway Research Center, McLean, VA.
- Philip, J. R., and D. A. De Vries. 1957. Moisture Movement in Porous Materials under Temperature Gradients. *Eos, Transactions American Geophysical Union*, Vol. 38, No. 2, pp. 222–232.
- Pradena, M., and L. Houben. 2018. Ride Quality Stability of Jointed Plain Concrete Road Pavements with Short Slabs. *Proceedings of the Institution of Civil Engineers: Transport*, Vol. 171, No. 3, pp. 166–173.
- Qin, Y. 2011. Numerical Study on the Curling and Warping of Hardened Rigid Pavement Slabs. PhD dissertation. Michigan Technological University, Houghton, MI.
- Qin, Y., J. E. Hiller, and D. Meng. 2019. Linearity between Pavement Thermophysical Properties and Surface Temperatures. *Journal of Materials in Civil Engineering*, Vol. 31, No. 11.
- Rao, C., D. E. J. Barenberg, M. B. Snyder, and S. Schmidt. 2001. Effects of Temperature and Moisture on the Response of Jointed Concrete Pavements. 7th International Conference on Concrete Pavements, September 9–13, Orlando, FL.
- Rao, S., J. R. Roesler, B. 2005. *Characterization of Effective Built-In Curling and Concrete Pavement Cracking on the Palmdale Test Sections*. University of Illinois at Urbana-Champaign, Urbana, IL.
- Rasmussen, R. O., A. Agosto, S. Cramer, and T. T. Group. 2007. *Analysis of Concrete Pavement Joints to Predict the Onset of Distress*. WHRP 07-13. Wisconsin Department of Transportation, Madison, WI.
- Roesler, J. R., V. G. Cervantes, and A. N. Amirhanian. 2012. Accelerated Performance Testing of Concrete Pavement with Short Slabs. *International Journal of Pavement Engineering*, Vol. 13, No. 6, pp. 494–507.
- Sayers, M. W., and S. M. Karamihas. 1996. *Interpretation of Road Roughness Profile Data*. FHWA-RD-96-101. Turner-Fairbank Highway Research Center, McLean, VA.

- Shafiee, M., O. Maadani, and H. Shirkhani. 2019. Evaluation of Climate Impacts on Jointed Plain Concrete Pavement Structures. *Proceedings of the 2019 TAC-ITS Canada Joint Conference & Exhibition, September 22–26, Halifax, Canada*, pp. 22–25.
- Siddique, Z., and M. Hossain. 2005. Finite Element Analysis of PCCP Curling and Roughness. *Proceedings of the 8th International Conference on Concrete Pavements: Innovations for Concrete Pavement: Technology Transfer for the Next Generation, August 14–18, Colorado Springs, CO*, pp. 1173–1188.
- Smith, K., and P. Ram. 2016. *Measures and Specifying Pavement Smoothness*. FHWA-HIF-16-032. Federal Highway Administration, Washington, DC.
- Suprenant, B. A. 2002. Why Slabs Curl. *Concrete International*, Vol. 24, No. 3, pp. 56–61.
- Tan, Z., Z. Ma, and X. Zou. 2013. Pavement Temperature Estimation Model Based on Field Temperature Data. *Journal of Tongji University (Natural Science)*, Vol. 41, No. 5, pp. 700–704.
- Tayabji, S. D., M. Swanlund, and S. Tyson. 2010. *Impact of Temperature Curling and Moisture Warping on Jointed Concrete Pavement Performance*. FHWA-HIF-10-010. Federal Highway Administration, Washington, DC.
- Teller, L. W., and E. C. Sutherland. 1935. *The Structural Design of Concrete Pavements*. Bureau of Public Roads, Washington, DC.
- Thomlinson, J. 1940. Temperature Variations and Consequent Stresses Produced by Daily and Seasonal Temperature Cycles in Concrete Slabs. *Concrete Constructional Engineering*, Vol. 36, No. 6, pp. 298–307.
- Tian, K., B. Yang, D. King, H. Ceylan, and S. Kim. 2021. Characterization of Curling and Warping Influence on Smoothness of Jointed Plain Concrete Pavements. *Airfield and Highway Pavements 2021: Airfield Pavement Technology*, pp. 110–119.
- Wang, D. 2016. Prediction of Time-Dependent Temperature Distribution within the Pavement Surface Layer during FWD Testing. *Journal of Transportation Engineering*, Vol. 142, No. 7.
- Wang, D., J. R. Roesler, and D. Z. Guo. 2009. Analytical Approach to Predicting Temperature Fields in Multilayered Pavement Systems. *Journal of Engineering Mechanics*. Vol. 135, No. 4.
- Wei, Y., and W. Hansen. 2011. Characterization of Moisture Transport and Its Effect on Deformations in Jointed Plain Concrete Pavement. *Transportation Research Record: Journal of the Transportation Research Board*, Vol. 2240, No. 1, pp. 9–15.
- Wei, Y., S. Liang, and X. Gao. 2017. Numerical Evaluation of Moisture Warping and Stress in Concrete Pavement Slabs with Different Water-to-Cement Ratio and Thickness. *Journal of Engineering Mechanics*, Vol. 143, No. 2.
- Wei, Y., Y. Wang, and X. Gao. 2015. Effect of Internal Curing on Moisture Gradient Distribution and Deformation of a Concrete Pavement Slab Containing Pre-Wetted Lightweight Fine Aggregates. *Drying Technology*, Vol. 33, No. 3, pp. 355–364.
- Wells, S. A. 2006. Early-Age Response of Jointed Plain Concrete Pavements to Environmental Loads. MS thesis. University of Pittsburgh, Pittsburgh, PA.
- Westergaard, H. M. 1926. Stresses in Concrete Pavements Computed by Theoretical Analysis. *Public Roads*. Vol. 7, No. 2, pp. 25–35.
- Yang, S. 2014. Health Monitoring of Pavement Systems Using Smart Sensing Technologies. MS thesis. Iowa State University, Ames, IA.

- Yang, S. 2019. Investigation of Curling and Warping Behavior of Iowa Concrete Pavements Using Advanced Technologies. PhD dissertation. Iowa State University, Ames, IA.
- Yang, S., A. Alhasan, H. Ceylan, S. Kim, and B. Yang. 2022. Accuracy Assessment of Light Detection and Ranging System Measurements for Jointed Concrete Pavement Surface Geometry. *Road Materials and Pavement Design*.
<https://doi.org/10.1080/14680629.2022.2093262>.
- Yang, S., H. Ceylan, K. Gopalakrishnan, S. Kim, P. C. Taylor, and A. Alhasan. 2018. Characterization of Environmental Loads Related Concrete Pavement Deflection Behavior Using Light Detection and Ranging Technology. *International Journal of Pavement Research and Technology*, Vol. 11, No. 5, pp. 470–480.
- Yang, S., Y. Zhang, O. Kaya, H. Ceylan, and S. Kim. 2020a. Investigation of Longitudinal Cracking in Widened Concrete Pavements. *The Baltic Journal of Road and Bridge Engineering*, Vol. 15, No. 1, pp. 211–231.
- Yang, S., Y. Zhang, O. Kaya, H. Ceylan, and S. Kim. 2020b. Investigation of Longitudinal Cracking in Widened Concrete Pavements. *The Baltic Journal of Road and Bridge Engineering*, Vol. 15, No. 1, pp. 211–231.
- Ytterberg, R. F. 1987. Shrinkage and Curling of Slabs on Grade: Part 2. *Concrete International*, Vol. 9, No. 5, pp. 54–61.
- Yu, H. and L. Khazanovich. 2001. Effects of Construction Curling on Concrete Pavement Behavior. 7th International Conference on Concrete Pavements, September 9–13, Orlando, FL.
- Yu, H. T., L. Khazanovich, and M. I. Darter. 2004. Consideration of JPCP Curling and Warping in the 2002 Design Guide. 83rd Annual Meeting of the Transportation Research Board, January 11–15, Washington, DC.
- Yu, H. T., L. Khazanovich, M. I. Darter, and A. Ardani. 1998. Analysis of Concrete Pavement Responses to Temperature and Wheel Loads Measured from Instrumented Slabs. *Transportation Research Record: Journal of the Transportation Research Board*, Vol. 1639, No. 1, pp. 94–101.
- Zhao, H., C. Li, L. Ma, Y. Tian, and J. Ling. 2020. Simple Empirical Temperature Gradient Prediction Model for Jointed Plain Concrete Pavements: Development and Validation. *Journal of Transportation Engineering, Part B: Pavements*, Vol. 146, No. 3.

APPENDIX A. ADDITIONAL MATERIAL

A.1. Operation Manual for SSI High-Speed Profiler

Profiler equipment to load:

1. Removable power cable
2. DMI assembly
3. Lasers
4. Camera
5. Laptop and its charging cable
6. Enough memory space on laptop for processing and storing the data
7. Marking spray (bright green or red)
8. Cones with reflector strips
9. Reflector vest
10. Strobe light for the truck
11. Hand-operated distance measuring wheel

Preparing the profiler:

1. Bolt in the DMI plate and the rod in its position at the rear left wheel. Adjust the position of the plate to find a balanced position for the plate.
2. Undo the Allen screws from the laser mounting brackets on the truck and carefully insert the laser units into their dovetail slots without exerting too much pressure. Tighten the Allen screws a reasonable amount but avoid overtightening.
3. Connect the three cables on the side laser units to their respective counterparts.
4. Undo the four screws on the control box and remove the cover. Fasten the two cables on the central laser unit. The black cable passes into the control unit from its bottom surface and is fastened to one of the two black cable counterparts.
5. Close the control unit cover and tighten back the four screws.
6. Ensure that the GPS antenna suction mounts are firmly locked on the truck hood.
7. Attach the suction cup-mounted camera on the windshield approximately to the middle position and at the highest possible available location to obtain the optimum viewing angle.
8. Start the truck. Then connect the power cable to the control unit power-in plug and the power output port outside the truck. Confirm that the blue light is on at the control unit box.
9. Attach the laptop to its housing and lock it in its position securely.
10. Connect the data cable, power cable, and camera cable to the laptop housing input ports or the laptop ports.
11. Turn on the laptop and open SSI Profiler software.
12. Go to Collect. Let the software search and find the SSI Profiler hardware and load the interface view. Wait for the GPS to load satellites and show the GPS coordinates.
13. At this point, the system should be green and good to go.
14. Check outside that all three lasers are armed and visible on the ground surface.
15. Each time the equipment is assembled, calibration of the accelerometer and DMI unit is required for the accuracy of the data collected.

Data collection:

1. Using the selected site data sheet, drive the truck to the starting point of the site to be surveyed.
2. Observe the station numbers marked on the side of the pavement near the shoulder. Using Google Maps, save this site on a mobile device (phone or tablet) for future visits. Use spray paint to mark the physical starting point location on the pavement and place a cone centered on the marker in the shoulder area.
3. If one cone is too lightweight, double it with another cone to prevent it from falling over from wind.
4. Ensure that the cone has a sufficient area of reflector strip to be visible by the truck's blue IR trigger sensor unit on the right-side laser unit.
5. Move to the end position of the site track and repeat steps 2 through 4 for the end point.
6. Drive the truck, search for a convenient U-turn, and be ready for data collection.
7. Provide sufficient distance between the truck and the starting point before accelerating and adjusting speed. Set the cruise speed to 60 to 70 mph for the truck before reaching the starting point.
8. On the Collect tab in the SSI Profiler software, click Collect. Select the run-up and run-out lengths, then click OK. Then approximately 25 ft before approaching the starting cone, click EE Start and pass the cone. Note that the EE (electric eye infrared) sensor should trigger data collection the instant it sees and passes the cone. Continue toward the end point.
9. Approximately 25 ft before the end cone, click EE Stop; the data collection will stop once the truck sees the end cone.
10. Let the data be processed then save the results as a new project. Name the project according to your site, run, time, station number, etc.

A.2. Data Processing Procedure Using MATLAB

The data processing procedure is as follows:

1. Pick one of multiple runs with three similar tracks (similar raw IRI profiles) in the SSI Profiler software.
2. Convert the SSI raw profile into a *.erd profile for use in ProVAL since the MATLAB-based algorithm can only recognize *.erd.
3. Open the MATLAB-based algorithm file and load the *.erd profile data.

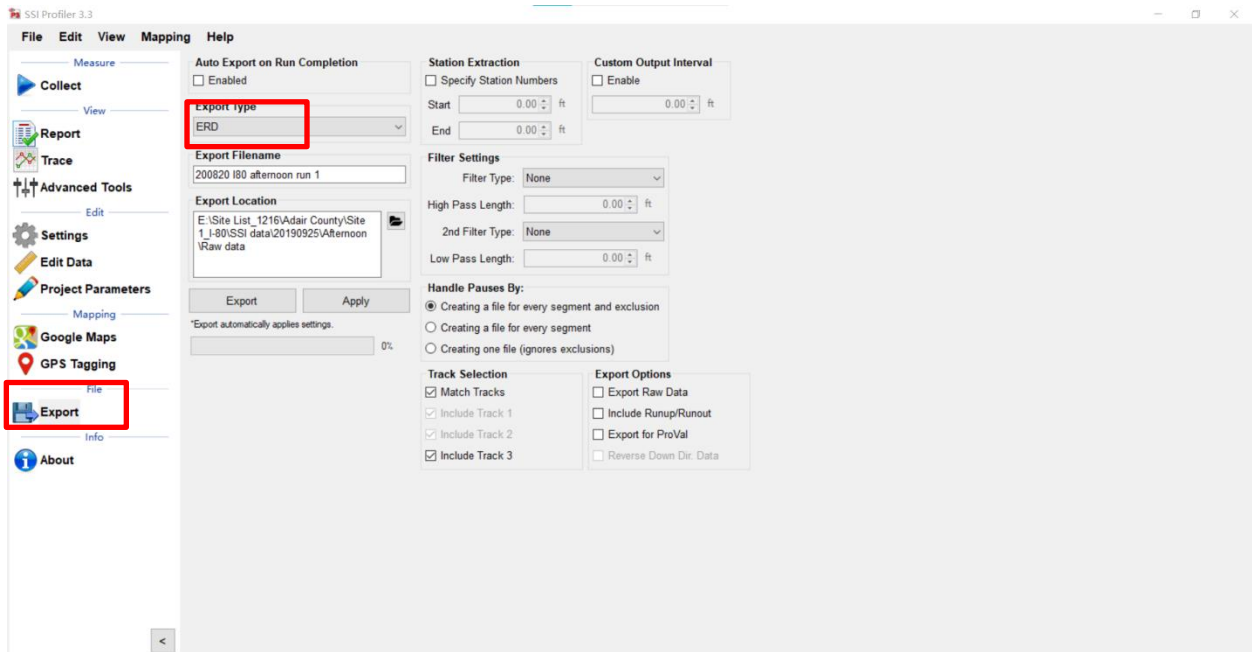


Figure A1. Exporting a *.erd profile in the SSI Profiler software

4. In MATLAB, the user will see the pop-up window shown in Figure A2. The user needs to identify the curling direction (zoom in on the raw profile, judge the curling direction, randomly select a few slabs, then determine the consistency of their curling direction).

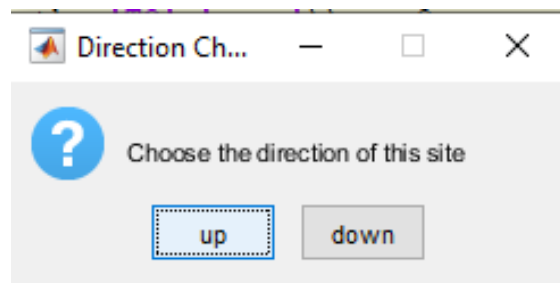


Figure A2. Selecting a curling direction in MATLAB

- Identify the joint locations for a given PCC pavement's *.erd profile using MATLAB (remembering to insert the correct transverse joint spacing, keep the window space as 2 or 3 ft, and usually start the data analysis from the second pavement slab).
- Run the 2GCI code and second-order polynomial code separately. You can check the data analysis progress as shown below:

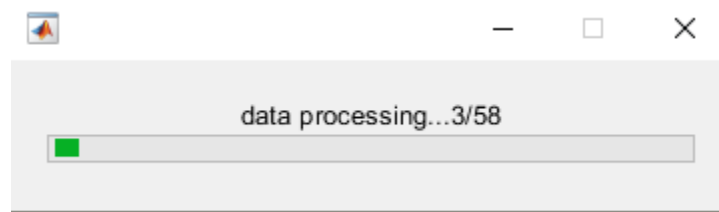


Figure A3. Data processing status in MATLAB

- Double-check the results of four indicators (curvature IRI, deflection, deflection ratio, and degree of curvature), and choose another run for analysis if the results are too high or too low compared to previous analysis results for the selected section. The following code will run automatically and save the results.

	<pre>P = d_1;</pre>
Joint Detection	<pre>[ind3, x6, y6]= Joint_Detection_3 (P, 1/12, 15, 15, 3, Dir);</pre>
2GCI outputs	<pre>[X,Z,ZF,Z_Fitted,ZC,C_PSG,C_L, RMSE, MAPE, R2, DFL]= Curling_Warping_3 (P, ind3, Dir);</pre>
Save all results as an excel sheet	<pre>T = table(X, Z, ZF, Z_Fitted,DFL,RMSE,MAPE,R2,C_L,C_PSG);</pre>
Calculate IRI value	<pre>[PI] = IRI2_1(Z_Fitted, 0.025, 80, 0.25, 25.4, 11, 653, 63.3, 6, 0.15)</pre>
	<pre>filename = [save_path_root, '_T1_', num2str(PI), '.xlsx'];</pre>
	<pre>writetable(T, filename);</pre>

Figure A4. Code view in MATLAB

MATLAB Code to Read *.erd Profile from ProVAL:

```
function [d_l,d_r] = erdRead_T12(filepath)
% return T1 and T2 data from .erd file
% [d_l,d_r] = erdRead(filepath), dir is the file path
% return [left data, right date, center data]
d_12 = importdata(filepath);
d_l = d_12.data(:,2);
d_r = d_12.data(:,3);
len = length(d_12.data);

info = d_12.textdata{2};
info = strsplit(string(info),',');
sp = str2double(info{6});

x_start = d_12.textdata{18};
x_start = strsplit(string(x_start),' ');
x_start = str2double(x_start{2});

x_end = (len-1)*sp + x_start;
dist = x_start:sp:x_end;
d_l = [dist',d_l];
d_r = [dist',d_r];

function [d_c] = erdRead_T3(filepath)
% return T3 data from .erd file
% [d_l,d_r] = erdRead(filepath), dir is the file path
% return [left data, right date, center data]
d_3 = importdata(filepath);
d_c = d_3.data(:,2);
len = length(d_3.data);

info = d_3.textdata{2};
info = strsplit(string(info),',');
sp = str2double(info{6});

x_start = d_3.textdata{18};
x_start = strsplit(string(x_start),' ');
x_start = str2double(x_start{2});

x_end = (len-1)*sp + x_start;
dist = x_start:sp:x_end;
d_c = [dist',d_c];
```

Joint Detection Code:

```
function [ind3, x6, y6]= Joint_Detection_3 (A, D, F, NS, B, Dir)
%% [ind3, x6, y6]= Joint_Detection_2 ('profile name', 1/12, start point (usually same as joint
spacing), joint spacing, 2 or 3, 'curling direction')
x = A(:,1);
y = A(:,2);
if strcmp(Dir,'down')
    y = 0-y;
end
x = x.';
y = y.';
z = csaps(x,y,0.000005,x);
z3 = y-z;
M = movmean(z3,23);
M2 =diff(M);
M3 = movmean(M2,9);
M4 = diff(M3);
X0 = ((F- x(1))/D)-1;
Del = B/D;
S = NS/D;
St = (NS/D)+Del;
x2 = x(3:end);
x4 =[];
while lt(St,(size(M4,2)-X0))
    C = X0 + S;
    Lb = C - Del;
    Ub = C + Del;
    W = M4 (Lb:Ub);
    [mm, I] = min(W);
    ind = Lb+I-1;
    x4 = horzcat(x4, ind);
    X0 = ind;
end

N = size(x4,2);
x5 = x4+2;
y6 = [];
x6 = [];
ind3 = [];
for i = 1:N
    Lbb = x5(i)-(1/D);
    Ubb = x5(i)+(1/D);
    if Lbb < 1
        Lbb = 1;
    end
end
```

```

if Ubb > length(A)
    Ubb = length(A);
end

W = z3 (Lbb:Ubb);
[m, I2] = max(W);
ind2 = Lbb+I2-1;
xx = x(ind2);
yy = y(ind2);
x6 = horzcat(x6, xx);
y6 = horzcat(y6, yy);
ind3 = horzcat(ind3, ind2);
end
if strcmp(Dir,'down')
    y = 0-y;
end
if strcmp(Dir,'down')
    y6 = 0-y6;
end
plot(x,y)
hold on
scatter(x6,y6)
x6 = x6.';
y6 = y6.';
ind3 = ind3.';
end

```

2GCI-Based MATLAB Code:

```
function [X,Z,ZF,Z_Fitted, ZC, C_PSG, C_L, RMSE, MAPE, R2, DFL]= Curling_Warping_3 (A,
B, Dir)
%% [X,Z,ZF,Z_Fitted, ZC, C_PSG, C_L, RMSE, MAPE, R2, DFL]= Curling_Warping_3
(profile name, ind3, curling direction)
F = size (B, 1)-1
Z_f = [];
Z_curl = [];
ZF = [];
Z_Fitted = [];
RMSE = [];
MAPE = [];
R2 = [];
Z = [];
DFL=[];
C_PSG = [];
C_L = [];
for i = 1:F
    st = B(i);
    fi = B(i+1);
    x = A(st:fi,1);
    z = A(st:fi,2);
    corr = z(1)+(((z(end)-z(1))/(x(end)-x(1)))).*(x- x(1)));
    z_corr = z-corr;
    [c,g,d] = fit_curling (x, z_corr, Dir);
    [z_f, z_curl] = filter_curling_s(x, z_corr, c.PSG, c.l);
    z_f = z_f - z_f(1);
    z_f_2 = z_f +corr;
    z_f_3 = z_f_2(2:end);
    size(z_f_3);
    ZF = vertcat (ZF,z_f_3);
    z_fitted = z - z_f;
    Z_Fitted = vertcat (Z_Fitted,z_fitted(2:end));
    Z = vertcat (Z,z(2:end));
    C_PSG = vertcat (C_PSG,repmat(c.PSG,size(z_fitted(2:end))));
    C_L = vertcat (C_L,repmat(c.l,size(z_fitted(2:end))));
    rmse = sqrt(mean((z_fitted-z).^2));
    RMSE = [RMSE;repmat(rmse,size(z_fitted(2:end)))];
    mape = mean(abs((z - z_fitted)./z));
    MAPE = [MAPE;repmat(mape,size(z_fitted(2:end)))];
    r2 = 1 - (sum((z_fitted - z).^2) / sum((z - mean(z)).^2));
    R2 = [R2;repmat(r2,size(z_fitted(2:end)))];
    dfl = max(abs(z_curl));
    DFL = [DFL;repmat(dfl,size(z_fitted(2:end)))];
end
```

```

size(ZF)
st = 1+B(1);
fi = B(end);
X = A(st:fi,1);
ZC = A(st:fi,2)-ZF;

plot (X, Z, X, ZF, X, Z_Fitted), xlabel('Distance (ft)'), ylabel('Elevation (in)'), legend('Raw
Profile','Non-curvated Profile','Curvated Profile')
title('Site name, curled down, all slabs')

plot (X, Z, X, ZF, X, Z_Fitted), xlabel('Distance (ft)'), ylabel('Elevation (in)'), legend('Raw
Profile','Non-curvated Profile','Curvated Profile')
axis([15 160 -40 80])
title('Site name, curled down, 10 slabs')
end

```

Second-Order Polynomial-Based MATLAB Code:

```
function [X,Z,ZF,Z_Fitted, ZC, C_PSG, C_L, RMSE, MAPE, R2, DFL]= Curling_Warping_3 (A,  
B, Dir)  
F = size (B, 1)-1  
Z_f = [];  
Z_curl = [];  
ZF = [];  
Z_Fitted = [];  
RMSE = [];  
MAPE = [];  
R2 = [];  
Z = [];  
DFL=[];  
C_PSG = [];  
C_L = [];  
for i = 1:F  
    st = B(i);  
    fi = B(i+1);  
    x = A(st:fi,1);  
    z = A(st:fi,2);  
    corr = z(1)+(((z(end)-z(1))/((x(end)-x(1)))).*(x- x(1)));  
    z_corr = z-corr;  
    [c,g,d] = fit_curling (x, z_corr, Dir);  
    [z_f, z_curl] = filter_curling_s(x, z_corr, c.PSG, c.l);  
    z_f = z_f - z_f(1);  
    z_f_2 = z_f +corr;  
    z_f_3 = z_f_2(2:end);  
    size(z_f_3);  
    ZF = vertcat (ZF,z_f_3);  
    z_fitted = z - z_f;  
    Z_Fitted = vertcat (Z_Fitted,z_fitted(2:end));  
    Z = vertcat (Z,z(2:end));  
    C_PSG = vertcat (C_PSG,repmat(c.PSG,size(z_fitted(2:end))));  
    C_L = vertcat (C_L,repmat(c.l,size(z_fitted(2:end))));  
    rmse = sqrt(mean((z_fitted-z).^2));  
    RMSE = [RMSE;repmat(rmse,size(z_fitted(2:end)))];  
    mape = mean(abs((z - z_fitted)./z));  
    MAPE = [MAPE;repmat(mape,size(z_fitted(2:end)))];  
    r2 = 1 - (sum((z_fitted - z).^2) / sum((z - mean(z)).^2));  
    R2 = [R2;repmat(r2,size(z_fitted(2:end)))];  
    dfl = max(abs(z_curl));  
    DFL = [DFL;repmat(dfl,size(z_fitted(2:end)))];  
end  
size(ZF)  
st = 1+B(1);
```

```

fi = B(end);
X = A(st:fi,1);
ZC = A(st:fi,2)-ZF;

plot(X, Z, X, ZF, X, Z_Fitted), xlabel('Distance (ft)'), ylabel('Elevation (in)'), legend('Raw
Profile','Non-curvated Profile','Curvated Profile')
title('Site name, all slabs')

plot(X, Z, X, ZF, X, Z_Fitted), xlabel('Distance (ft)'), ylabel('Elevation (in)'), legend('Raw
Profile','Non-curvated Profile','Curvated Profile')
axis([15 160 -40 80])
title('Site name, 10 slabs')
end

% %% The directory of your files
% str = [uigetdir('folder name'),''];
% %% dir set by depth-first walk
filepath = [uigetdir('folder name'),''];
answer = questdlg('Choose the direction of this site','Direction Choose', ...'up', 'down','up');
Dir = answer; % for each site;

mFiles = [];
[mFiles, iFilesCount] = DeepTravel(filepath,mFiles,0);
mFiles = mFiles';
erd_set = regexp(mFiles, '.ERD');
% len = length(cell2mat(erd_set));
% bar = waitbar(0,'data processing...');
log = fopen(fullfile(filepath,'error_log.txt'),'a');
cur_num = 0;
% %% solve
for k = 1:length(erd_set)

    if isempty(erd_set{k}) == 1
        continue
    end

    % cur_num = cur_num + 1;
    % str=['data processing...',num2str(cur_num),',',num2str(len)];
    % waitbar(cur_num/len,bar,str);
    % fprintf('Running: %d/%d\n',[cur_num,len]);
    % filepath = mFiles{k};
    % if regexpi(filepath, '\\dir_Down\\')
    %     dir = 'down';
    % elseif regexpi(filepath, '\\dir_Up\\')
    %     dir = 'up';
    % else
    %     warning(['Cannot get direction of file:', filepath])

```

```

%     continue
%     end
indx = regexpi(filepath, 'folder name\');
js = findFirstNumber(filepath(indx:end));
D = 1/12;
F = js;
NS = js;
B = 3;
[filenames, profiles, num_file] = erd_read_his(filepath);
for i = 1:num_file
    %bar = waitbar(0,[filenames(i,:), ' processing...']);
    fig_path = [filenames(i,),'_slabImages'];
    mkdir(fig_path);
    filename = [filenames(i,),'xlsx'];
    profile = profiles(:,[1,i+1]);
    try
        [ind3, x6, y6] = Joint_Detection_2 (profile, D, F, NS, B, dir);
    catch
        warning(['Cannot get ind3, skip: ',filename]);
        filename = strrep(filename,'\','\');
        fprintf(log,['Cannot get ind3, skip: ',filename,'\n']);
        continue;
    end
    cur_index = 1;
    prev_index = 1;
    x_cur = 0;
    [row,~] = size(profile);
    rst = zeros(row,7);
    stat = zeros(length(ind3)+1, 6);
    for j = 1:length(ind3)+1

        if j == length(ind3) + 1
            last_idx = row;
        else
            last_idx =ind3(j);
        end
        section = profile(cur_index:last_idx,:);
        prev_index = cur_index;
        cur_index = last_idx;
        x = section(:,1);
        y = section(:,2);
        x_fit = x - x(1);
        [p,S] = polyfit(x_fit,y,2);
        R2 = 1 - (S.normr/norm(y - mean(y)))^2;
        y1 = polyval(p,x_fit);
        angle = atan((y1(end) - y1(1))/(x_fit(end) - x_fit(1)));
    end
end

```

```

fit_rotated = rotate_curve([x_fit,y1], [x_fit(1), y1(1)], angle);
raw_rotated = rotate_curve([x_fit,y], [x_fit(1), y1(1)], angle);
raw_rotated(:,2) = raw_rotated(:,2) - fit_rotated(1,2);
fit_rotated(:,2) = fit_rotated(:,2) - fit_rotated(1,2);
raw_rotated(:,1) = raw_rotated(:,1) - raw_rotated(1,1) + x_cur;
fit_rotated(:,1) = fit_rotated(:,1) - fit_rotated(1,1) + x_cur;
rst(prev_index:cur_index,1:7) = [raw_rotated(:,1:2), fit_rotated(:,1:2),x,y,y1];
stat(j,:) = [j, max(abs(fit_rotated(:,2))),p, R2];
x_cur = raw_rotated(end,1);
fig_name = ['fig_slab_',num2str(j, '%.5d'),'tiff'];

%%%%%% ouput image if needed %%%%%%%%%
%   if R2 >= 0.993
%       h = figure;
%       set(h,'visible','off');
%       scatter(raw_rotated(:,1),raw_rotated(:,2),80,'.');
%       hold on
%       plot(fit_rotated(:,1),fit_rotated(:,2),'-
d','LineWidth',2,'MarkerIndices',1:10:length(fit_rotated(:,2)));
%       line(xlim(), [0,0],'LineStyle','-.', 'LineWidth', 1, 'Color', 'k');
%       h = modify_Fig(h);
%       saveas(h,fullfile(fig_path,fig_name));
%       print(h,fullfile(fig_path,fig_name),'-r600','-dtiff');
%       close(h);
%       % waitbar(j/(length(ind3)+1),bar)
%       fprintf('got slab: %d/%d\n',[j,length(ind3)+1]);
%   end

end

raw_x = rst(:,1);
raw_y = rst(:,2);
fitted_x = rst(:,3);
fitted_y = rst(:,4);
fitted_y_abs = abs(rst(:,4));
x_unrotated = rst(:,5);
y_unrotated = rst(:,6);
y_fitted_unrotated = rst(:,7);
csvwrite([filenames(i:),'_fitted_y.csv'],y_fitted_unrotated);

T1 = table(raw_x, raw_y, fitted_x, fitted_y, fitted_y_abs, x_unrotated, y_unrotated,
y_fitted_unrotated);
slab_index = stat(:,1);
deflection = stat(:,2);
ind3 = [ind3:length(profile)];
p = stat(:,3:5);
R = stat(:,6);

```

```

culvature_degree = 2.*p(:,1)./144./12.*100000;
deflection_mean = mean(deflection);
culvature_degree_mean = mean(culvature_degree);
T2 = table(slab_index, ind3, deflection, p, R, culvature_degree);
T3 = table(deflection_mean, culvature_degree_mean);

writetable(T1, filename, 'Sheet',1);
writetable(T2, filename, 'Sheet',2);
writetable(T3, filename, 'Sheet',2, 'Range','I1:J6');

disp(['Finished:', filename]);
end

end
fclose(log);
disp('Done!');

function hfig = modify_Fig(hfig)
set(0, 'CurrentFigure', hfig)
xlabel('Distance (ft)', 'FontSize',10)
ylabel('Elevation (in)', 'FontSize',10)
title('Elevation distribution', 'FontSize',12)
legend({'Raw data', 'Fitted curve'}, 'Location', 'northwest', 'FontSize',6);
figWidth = 5;
figHeight = figWidth * 0.618;
set(hfig, 'PaperUnits', 'inches');
set(hfig, 'PaperPosition', [0 0 figWidth figHeight]);

end

```

A.3. Site List and Visited Seasons

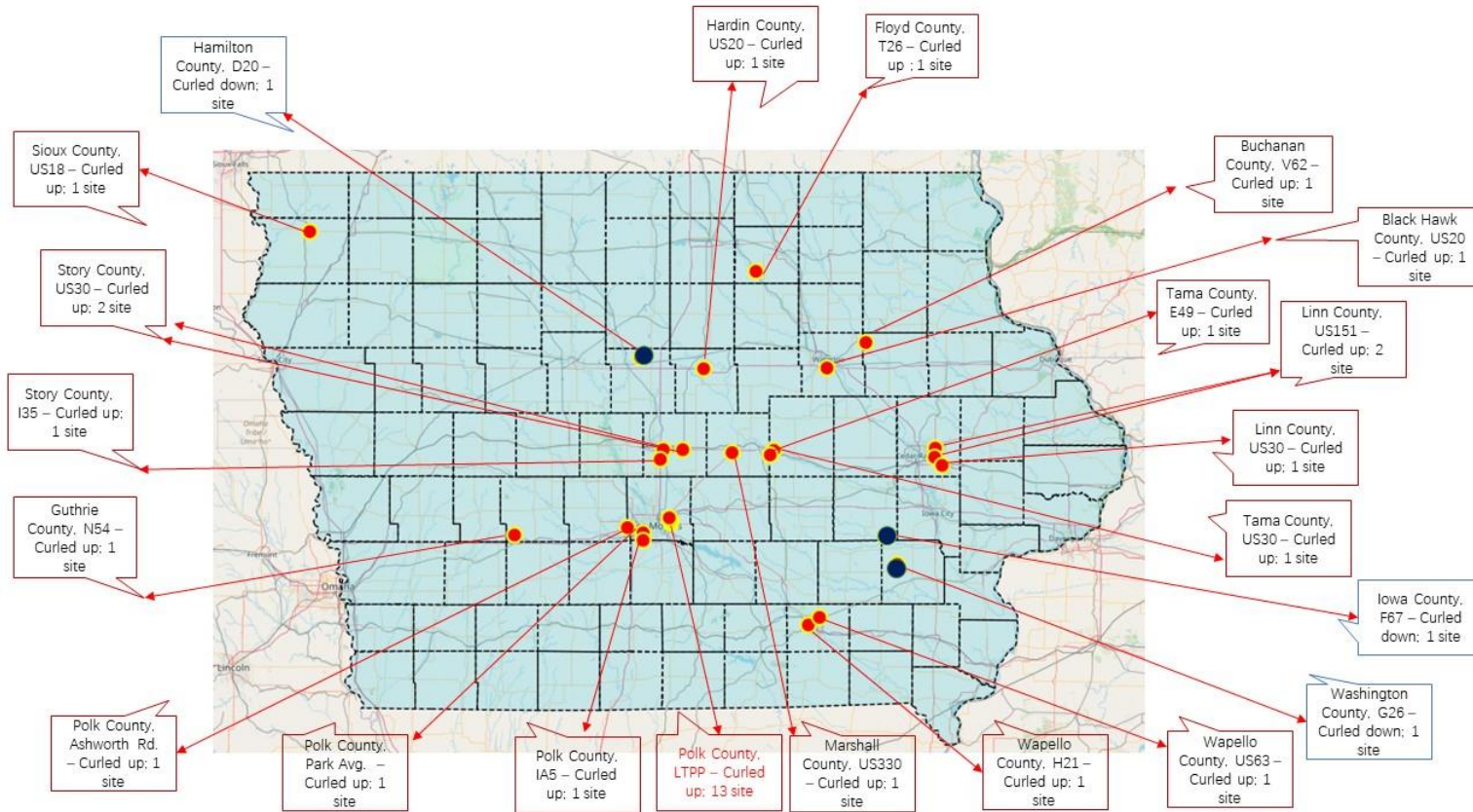


Figure A5. Detailed site list

Table A1. Site list and visited seasons

Group	City	County	Route	Scan Times	2019				2020				2021	
					Spring	Summer	Fall	Winter	Spring	Summer	Fall	Winter	Spring	
Highway	Waterloo	Black Hawk County	US 20	3		<input checked="" type="checkbox"/>					<input checked="" type="checkbox"/>	<input checked="" type="checkbox"/>		
Highway	Cedar Rapids	Linn County	US 151 (1)	5		<input checked="" type="checkbox"/>					<input checked="" type="checkbox"/>	<input checked="" type="checkbox"/>	<input checked="" type="checkbox"/>	<input checked="" type="checkbox"/>
Highway	Cedar Rapids	Linn County	US 151 (2)	5		<input checked="" type="checkbox"/>					<input checked="" type="checkbox"/>	<input checked="" type="checkbox"/>	<input checked="" type="checkbox"/>	<input checked="" type="checkbox"/>
Highway	Cedar Rapids	Linn County	US 30	5		<input checked="" type="checkbox"/>					<input checked="" type="checkbox"/>	<input checked="" type="checkbox"/>	<input checked="" type="checkbox"/>	<input checked="" type="checkbox"/>
Highway	Marshalltown	Marshall County	US 330	5			<input checked="" type="checkbox"/>				<input checked="" type="checkbox"/>	<input checked="" type="checkbox"/>	<input checked="" type="checkbox"/>	<input checked="" type="checkbox"/>
Highway	Pleasant Hill	Polk County	US 65 (1)	6		<input checked="" type="checkbox"/>			<input checked="" type="checkbox"/>					
Highway	Pleasant Hill	Polk County	US 65 (2)	6		<input checked="" type="checkbox"/>			<input checked="" type="checkbox"/>					
Highway	Pleasant Hill	Polk County	US 65 (3)	6		<input checked="" type="checkbox"/>			<input checked="" type="checkbox"/>					
Highway	Pleasant Hill	Polk County	US 65 (4)	6		<input checked="" type="checkbox"/>			<input checked="" type="checkbox"/>					
Highway	Pleasant Hill	Polk County	US 65 (5)	6		<input checked="" type="checkbox"/>			<input checked="" type="checkbox"/>					
Highway	Pleasant Hill	Polk County	US 65 (6)	6		<input checked="" type="checkbox"/>			<input checked="" type="checkbox"/>					
Highway	Pleasant Hill	Polk County	US 65 (7)	6		<input checked="" type="checkbox"/>			<input checked="" type="checkbox"/>					
Highway	Pleasant Hill	Polk County	US 65 (8)	6		<input checked="" type="checkbox"/>			<input checked="" type="checkbox"/>					
Highway	Pleasant Hill	Polk County	US 65 (9)	6		<input checked="" type="checkbox"/>			<input checked="" type="checkbox"/>					
Highway	Pleasant Hill	Polk County	US 65 (10)	6		<input checked="" type="checkbox"/>			<input checked="" type="checkbox"/>					
Highway	Pleasant Hill	Polk County	US 65 (11)	6		<input checked="" type="checkbox"/>			<input checked="" type="checkbox"/>					
Highway	Pleasant Hill	Polk County	US 65 (12)	6		<input checked="" type="checkbox"/>			<input checked="" type="checkbox"/>					
Highway	Pleasant Hill	Polk County	US 65 (13)	6		<input checked="" type="checkbox"/>			<input checked="" type="checkbox"/>					
Highway	Hull City	Sioux County	US 18	4				<input checked="" type="checkbox"/>		<input checked="" type="checkbox"/>				
Highway	Ames	Story County	US 30	5		<input checked="" type="checkbox"/>			<input checked="" type="checkbox"/>					
Highway	Nevada	Story County	US 30	5		<input checked="" type="checkbox"/>			<input checked="" type="checkbox"/>					
Highway	Ames	Story County	I-35	4		<input checked="" type="checkbox"/>			<input checked="" type="checkbox"/>					
Highway	Toledo	Tama County	US 30	4		<input checked="" type="checkbox"/>				<input checked="" type="checkbox"/>				
County Road	Jesup	Buchanan County	V62 (1)	3		<input checked="" type="checkbox"/>				<input checked="" type="checkbox"/>	<input checked="" type="checkbox"/>	<input checked="" type="checkbox"/>	<input checked="" type="checkbox"/>	

Group	City	County	Route	Scan Times	2019				2020				2021	
					Spring	Summer	Fall	Winter	Spring	Summer	Fall	Winter	Spring	
County Road	Marble Rock	Floyd County	T26	3		<input checked="" type="checkbox"/>					<input checked="" type="checkbox"/>	<input checked="" type="checkbox"/>		
County Road	Guthrie Center	Guthrie County	N54	3			<input checked="" type="checkbox"/>				<input checked="" type="checkbox"/>	<input checked="" type="checkbox"/>		
County Road	Webster City	Hamilton County	D20	5			<input checked="" type="checkbox"/>		<input checked="" type="checkbox"/>	<input checked="" type="checkbox"/>	<input checked="" type="checkbox"/>	<input checked="" type="checkbox"/>		
County Road	North English	Iowa County	F67	5		<input checked="" type="checkbox"/>					<input checked="" type="checkbox"/>	<input checked="" type="checkbox"/>	<input checked="" type="checkbox"/>	<input checked="" type="checkbox"/>
County Road	Marshalltown	Tama County	E49	5		<input checked="" type="checkbox"/>					<input checked="" type="checkbox"/>	<input checked="" type="checkbox"/>	<input checked="" type="checkbox"/>	<input checked="" type="checkbox"/>
County Road	Ottumwa	Wapello County	H21	5		<input checked="" type="checkbox"/>					<input checked="" type="checkbox"/>	<input checked="" type="checkbox"/>	<input checked="" type="checkbox"/>	<input checked="" type="checkbox"/>
County Road	Washington	Washington County	G26 (2)	6		<input checked="" type="checkbox"/>			<input checked="" type="checkbox"/>					
City Street	Des Moines	Polk County	Park Avg.	5			<input checked="" type="checkbox"/>				<input checked="" type="checkbox"/>	<input checked="" type="checkbox"/>	<input checked="" type="checkbox"/>	<input checked="" type="checkbox"/>
City Street	West Des Moines	Polk County	Ashworth Rd.	5			<input checked="" type="checkbox"/>				<input checked="" type="checkbox"/>	<input checked="" type="checkbox"/>	<input checked="" type="checkbox"/>	<input checked="" type="checkbox"/>
Highway	Des Moines	Polk County	IA 5	4							<input checked="" type="checkbox"/>	<input checked="" type="checkbox"/>	<input checked="" type="checkbox"/>	<input checked="" type="checkbox"/>
Highway	Iowa Falls	Hardin County	US 20	4							<input checked="" type="checkbox"/>	<input checked="" type="checkbox"/>	<input checked="" type="checkbox"/>	<input checked="" type="checkbox"/>
Highway	Ottumwa	Wapello County	US 63	4							<input checked="" type="checkbox"/>	<input checked="" type="checkbox"/>	<input checked="" type="checkbox"/>	<input checked="" type="checkbox"/>

A.4. Equivalent Temperature Difference Calculation in PMED

The overall equivalent temperature difference is calculated by the following equation:

$$\Delta T = \Delta T_{\text{Permanent}} + \Delta T_{\text{Hourly}} + \Delta T_{\text{Shrinkage}}$$

- In the MEPDG, the permanent effective curling/warping temperature difference ($\Delta T_{\text{Permanent}}$) is represented by a default value of -10°F .
- The hourly pavement temperature difference (ΔT_{Hourly}) for the JPCP layer can be found in the “ThermalPCC.dat” output/intermediate file.
 - The spacing information can be found in the “input.tmp” file, which is the input file for the EICM.
 - PCC,10,0.909090909090909,12,'Material, Thickness, Nodal spacing, Last Node'

1	1979060100	53.7	53.7	53.7	53.7	53.7	53.7	53.7	53.7	53.7	53.7	53.7
2	1979060101	69.1	65.6	62.5	59.8	57.7	56.3	55.3	54.6	54.3	54.0	53.9
3	1979060102	68.4	66.1	63.9	61.9	60.1	58.5	57.2	56.2	55.5	54.9	54.6
4	1979060103	67.8	66.0	64.4	62.7	61.2	59.8	58.5	57.4	56.6	56.0	55.4
5	1979060104	68.0	66.4	64.8	63.3	61.9	60.6	59.4	58.5	57.5	56.9	56.3
6	1979060105	68.2	66.7	65.2	63.8	62.4	61.3	60.2	59.2	58.3	57.7	57.0
7	1979060106	69.1	67.1	65.6	64.2	63.0	61.9	60.8	59.8	59.0	58.3	57.7
8	1979060107	75.0	71.3	68.4	66.2	64.4	62.9	61.6	60.6	59.6	59.0	58.3
9	1979060108	81.4	76.6	72.7	69.5	67.0	64.9	63.2	61.8	60.7	59.8	59.0
10	1979060109	87.6	82.0	77.4	73.5	70.3	67.7	65.4	63.6	62.1	61.0	60.0
11	1979060110	92.2	86.6	81.7	77.4	73.7	70.6	68.0	65.8	64.0	62.5	61.4
12	1979060111	95.3	89.9	85.0	80.7	76.8	73.4	70.6	68.1	66.0	64.3	63.0
13	1979060112	97.6	92.5	87.8	83.5	79.5	76.1	73.1	70.5	68.2	66.3	64.7

Figure A6. ThermalPCC.dat image

To obtain the shrinkage temperature difference ($\Delta T_{\text{shrinkage}}$), relative humidity can be converted to an equivalent temperature difference for every month. The hourly humidity values are available in the selected HCD file.

- Monthly averages are calculated based on the relative humidity values for the length of the entire HCD file.
- The monthly relative humidity values can be verified using the “JPCP_Faulting.csv” intermediate output file.

**THE INSTITUTE FOR TRANSPORTATION IS THE FOCAL POINT FOR TRANSPORTATION
AT IOWA STATE UNIVERSITY.**

InTrans centers and programs perform transportation research and provide technology transfer services for government agencies and private companies;

InTrans contributes to Iowa State University and the College of Engineering's educational programs for transportation students and provides K–12 outreach; and

InTrans conducts local, regional, and national transportation services and continuing education programs.



**IOWA STATE
UNIVERSITY**

Visit InTrans.iastate.edu for color pdfs of this and other research reports.